Development and application of an experimental concept for surface characterization of semiconductor based substrates using scanning electrochemical microscopy

Dissertation

Zur Erlangung des Doktorgrades der Naturwissenschaften (Dr. rer. nat.)

der Fakultät für Chemie und Pharmazie

der Universität Regensburg

vorgelegt von

Patrick Hanekamp

aus Laaber

im Jahr 2018

Die vorgelegte Dissertation entstand in der Zeit von März 2016 bis September 2018 am Institut für Analytische Chemie, Chemo- und Biosensorik der naturwissenschaftlichen Fakultät IV- Chemie und Pharmazie - der Universität Regensburg.

Die Arbeit wurde angeleitet von: Prof. Dr. Frank Michael-Matysik.

Das Promotionsgesuch wurde eingereicht am: 17. Dezember 2018

Termin des Kolloquiums: 15.03.2019

Dem Prüfungsausschuss saß Prof. Dr. Alkwin Slenczka vor. Erstgutachter war Prof. Dr. Frank-Michael Matysik, Zweitgutachter war Prof. Dr. Alfred Lechner und Drittprüfer war Prof. Dr. Arno Pfitzner.

List of content

List of content ... I
Oral and poster presentations ... III
List of publications ... IV
Declaration of collaboration ... VII
List of abbreviations ... VIII
1 Introduction ... 1
2 Theory ... 5
2.1 Voltammetry ... 5
2.1.1 Fundamentals of voltammetry ... 5
2.1.2 Mass transfer towards the electrode surface ... 9
2.1.3 Voltammetric behavior of macroelectrodes and microelectrodes ... 11
2.1.4 Voltammetric techniques ... 15
2.2 Scanning electrochemical microscopy ... 19
2.2.1 Measurement setup of scanning electrochemical microscopy ... 19
2.2.2 Electrochemical mediators ... 20
2.2.3 Working modes in scanning electrochemical microscopy ... 21
2.2.4 Imaging process ... 26
2.3 Electrochemical deposition of copper ... 27
2.3.1 Electroplating of copper in semiconductor industry ... 27
2.3.2 Barrier films for copper ... 30
2.3.3 Nucleation process ... 32
2.3.4 Electrochemical deposition of copper on barrier films ... 35
3 Experimental ... 48
3.1 Materials ... 48
3.2 Mediators ... 50
3.3 Copper electrolytes ... 51
3.4 SECM probe fabrication and characterization ... 52
3.4.1 Fabrication of ultramicroelectrodes ... 52
3.4.2 Characterization of ultramicroelectrodes ... 53
3.5 Multipurpose cell ... 55

4 Results and discussion 58
4.1 Development and application of a multipurpose electrodeposition cell configuration 58
4.1.1 Introduction 59
4.1.2 Experimental 60
4.1.3 Result and discussion 63
4.1.4 Conclusion 68
4.2 Probe approach curves on barrier films on semiconductor substrates 73
4.2.1 Introduction 73
4.2.2 Experimental 74
4.2.3 Result and discussion 75
4.2.4 Conclusion 80
4.3 Material contrast studies of conductive thin films on semiconductor substrates using scanning electrochemical microscopy 83
4.3.1 Introduction 84
4.3.2 Experimental 85
4.3.3 Result and discussion 89
4.4 Nucleation studies on ruthenium from various electrolytes 102
4.4.1 Introduction 102
4.4.2 Experimental 103
4.4.3 Result and discussion 106
4.4.4 Conclusion 113
5 Summary 116
6 Zusammenfassung in deutscher Sprache 118

Oral and poster presentations

Oral presentations

1st Cross-Border Seminar on Electroanalytical Chemistry (ELACh), 4.-6. April 2018, Furth im Wald, Germany

Multipurpose electrochemical cell concept: Surface modification and characterization of semiconductor substrates

Scanning electrochemical microscopy (SECM) is a unique scanning probe method to study samples like coatings, electrodes and membranes in liquid environments. With this technique the electrochemical reactivity and the topography of the substrate can be measured by scanning the probe across the surface. Therefore SECM is a promising technique for the investigation of the electrochemical deposition of copper onto metallic barrier materials or the density of barrier films on semiconductor substrates.

In the frame of this contribution a versatile experimental cell configuration for semiconductor thin film materials is presented [1]. This multipurpose cell setup is designed to conduct semiconductor plating processes in laboratory scale and also to characterize the electrochemical activity of the surface with SECM. For this purpose the silicon substrates with the thin-film barrier materials are placed in a special sample holder ensuring electrical contact of the sample surface with a small circular area of 16 mm^2 exposed to the electrolyte solution.

The multipurpose electrochemical cell configuration was used to obtain information concering film coalescences, grainsize and growth mode during potentiostatic copper deposition on thin-film ruthenium. In addition, thin film copper, titanium, and silicon nitride are studied with SECM concerning their local electrochemical activity. The gained results indicate that biasing of the substrate is essential for non-destructive and interaction-free measurements of semiprecious films and structures in the case of ferrocenemethanol mediator solution.

Literature:

[1] Hanekamp P, Robl W, Matysik F-M (2017) J. Appl. Electrochem.47(12):1305-1312

Poster presentations

Electrochemistry 2016, 26.-28.9.2016, Goslar, Germany

Characterisation of barrier materials on semiconductor substrates by means of scanning electrochemical microscopy

Patrick Hanekamp and Frank-Michael Matysik

ANAKON 2017, 3.-6.4.2017, Tübingen

Characterisation of barrier materials on semiconductor substrates by means of scanning electrochemical microscopy

Patrick Hanekamp and Frank-Michael Matysik

List of publications

Peer reviewed articles

Development and application of a multipurpose electrodeposition cell configuration

Patrick Hanekamp, Werner Robl and Frank-Michael Matysik,

Journal of Applied Electrochemistry 47 (2017): 1305-1312.

Abstract

In this report a versatile experimental concept for electrochemical deposition and subsequent surface characterization studies is presented. This concept can be utilized to perform semiconductor plating processes at laboratory scale followed by scanning electrochemical microscopy (SECM). The same sample holder used for electroplating experiments could be integrated into the SECM instrument. Conductive thin-film barrier materials were deposited on planar silicon wafers. The substrate samples were fixed in the multipurpose sample holder ensuring a large electrical contact area to minimize ohmic drop across the sample surface with a small circular area of the substrate material of 16 mm^2 exposed to electrolyte solution. In order to investigate the capabilities of the electrochemical cell configuration, a potentiostatic copper deposition on ruthenium was carried out. Thus, information on film coalescences, grainsize and

growth mode could be derived. SECM was used to study the effect of biasing during probe approach curves on a titanium surface. Furthermore, microstructured copper layers were imaged using ferrocenemethanol (FcMeOH) as mediator. The results show that biasing the substrate is essential for nondestructive and interaction-free measurements of semiprecious thin-film materials and copper structures, if FcMeOH is used as electrochemical mediator.

Material contrast studies of conductive thin films on semiconductor substrates using scanning electrochemical microscopy

Patrick Hanekamp, Timo Raith, Christian Iffelsberger, Tobias Zankl, Werner Robl and Frank-Michael Matysik

Journal of Applied Electrochemistry (2019): 1-9

Abstract

In this paper a mediator-free scanning electrochemical microscopy (SECM) imaging concept is presented, which is capable of generating high electrochemical contrast and high spatial resolution between two conductive materials. The methodical approach is based on the hydrogen evolution reaction which shows potential dependent material selectivity. Various conductive thin films deposited on silicon substrates were studied. The investigated materials included copper, ruthenium, platinum, tantalum nitride, and titanium nitride. The hydrogen evolution was studied with chronoamperometry ($E_{substrate}$ = -1 V vs. Ag/AgCl/3 M KCl) to characterize the material selectivity of this reaction for the above listed thin films. SECM imaging in the substrate generation-tip collection (SG/TC) mode was carried out and applied to study the boundary regions of thin copper films in combination with the aforementioned thin film materials. In addition, the spatial resolution of hydrogen based SG/TC SECM imaging was characterized using lithographically fabricated platinum/copper structures as test substrates. For comparison, the common feedback mode was also applied for SECM imaging of the conducting thin film combinations. It was found, that only the hydrogen based SG/TC mode enabled SECM imaging with clear material contrast between different conductive materials which was not possible in the feedback mode.

Non-Peer reviewed articles

Trends in der elektrochemischen Rastermikroskopie

Christian Iffelsberger, Timo J. Raith, Patrick J. Hanekamp, Preety Vatsayayan und Frank- Michael Matysik, chrom+food FORUM 4 (2017) 20-22

Declaration of collaboration

The majority of the theoretical and practical research of the presented work was created by the author alone. However, some of the obtained results were achieved in cooperation with other researchers. In accordance with § 8 Abs. 1 Satz 2 Punkt 7 of the Ordnung zum Erwerb des akademischen Grades eines Doktors der Naturwissenschaften (Dr. rer. nat.) an der Universität Regensburg vom 18. Juni 2009, this section describes the nature of these collaborations. In the following, the proportion of these cooperations are specified in dependence of their appearance in the chapter sequence.

4.1 Development and application of a multipurpose electrodeposition cell configuration

SECM measurements, electroplating experiments and the theoretical work were performed by the author. SEM images were taken by Walter Früchtl. Thin film samples on wafer specimen were provided by Infineon Technologies AG. Werner Robl and Frank-Michael Matysik were involved in discussions.

4.2 Probe approach curves on barrier films on semiconductor substrates

Experiments were performed solely by the author. Thin film samples on wafer specimen were provided by Infineon Technologies AG. Some of the obtained results are published in: Material contrast studies of conductive thin films on semiconductor substrates using scanning electrochemical microscopy (submitted for publication). Christian Iffelsberger, Frank-Michael Matysik and Werner Robl were involved in the discussions.

4.3 Material contrast studies of conductive thin films on semiconductor substrates using scanning electrochemical microscopy

Experiments were performed solely by the author. Thin film samples on wafer specimen were provided by Infineon Technologies AG. Fabrication of lithographically structured thin films was done by Tobias Zankl. The artwork of the graphical abstract was done in cooperation with Thomas Herl. Timo Raith, Christian Iffelsberger, Frank-Michael Matysik and Werner Robl were involved in the discussions. Furthermore, Timo Raith was involved in the writing process.

4.4 Nucleation studies on ruthenium from various electrolytes

Electroplating experiments and interpretation were done by the author. Thin film samples on wafer specimen were provided by Infineon Technologies AG. SEM images were recorded by Daniel Fruechtl. Werner Robl was involved in discussions.

List of abbreviations

A	a) Area	[m^2]
	b) Accelerator	
A'	Nucleation rate constant	[s^{-1}]
$A_{Cu\%}$	Copper surface coverage	[%]
A_{dep}	Area of deposition	[m^2]
ALD	Atomic layer deposition	
c	Concentration	[mol l^{-1}]
c^0	Bulk concentration	[mol l^{-1}]
C_{DL}	Capacity of the double layer	[F]
CE	Counter electrode	
D	Diffusion coefficient	[cm^2 s^{-1}]
d_{coal}	Layer thickness of coalescence	[µm]
d_{inner}	Inner diameter	[m]
D_O	Diffusions coefficient of oxidized species	[cm^2 s^{-1}]
d_{outer}	Outer diameter	[m]
D_R	Diffusions coefficient of reduced species	[cm^2 s^{-1}]
E	Potential	[V]
e^-	Electron	
ECD	Electrochemical deposition	
E_{eff}	Effective applied potential	[V]
F	Faraday constant	$9.64853 \cdot 10^4$ C mol^{-1}
FcMeOH	Ferrocenemethanol	
HER	Hydrogen evolution reaction	
I	Current	[A]
I_C	Charging current	[A]
I_{diff}	Current based on diffusion	[A]
I_F	Faradaic current	[A]
I_{kin}	Current based on kinetics	[A]
I_L	Normalized current	[A]
I_S	Substrate current	[A]

I_{SS}	Steady-state current	[A]
$I_{t/d}$	Current based on thermodynamics and diffusion	[A]
$I_{T,\infty}$	Tip current in bulk solution	[A]
I_T	Tip current	[A]
J	Flux	[mol cm^{-2} s^{-1}]
j	Current density	[mA cm^{-2}]
JGB	Janus Green B	
k	Reaction rate constant	[s^{-1}]
L	a) Normalized distance	
	b) Leveler	
L^2	Cross section	[m^2]
Me-B	Metal-boron compound	
Me-C	Metal-carbon compound	
Me-N	Metal-nitrogen compound	
Me-O	Metal-oxide compound	
Me-Si	Metal-silicone compound	
m_T	Mass transport coefficient	[m s^{-1}]
n	Amount of substance	[mol]
N	Nucleation center	
N_0	Active sites on the surface	
N_d	Nucleation density	[m^{-2}]
O^{bulk}	Oxidized active species in bulk solution	
$O^{surface}$	Oxidized active species at the surface	
PECVD	Plasma enhanced physical vapor deposition	
PVD	Physical vapor deposition	
PVP	Polyvinylpyrridone	
Q	Charge	[C]
R	Universal gas constant	8.31447 J mol^{-1} K^{-1}
r	Radius	[m]
R^{bulk}	Reduced active species in bulk solution	
RE	Reference electrode	
RG	RG value	

r_g	Radius of glass mantle	[m]
R_{sol}	Resistance of solution	[Ω]
$R^{surface}$	Reduced active species at the surface	
r_{tip}	Radius of the tip of the electrode	[m]
S	Suppressor	
SECM	Scanning electrochemical microscopy	
SG/TC	Substrate generation/tip collection	
T	Temperature	[K]
t	Time	[s]
TG/SC	Tip generation/substrate collection	
T_M	Melting temperature	[K]
UME	Ultramicroelectrode	
VMS	Virgin make-up solution	
WE	Working electrode	
WD	Working distance	
X, Y, Z	Axis in three-dimensional Cartesian space	
x, y, z	Distance in three-dimensional Cartesian space	[m]
z	Number of electrons transferred	
z’	Correlation factor	[m]
Z_F	Faraday impedance	[Ω]
δ	Diffusion layer thickness	[µm]
η	Efficiency	
Θ	Coverage	
ρ	Density	[kg m^{-3}]
υ	Flow velocity	[m s^{-1}]
Φ	Electric potential	[V]
ΔG^a	Gibbs free energy of formation	[J]
∇^2	Laplacian operator	

1 Introduction

The demand of efficient and more compact microelectronic devices causes a continuous process of miniaturization in the semiconductor industry. Consequently, new materials and processes are developed and introduced to the manufacturing steps in order to achieve these requirements. Recently, copper (Cu) has become increasingly important as metallization material due to its good electrical and thermal conductivity and its higher resistance to electromigration in comparison to aluminum (Al). The Cu metallization in the semiconductor industry can be formed by different deposition techniques such as physical vapor deposition (PVD), chemical vapor deposition (CVD), or electrochemical deposition (ECD). Due to its cost-effectiveness ECD is commonly used for Cu deposition on the wafer scale level [1]. In the ECD process, Cu is usually deposited by galvanic electroplating from an acidic copper electrolyte containing various bath additives on a Cu seed layer [2]. This conductive thin film acts as starting layer for the ECD process and is formed by a PVD, a CVD or an ALD technique. Prior to seed layer coating, deposition of a thin barrier film is carried out to prevent the diffusion of copper into the surrounding dielectric and to enhance the adhesion of the seed film on the substrate. These thin films are typically based on tantalum (Ta), titanium (Ti), or tungsten (W) and may have a nitrogen (N) content [3]. As structure dimensions continue to shrink, the deposition of a thin and conformal Cu seed layer into structured surfaces such as trenches or vias is challenging with the abovementioned techniques [4]. Accordingly, alternative concepts are under investigation to address this issue. One promising approach is the direct electrochemical deposition of Cu onto the thin film barrier as it was shown for Ru, TaN, TiN, W_xN, Os or Ir in laboratory scale [5–10]. Based on these results, characterization of these direct electroplating procedures has to be carried out in terms of process integrability in semiconductor manufacturing to get further insight into the Cu growth process as well. For this purpose, dedicated laboratory equipment is required, which is capable of simulating wafer scale processes on miniaturized laboratory level without any complex sample preparation steps to reduce the risk of damaging the deposited thin films prior to the characterization step. In addition, such equipment should also be connectable and capable of being integrated with scanning probe techniques to obtain local information of the sample surface. Thereby, scanning electrochemical microscopy (SECM) has proven to be a powerful electroanalytical tool to investigate the electrochemical activity of a surface of interest and is promising for the application in semiconductor industry due to its strength to gain local electrochemical information on nucleation [11], corrosion [12–14], dissolution of metals [15], and the chemical stability of inhibitor thin films [16–18]. Applying this

analytical method can give complementary information to typically applied characterization procedures in semiconductor manufacturing.

The following objectives were the basis of this thesis:

- Development and characterization of a multipurpose cell for electrochemical surface modification and electrochemical surface characterization of thin film materials on a silicon substrate
- Examination of applicability of SECM for electrochemical surface characterization for typically used thin films in semiconductor industry
- Development of a SECM concept to study structured conductive semiprecious thin film materials with high contrast and spatial resolution
- Characterization of the influence of electrolyte composition on the nucleation process and growth behavior of electrochemically deposited copper on a suitable barrier material

References

[1] J.R. Eid, Copper Electrodeposition : Principles and Recent Progress Copper Electrodeposition : Principles and Recent Progress, 2650 (n.d.).

[2] P.M. Vereecken, R. a. Binstead, H. Deligianni, P.C. Andricacos, The chemistry of additives in damascene copper plating, IBM J. Res. Dev. 49 (2005) 3–18. doi:10.1147/rd.491.0003.

[3] M. Baklanov, P.S. Ho, E. Zschech, Advanced interconnects for ULSI technology, John Wiley & Sons, 2012.

[4] A. Radisic, M. Nagar, K. Strubbe, S. Armini, Z. El-Mekki, H. Volders, W. Ruythooren, P.M. Vereecken, Copper Plating on Resistive Substrates, Diffusion Barrier and Alternative Seed Layers, ECS Trans. . 25 (2010) 175–184. doi:10.1149/1.3318516.

[5] M. Nagar, A. Radisic, K. Strubbe, P.M. Vereecken, The Effect of the Substrate Characteristics on the Electrochemical Nucleation and Growth of Copper, J. Electrochem. Soc. 163 (2016) D3053--D3061.

[6] A. Radisic, Y. Cao, P. Taephaisitphongse, A.C. West, P.C. Searson, Direct Copper Electrodeposition on TaN Barrier Layers, J. Electrochem. Soc. 150 (2003) C362–C367. doi:10.1149/1.1565137.

[7] L. Magagnin, A. Vicenzo, M. Bain, H.W. Toh, H.S. Gamble, P.L. Cavallotti, Nucleation and growth of

ECD Cu on PVD TiN from low acid sulfate electrolyte, Microelectron. Eng. 76 (2004) 131–136. doi:10.1016/j.mee.2004.07.006.

[8] M.J. Shaw, S. Grunow, D.J. Duquette, “Seedless” electrochemical deposition of copper on physical vapor deposition-W2N liner materials for ultra large scale integration (ULSI) devices, J. Electron. Mater. 30 (2001) 1602–1608. doi:10.1007/s11664-001-0179-8.

[9] D. Josell, J.E. Bonevich, T.P. Moffat, T. Aaltonen, M. Ritala, M. Leskelä, Osmium Barriers for Direct Copper Electrodeposition in Damascene Processing, Electrochem. Solid-State Lett. 9 (2006) C48-50. doi:10.1149/1.2179770.

[10] D. Josell, J.E. Bonevich, T.P. Moffat, T. Aaltonen, M. Ritala, M. Leskelä, Iridium Barriers for Direct Copper Electrodeposition in Damascene Processing, Electrochem. Solid-State Lett. 9 (2006) C48–C50. doi: 10.1149/1.2150165.

[11] J. Kim, C. Renault, N. Nioradze, N. Arroyo-Currás, K.C. Leonard, A.J. Bard, Electrocatalytic Activity of Individual Pt Nanoparticles Studied by Nanoscale Scanning Electrochemical Microscopy, J. Am. Chem. Soc. 138 (2016) 8560–8568. doi:10.1021/jacs.6b03980.

[12] C. Gabrielli, E. Ostermann, H. Perrot, V. Vivier, L. Beitone, C. Mace, Concentration mapping around copper microelectrodes studied by scanning electrochemical microscopy, Electrochem. Commun. 7 (2005) 962–968. doi:10.1016/j.elecom.2005.06.018.

[13] J. Izquierdo, A. Eifert, C. Kranz, R.M. Souto, In situ investigation of copper corrosion in acidic chloride solution using atomic force- scanning electrochemical microscopy, Electrochim. Acta. 247 (2017) 588–599. doi:10.1016/j.electacta.2017.07.042.

[14] A. Asserghine, D. Filotás, L. Nagy, G. Nagy, Scanning electrochemical microscopy investigation of the rate of formation of a passivating TiO 2 layer on a Ti G4 dental implant, Electrochem. Commun. (2017). doi:10.1016/j.elecom.2017.08.018.

[15] J. Izquierdo, B.M. Fernández-Pérez, A. Eifert, R.M. Souto, C. Kranz, Simultaneous Atomic Force-Scanning Electrochemical Microscopy (Afm-Secm) Imaging of Copper Dissolution, Electrochim. Acta. 201 (2015) 320–332. doi:10.1016/j.electacta.2015.12.160.

[16] C. Li, L. Li, C. Wang, Study of the inhibitive effect of mixed self-assembled monolayers on copper with SECM, Electrochim. Acta. 115 (2014) 531–536. doi:10.1016/j.electacta.2013.11.029.

[17] K. Mansikkamäki, P. Ahonen, G. Fabricius, L. Murtomäki, K. Kontturi, Inhibitive Effect of Benzotriazole on Copper Surfaces Studied by SECM, J. Electrochem. Soc. 152 (2005) B12–B16. doi:10.1149/1.1829413.

[18] M. Pähler, J.J. Santana, W. Schuhmann, R.M. Souto, Application of AC-SECM in corrosion science: Local visualisation of inhibitor films on active metals for corrosion protection, Chem. - A Eur. J. 17 (2011) 905–911. doi:10.1002/chem.201000689.

2 Theory

The theoretical fundamentals of this work are presented in this chapter, divided into three subsections. In the first part, an introduction to voltammetry is given. A detailed overview on electrode processes and commonly used voltammetric techniques is shown. Next, the scanning electrochemical microscopy will be introduced based on these fundamental aspects. On this occasion, a description of the experimental setup and the working modes of this electrochemical characterization technique is given. In the third part the focus is set on the electrochemical deposition process of copper. Here, an overview of industry scaled Cu deposition and the theoretical aspects of electrochemical nucleation and growth will be presented. Based on these fundamentals, an introduction of a rather new approach of direct electrochemically copper deposition on barrier films will be given.

2.1 Voltammetry

The onset of voltammetry began with the discovery of polarogaphy by Jaroslav Heyrovský, awarded with the Nobel Prize in 1922 [1]. In voltammetry, the current I is measured in dependence of the potential E in presence of an electrochemically convertible analyte.

2.1.1 Fundamentals of voltammetry

From the I-E curves qualitative and quantitative information of the studied system can be obtained. Voltammetry is usually performed in a three electrode configuration with a working electrode WE, a reference electrode RE and a counter electrode CE [2]. A schematic layout of an electrochemical cell in three electrode configuration and the corresponding equivalent circuit diagram are depicted in Fig. 2.1.

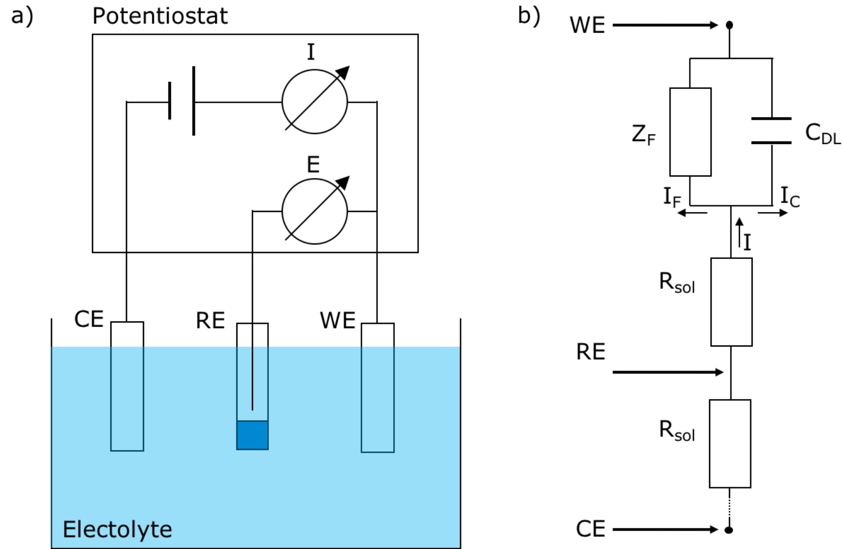

Figure 2.1: Schematic representation of an electrochemical cell. (a) Schematic layout of the three electrode configuration with working electrode (WE), counter electrode (CE) and reference electrode (RE). The potential (E) of the WE is measured and controlled versus the RE and the current (I) is measured versus CE with a potentiostat. (b) Equivalent circuit diagram of the electrochemical cell with the ohmic resistance of the solution R_{sol}, the capacity of the double layer at the electrolyte/electrode interface C_{DL} and the Faraday impedance Z_F representing material conversion. The corresponding current I can be divided in the charging current I_C and the faradaic current I_F. Adapted from [2].

As it can be seen in the schematic layout in Fig. 2.1, the applied potential E at the WE is measured versus RE and the corresponding current I is measured versus CE with a potentiostat. The measurement of E should preferably be carried out currentless versus RE as otherwise a proportion of the applied potential E is lost at the resistance of the solution R_{sol}. The effective applied potential E_{eff} at the WE is therefore described as:

$$E_{eff} = E - I \cdot R_{sol} \quad (1)$$

Accordingly, electrochemical measurements should be performed in electrolytes with a low resistivity to reduce this parasitic effect (IR-drop) on the measurement results. From Fig. 2.1 b) it is evident that I is the

sum of two superimposed and inseparable current components, consisting of the charging current I_C and the faradaic current I_F.

$$I = I_C + I_F \tag{2}$$

Here, I_C represents the charging of the double layer at the electrolyte/substrate at a potential step. The double layer can therefore be illustrated as a capacity element C_{DL} in the equivalent circuit. Consequently, I_c is a time dependent function in dependence of C_{DL} and R_{sol} at a potential step from E_1 to E_2.

$$I_C = \frac{E_2 - E_1}{R_{sol}} \cdot \exp\left(\frac{-t}{R_{sol} \cdot C_{DL}}\right) \tag{3}$$

Contrary, I_F is a result of the electrochemical conversion of the active species at the WE and starts at the characteristic half-wave potential of a reaction. This process is represented as the Faraday impedance Z_F in the equivalent circuit diagram [3]. Since the information of the reaction is only represented by I_F, a large ratio I_F/I_C is favorable. This can be achieved by exploiting the time dependency of both current components by using pulsed techniques [4] or by utilizing microelectrodes (chapter 2.1.3.2). The process of the electrochemical conversion of the active species consists of three major steps and will representatively be explained for a reduction process. The overall process can be described schematically as:

$$O^{bulk} \rightarrow O^{surface} \overset{n \cdot e^-}{\longleftrightarrow} R^{suface} \rightarrow R^{bulk} \tag{4}$$

In the first step, the oxidized form of the active species O is transported towards the electrode surface at a diffusion-controlled rate D_O. This mass transport can be described by the mass transport coefficient m_T in dependence of D_O and the corresponding diffusion layer thickness δ:

$$m_T = \frac{D_0}{\delta} \quad (5)$$

In the second step, the electrons are transferred at the electrode surface, whereas the species O is reduced to its reduced form R. The reaction is kinetically controlled by the potential dependent reaction rate constant k. In the third step, the conversed species R is transported away from the electrode, controlled jointly by thermodynamics and diffusion D_R of the reduced species. Each of the three steps contributes to I_F by their partial currents of I_{dif}, I_{kin} and $I_{t/d}$. Consequently, the measured faradaic current is expressed by the reciprocal formula [5]:

$$\frac{1}{I_F} = \frac{1}{I_{dif}} + \frac{1}{I_{kin}} + \frac{1}{I_{t/d}} \quad (6)$$

As it can be seen in (6), electrochemical conversion can be limited by one of the steps mentioned before. Therefore, this process can basically be limited by mass transport or kinetics. Accordingly, an electrochemical conversion process can be categorized into reversible (fast kinetics) or irreversible (slow kinetics) processes by comparing m_T with k [6]:

$$k \gg m_T \text{ (reversible)} \quad (7)$$

$$k \ll m_T \text{ (irreversible)} \quad (8)$$

For the following theoretical considerations, it is assumed that the electrode processes are reversible. As previously described, electrochemical conversion is dependent on mass transport towards the surface in this case. A more detailed description of the process of mass transfer will be given in the next chapter which is required to understand the behavior of macro- and microelectrodes.

2.1.2 Mass transfer towards the electrode surface

Mass transport is defined as the flux J of a mass or a species from one place to another place in the solution. The flux is the result of a change of chemical potential or electrical potential between two locations or the movement of a volume element in this solution. It can be described by the Nernst-Planck equation in dependence of the aforementioned factors. For the one-dimensional stationary transport towards the electrode in x-direction J can be expressed in dependence of the active species i with diffusion coefficient D_i, concentration c_i, number of electrons transferred z_i, electric potential Φ and velocity υ, the faraday constant F, universal gas constant R and temperature T as [7]:

$$J_i(x) = -D_i \cdot \frac{\partial c_i(x)}{\partial x} - \frac{z_i \cdot F}{R \cdot T} \cdot D_i \cdot c_i \cdot \frac{\partial \Phi(x)}{\partial x} + c_i \cdot \upsilon(x) \tag{9}$$

One can see that J is the result of three independent terms. The first term of equation (9) describes the influence of diffusion on J. It is based on a concentration gradient arising from a difference in chemical potential. The second term of eq. 9 shows the impact of migration on the basis of the movement of charged particles in an electric field. The third term of eq. 9 characterizes the effect of natural or forced convection on J. Since these three terms are independent from each other, a simplification of eq. 9 is possible by suppression of one or two of the contributing terms. On this occasion, influence of migration can be eliminated by using a supporting electrolyte and the effect of convection can be suppressed by working in quiescent solution. Accordingly, mass transfer can be restricted to diffusive flux. In this case eq. 9 is simplified to the one-dimensional stationary Fick's first law:

$$-J_i(x) = D_i \cdot \frac{\partial c_i(x)}{\partial x} \tag{10}$$

Considering mass conservation without any chemical reactions in eq. 10, Fick's second law can be obtained. This partial differential equation describes the diffusion dependent change of the concentration gradient with time.

$$\frac{\partial c_i(x,t)}{\partial t} = D_i \cdot \left(\frac{\partial^2 c_i(x,t)}{\partial x^2}\right) \quad (11)$$

Or the general form of Fick's second law for any geometry with the Laplacian operator ∇^2:

$$\frac{\partial c_i}{\partial t} = D_i \cdot \nabla^2 c_i \quad (12)$$

This Laplacian operator has to be modified dependent on electrode geometry. The corresponding Laplace operators are depicted in table 2.1.

Table 2.1: Laplacian operator for various electrode geometries. Adapted from [8].

Type	Variables	Laplacian operator ∇^2	Example
Linear	x	$\frac{\partial^2}{\partial x^2}$	Shielded disk electrode
Spherical	r	$\frac{\partial^2}{\partial r^2} + \frac{2}{r} \cdot \left(\frac{\partial}{\partial r}\right)$	Hanging drop electrode
Cylindrical (axial)	r	$\frac{\partial^2}{\partial r^2} + \frac{1}{r} \cdot \left(\frac{\partial}{\partial r}\right)$	Wire electrode
Disc	r, z	$\frac{\partial^2}{\partial r^2} + \frac{1}{r} \cdot \left(\frac{\partial}{\partial r}\right) + \frac{\partial^2}{\partial z^2}$	Inlaid disk ultramicroelectrode
Band	x, z	$\frac{\partial^2}{\partial x^2} + \frac{\partial^2}{\partial z^2}$	Inlaid band electrode

By solving the general form of Fick's second law, the time dependent current response at a fixed potential can be obtained in the case of diffusion limited processes. In the next chapter, a more detailed description of the current response of different planar electrodes will be presented.

2.1.3 Voltammetric behavior of macroelectrodes and microelectrodes

The solution of the general form of the partial equation of Fick's second law is strongly dependent on the boundary conditions [8] and the Laplacian operator for the corresponding electrode geometry as it can be seen in table 2.1. Consequently, the current response of macro- and microelectrodes are not identical and have to be derived separately.

2.1.3.1 Macroelectrodes

The active area of a planar macroelectrode is large in comparison to the edges of aforementioned surface. Accordingly, it can be assumed that the flux towards the electrode surface is controlled by linear diffusion since boundary effects at these edges are negligible. Due to this simplification, the one-dimensional form of Fick's second law (eq. 11) can be used for calculation. This partial differential equation is solved by the Cottrell equation [6]:

$$I(t) = \frac{n \cdot F \cdot A \cdot \sqrt{D_i}}{\sqrt{\pi \cdot t}} \cdot c_i^0 \qquad (13)$$

The Cottrell equation describes the time dependent decrease of current based on the consumption of initial concentration of the active species c_i^0 on an electrode area A and the amount of substance n. This equation can be used to predict the faradaic current response of a potential step experiment from E_1 (no electrode reaction) to E_2 (reaction at a diffusion-controlled rate) and is used to describe current transients in chronoamperometry (chapter 2.1.4.2). Since this equation is based on eq. 11, it is only valid for diffusion limited electrochemical conversion. The depletion of the active species at the electrode surface can be prevented by applying forced convection to the system for example by stirring or using a rotating disc electrode (RDE). Due to the enhancement of mass transfers (eq. 9), a time-independent stable diffusion layer is formed, and a constant faradaic current is obtained which does not follow the predicted Cottrellian behavior.

2.1.3.2 Microelectrodes

In the case of microelectrodes, boundary effects cannot be neglected since they provide a significant share to the mass transport. Accordingly, diffusion from the edges of the electrode surface has to be considered in eq. 12 by adapting the Laplacian operator according to table 2.1. Thus, Fick's second law can be written in spherical coordinates for microelectrodes with an insulating mantle of infinite thickness as depicted in Fig. 2.2:

$$\frac{\partial c_i(r,z,t)}{\partial t} = D_i \cdot \left[\frac{\partial^2 c_i(r,z,t)}{\partial r^2} + \frac{1}{r} \cdot \frac{\partial c_i(r,z,t)}{\partial r} + \frac{\partial^2 c_i(r,z,t)}{\partial z^2}\right] \quad (14)$$

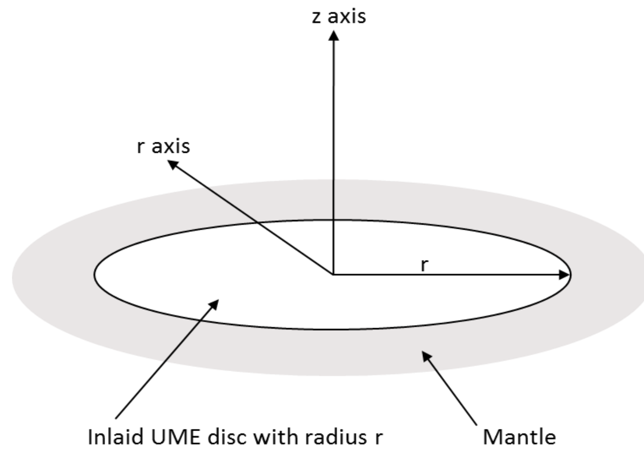

Figure 2.2: Schematic representation of an inlaid microelectrode with radius r and spherical coordinates. Adapted from [5].

The time dependent current response for inlaid microelectrodes of a radius r with infinite mantle thickness is obtained by solving eq. 14 [5]. Since the solution is derived from Fick's law, it is only valid for diffusion-controlled process:

$$I(t) = \frac{n \cdot F \cdot \pi \cdot r^2 \cdot \sqrt{D_i}}{\sqrt{\pi \cdot t}} \cdot c_i^0 + 4 \cdot n \cdot F \cdot D_i \cdot r \cdot c_i^0 \quad (15)$$

As it can be seen, the current response of microelectrodes is described by two independent terms. The first term represents the time dependent current response based on linear diffusion. This term shows a Cottrellian behavior analogous to macroelectrodes (eq. 13). The second term is time independent due to the formation of a time independent spherical diffusion field at the edges of the electrode. Thus, the current response of this term represents a steady-state current behavior. Both terms are schematically depicted in Fig. 2.3.

Figure 2.3: Schematic representation of diffusion fields at a disc electrode with infinite mantle thickness. (a) linear diffusion field and (b) spherical diffusion field of a microelectrode with radius r. Adapted from [5].

Since the Cotrellian term shows a quadratic dependency on electrode radius ($I \propto r^2$), its influence on the current response diminishes with decreasing electrode size in comparison to the second term ($I \propto r$). Thus, for very small electrodes with $r \ll 50\ \mu m$, also referred to as ultramicroelectrodes (UME), the linear diffusion term approaches zero and the term for the spherical diffusion represents the significant fraction. Consequently, the current response of microelectrodes in an insulating mantle of infinite thickness is described by a steady state current I_{ss}, since the mass transport of the reactive species is controlled by a constant spherical diffusion layer formed around the microelectrode:

$$I_{ss} = 4 \cdot n \cdot F \cdot D_i \cdot c_i^0 \cdot r \tag{16}$$

For microelectrodes with finite mantle thickness, the flux from behind the electrode surface has to be considered as otherwise I_{ss} will strongly differ from the value predicted by eq. 16. The mantle thickness r_g is usually normalized on the corresponding electrode radius r in order to be able to compare different microelectrodes sizes. Thus, the RG-value is calculated from the ratio between r_g and r:

$$\mathrm{RG} = \frac{\mathrm{r_g}}{\mathrm{r}} \tag{17}$$

Accordingly, the influence of the mantle thickness on I_{ss} can be expressed by a β-function in dependence of RG with an error of less than 0.3% for RG > 1 [9].

$$\mathrm{I_{ss}} = 4 \cdot \mathrm{n} \cdot \mathrm{F} \cdot \mathrm{D_i} \cdot \mathrm{c_i^0} \cdot \mathrm{r} \cdot \beta(\mathrm{RG}) \tag{17}$$

With the β-function [9]:

$$\beta(\mathrm{RG}) = 1 + \frac{0.23}{(\mathrm{RG}^3 - 0.81)^{0.36}} \tag{18}$$

Besides their steady-state behavior, the usage of microelectrodes has further advantages in comparison to macroelectrodes. Since the electrode radius is proportional to the RC element ($r \propto RC$, [5]), the utilization of smaller electrodes will minimize I_C according to eq. 3. Consequently, a high I_F/I_C ratio can be obtained, which is advantageous for studying fast reactions. Moreover, the impact of IR-drops on E_{eff} is significantly reduced. Since the measured current for microelectrodes is usually in the range of nA to pA, the IR-drop is much lower according to eq. 1. Consequently, it can be assumed that $E_{eff} \approx E$. For that reason, it is possible to work in high resistive solutions without the addition of a conductive salt. Furthermore, experimental studies can be carried out in two electrode configuration without the presence of a reference electrode when using microelectrodes. In the next chapter, common techniques in voltammetry are described. The impact of electrode sizes of macro- and microelectrodes in these methods are discussed.

2.1.4 Voltammetric techniques

There is a broad range of voltammetric techniques for quantitative and qualitative characterization in different application areas [7]. Since only cyclic voltammetry and chronoamperometry were used in this work, the focus is set on these techniques in the following chapter.

2.1.4.1 Cyclic voltammetry

In cyclic voltammetry a saw tooth voltage profile is applied to the working electrode. The saw tooth voltage is thereby defined by a low and high vortex potential as initial/end potential. The selection of the vortex potentials is dependent on the conversion process of the redox active species. A cycle contains a linear increase of voltage from the initial potential to the end potential followed by linear decrease until the initial potential is reached by a predefined scan rate. The cycles are repeated as often as desired. During controlled potential cycling, the current at the WE is monitored. The logged current during measurement is plotted versus the applied potential, which is called a cyclic voltammogram. This diagram can be used to obtain electrochemical properties of a redox active species [6]. A representative measurement with ferrorecenemethanol (FcMeOH) as electroactive species is shown in Fig. 2.4.

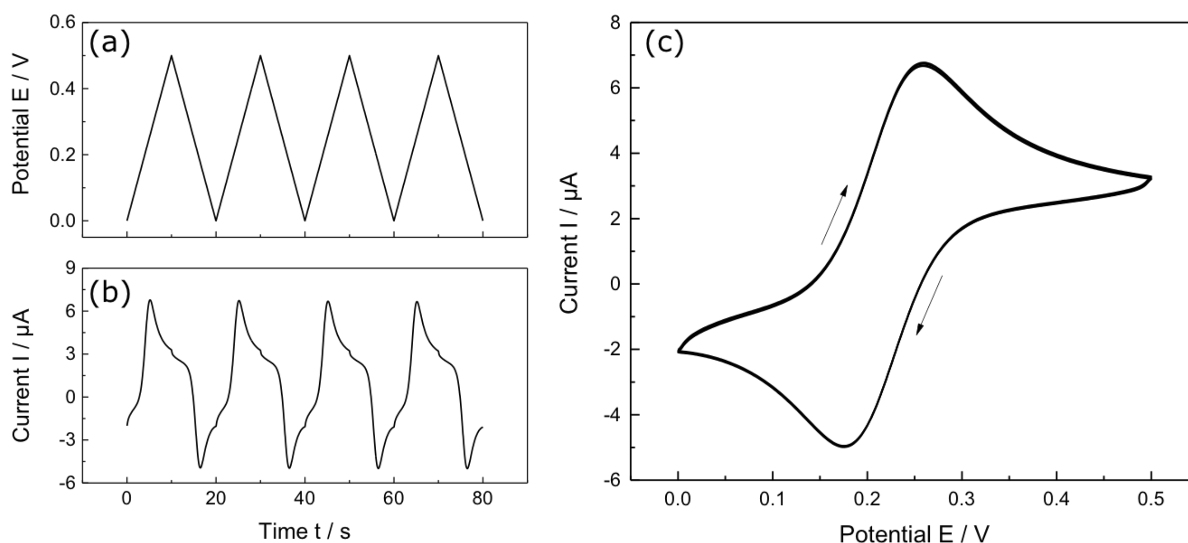

Figure 2.4: Different data parts of a measurement in cyclic voltammetry. (a) Applied saw tooth potential E at the working electrode in dependence of time. (b) Measured current I due to potential change in dependence of time and (c) plot of cyclic voltammogramm I vs E resulting from the data of (a) and (b) with a Pt-macroelectrode (r = 1 mm) in a 1.5 mM FcMeOH and 0.2 M KNO_3 mediator.

In cyclic voltammetry, different current responses are obtained based on electrode size. As shown in chapter 2.1.3, current response is dependent of the geometrical size of the active electrode area in the case of a diffusion limited reaction. Accordingly, current response for macroelectrodes and microelectrodes differs strongly as can be seen in Fig. 2.5 for a) a macroelectrode with r = 1 mm and b) an ultramicroelectrode with r = 12.5 µm (RG = 10).

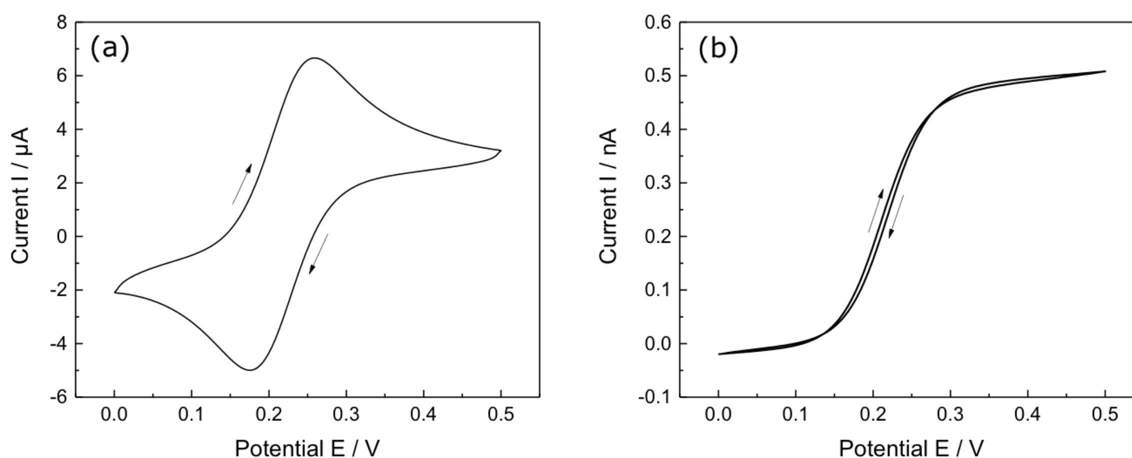

Figure 2.5: Comparison of cyclic voltammograms at different electrodes. (a) Pt-macroelectrode (r = 1mm) and (b) Pt-microelectrode (r = 300 nm, RG = 10) in 1.5 mM FcMeOH and 0.2 M KNO_3.

As can be seen, FcMeOH is oxidized at a heterogenous reaction rate at a certain starting potential. For the macroelectrode, a peak shaped response is obtained due to its Cottrellian behavior predicted by eq. 13. The observed peak during potential increase is consequently the result of the current decay ($I \propto 1/\sqrt{t}$) on the basis of the depletion of the surface concentration of FcMeOH. Furthermore, an offset between forward- and backward scan is observable. This effect can be attributed to the influence of I_c on the measured current due to the double layer charging during potential sweep as explained in chapter 2.1.1. In contrast to the macroelectrode, a steady-state current response is obtained for microelectrodes. The plateau of the sigmoidal steady state voltammogram corresponds to the steady state current response of microelectrodes according to eq. 17. No offset between forward- and backward scan can be observed as the influence of I_c is strongly reduced for microelectrodes due to dependence of the RC element on tip size (chapter 2.1.3.2).

2.1.4.2 Chronoamperometry

In chronoamperometry, the potential of the working electrode is set to a fixed value and the current response is logged during measurement time. The obtained current responses are also referred to as current transients. This technique can be used to study nucleation processes, kinetics and diffusion processes [10]. Typical current transients for a diffusion limited reaction are plotted in Fig. 2.6.

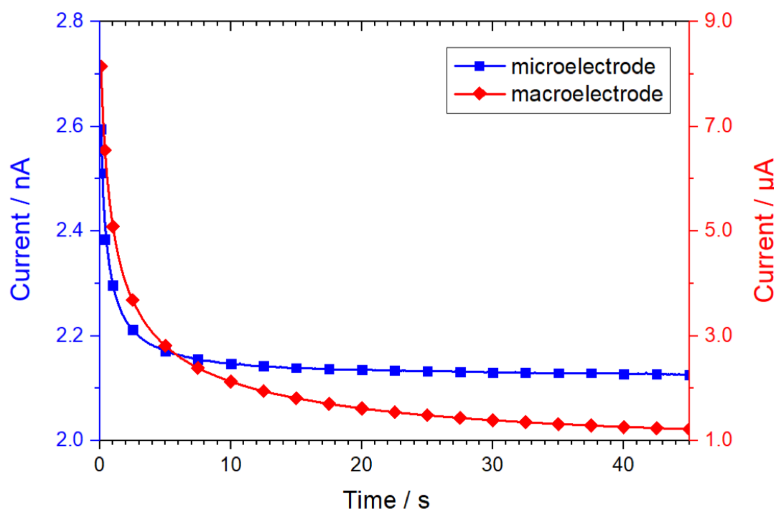

Figure 2.6: Current transients of a Pt-microelectrode (r = 6.25 µm, RG = 3) and a Pt-macroelectrode (r = 1 mm) at E = 0.5 V in 1.5 mM FcMeOH and 0.2 M KNO_3.

As theoretically predicted in chapter 2.1.3, the current response is dependent on the size of the electrode. For the macroelectrode, a decay of current is observed due to the Cottrellian behavior ($I \propto 1/\sqrt{t}$) at the large active electrode according to eq. 13. The current is steadily decreasing due to the depletion of the active species at the electrode surface until the reaction is limited by diffusion of the species from the bulk solution. Contrary, a steady-state current response is obtained for microelectrodes due to the diffusion limited transport of the active species caused by the spherical diffusion field as predicted by eq. 17. Due to this steady state behavior as well as the fast response times according to chapter 2.3.1.2, it is possible to obtain electrochemical information in small spots of the solution with microelectrodes. These

advantageous properties are applied in the scanning electrochemical microscope (SECM). This measuring technique will be presented in the following chapter.

2.2 Scanning electrochemical microscopy

Scanning electrochemical microscopy (SECM) was developed and characterized by Bard and coworkers in 1989 [11]. SECM belongs to the class of scanning probe microcopy (SPM). In SPM a small probe is scanned across the surface whereby an image of the surface is obtained through the interaction of the probe with the surface. Using SECM, local information of the electrochemical behavior at the liquid/solid, liquid/gas and liquid/liquid interface can be obtained through the interaction of an ultramicroelectrode with the interface of interest. Consequently, insight into surface reactivity, chemical kinetics, and the local concentration of reactants can be obtained [11]. An introduction into this versatile electrochemical characterization tool will be presented in the following chapter.

2.2.1 Measurement setup of scanning electrochemical microscopy

A schematic illustration of the SECM setup is depicted in Fig. 2.7. The electrochemical measurement cell (SECM cell) contains the counter- and reference electrode, a mounting platform for a substrate, and the mediator. The design of the SECM cell is dependent of the substrate of interest. Measurements are usually performed in a four-electrode configuration with an UME as probe (WE1), a counter electrode (CE), a reference electrode (RE), and the substrate of interest as the second working electrode (WE2). The control of the electrode potentials and the data acquisition is achieved with a bipotentiostat [11].

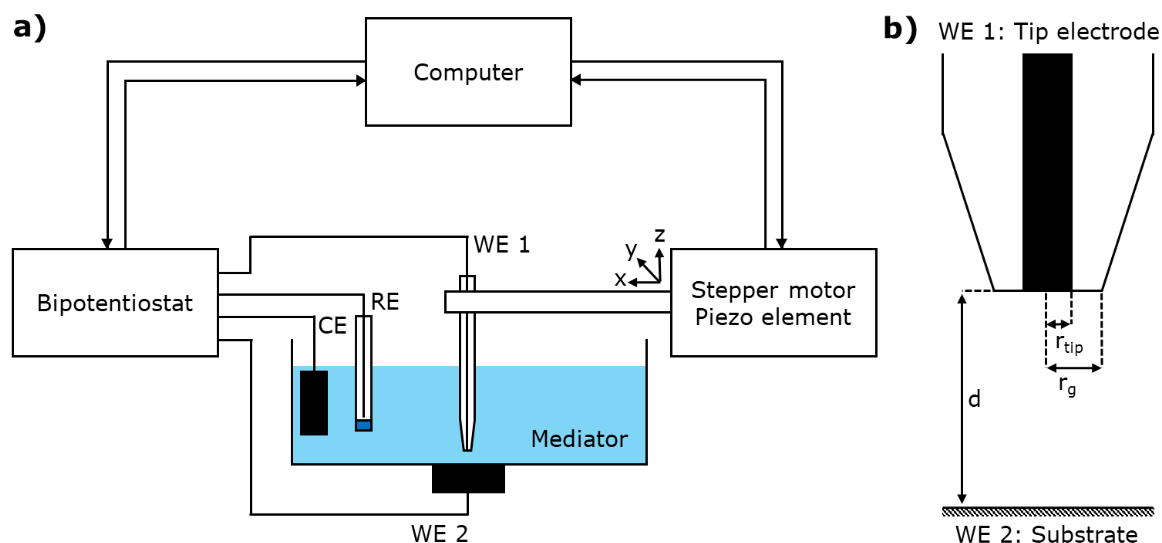

Figure 2.7: (a) Schematic illustration of a scanning electrochemical microscope setup. (b) Geometry of a tip electrode with characterizing parameters: tip radius r_{tip}, radius of insulating mantle r_g and distance between tip and substrate d. Adapted from [12].

The position of the ultramicroelectrode is controlled with a stepper motor for large movements and a piezoelectric motor for very fine movements in three orthogonal directions. Thus, one can approach to the interaction range of the UME in z-direction and scan in the xy-plane for surface imaging. Data acquisition and probe movement is simultaneously controlled by software.

2.2.2 Electrochemical mediators

The choice of the mediator system is strongly dependent on the investigated substrate of interest (redox potential, pH condition, concentration). A mediator is basically characterized by a kinetically rapid one-electron reversible transfer reaction which is selective for the substrate of interest. Consequently, both mediator species, the reduced form R and an oxidized form O, have to be stable in solution. The solvent is usually water but other organic solvents like acetonitrile can also be used. In order to prevent the influence of dissolved oxygen on measurement results at the electrodes, the mediator solution is usually deaerated before measurement [11]. In this study, ferrocenemethanol (FcMeOH), hexamineruthenium (III) chloride

($Ru(NH_3)_6Cl_3$) and potassium octacyanotungstate (IV) dihydrate ($K_4W(CN)_8{\cdot}2H_2O$) were used for surface characterization with SECM. Their half-cell reaction is depicted in table 2.2.

Table 2.2: Half-cell reaction of selected mediators. Adapted from [11].

Mediator	Half cell reaction	Standard potential (vs. NHE)
Octacyanotungstate (IV) dihydrate	$[W(CN)_8]^{4-/3-}$	0.49 V
Ferrocenemethanol (FcMeOH)	$[C_{11}H_{12}FeO]^{0/1+}$	0.44 V
Hexaamineruthenium (III) chloride	$[Ru(NH_3)_6]^{2+/3+}$	0.05 V

2.2.3 Working modes in scanning electrochemical microscopy

In this chapter the basic working modes of SECM are covered. Since the presented studies are based on amperometric methods, a short overview of the major amperometric SECM techniques will be provided: the feedback mode, the generation/collection modes and the competition mode. The choice of working mode is usually strongly dependent on the field of application. These working modes of SECM can be utilized for the characterization of surface reactivity of solid-state materials, electrocatalytic materials and enzyme activity in biochemistry [13].

2.2.3.1 Feedback mode

The feedback mode is the most commonly used working mode in SECM. This mode can be utilized in either a four-electrode or a three-electrode configuration in the case where biasing of the substrate at a fixed potential is not necessary. This technique allows for the precise positioning of the tip at a defined distance with respect to the substrate. The UME is set on a fixed potential E where the reactive species of the mediator is oxidized or reduced. As already shown in chapter 2.1.3.2, the electrochemical conversion at the UME tip is mass transport limited. Thus, the steady-state current in the bulk solution $I_{T,\infty}$ can be measured at the electrode tip according to eq. 17. Approaching the UME towards a substrate will result in a change of the measured tip current I_T. In order to be able to compare the results of UME with different sizes, I_T is normalized to $I_{T,\infty}$ and the tip-to-substrate distance d is normalized to r_{tip}.

$$I_L = \frac{I_T}{I_{T,\infty}} \tag{19}$$

$$L = \frac{d}{r_{tip}} \tag{20}$$

In feedback mode, there are two limiting cases dependent on the surface conductivity. If the tip is approached towards an insulating surface (e.g. PTFE or glass) the diffusion of the reactive species towards the UME is blocked by the substrate, resulting in a decrease in measured current $I_T < I_{T,\infty}$. The measured current reaches $I_T = 0$ as the tip-to-substrate distance d reaches d = 0. This effect of current decrease is called a negative feedback. If the tip approaches a conductive surface (e.g. platinum or gold) the tip-generated species is regenerated at the substrate and diffuses back to the UME. As a result, the measured current will increase $I_T > I_{T,\infty}$ due to an increase of the reactive species at the UME. The current can reach large values as the tip-to-substrate distance moves toward zero. The effect of current increase is called a positive feedback. Feedback is strongly dependent on r_{tip} and and r_g due to additional flux of mediator from the backside of the electrode. Accordingly, the influence of the RG-value on feedback has to be taken into account. Thus, the normalized tip current response for negative feedback I_L^{ins} and positive feedback I_L^C can be described in dependence of L and RG for a diffusion controlled reaction according to [14,15]. Since these analytical equations can be correlated with experimental approach curves, UME characterization (r_{tip}, r_g) in a known mediator solution is possible.

$$I_L^{ins}(L, RG) = \frac{\frac{2.08}{RG^{0.358}} \cdot \left(L - \frac{0.145}{RG}\right) + 1.585}{\frac{2.08}{RG^{0.358}} \cdot (L + 0.0023 \cdot RG) + 1.57 + \frac{\ln(RG)}{L} + \frac{2}{\pi \cdot RG} \cdot \ln\left(1 + \frac{\pi \cdot RG}{2 \cdot L}\right)} \tag{21}$$

$$I_L^C(L, RG) = \alpha + \frac{\pi}{4 \cdot \beta \cdot \arctan(L)} + \left(1 - \alpha - \frac{1}{2 \cdot \beta}\right) \cdot \frac{2}{\pi} \cdot \arctan(L) \tag{22}$$

with α and β in dependence of RG:

$$\alpha(\mathrm{RG}) = \ln(2) + \ln(2) \cdot \left(1 - \frac{2}{\pi} \cdot \arccos\left(\frac{1}{\mathrm{RG}}\right)\right) - \ln(2) \cdot \left(1 - \left(\frac{2}{\pi} \cdot \arccos\left(\frac{1}{\mathrm{RG}}\right)\right)^2\right) \tag{23}$$

$$\beta(\mathrm{RG}) = 1 + 0.639 \cdot \left(1 - \frac{2}{\pi} \cdot \arccos\left(\frac{1}{\mathrm{RG}}\right)\right) - 0.186 \cdot \left(1 - \left(\frac{2}{\pi} \cdot \arccos\left(\frac{1}{\mathrm{RG}}\right)\right)^2\right) \tag{24}$$

For positive feedback a simplified approximation can be used as feedback is less influenced by mediator flux from the backside of the UME. The accuracy of I_L^C fits within 1% for $1.1 \leq \mathrm{RG} \leq 10$ [16].

$$I_L^C(L, \mathrm{RG}) = A + \frac{B}{L} + C \cdot \exp\left(\frac{D}{L}\right) \tag{25}$$

The empirical parameters A, B, C, and D in dependence of the RG-value are depicted in table 2.3.

Table 2.3: Parameter values for eq. 25, adapted from [16].

RG	A	B	C	D
1.1	0.5882629	0.6007009	0.3872741	-0.869822
1.5	0.6368360	0.6677381	0.3581836	-1.496865
2.0	0.6686604	0.6973984	0.3218171	-1.744691
5.1	0.72035	0.75128	0.26651	-1.62091
10	0.7449932	0.7582943	0.2353042	-1.683087

A schematic illustration of the feedback modes with the corresponding tip reactions is depicted in Fig. 2.8. The approach curves were recorded in 1.5 mM FcMeOH and 0.2 M KNO_3 with an UME of r_{tip} = 13µm (RG > 10) towards insulating glass (red) and conductive platinum (blue) as substrate. The measured data are fitted with eq. 21 for negative feedback and eq. 25 for positive feedback.

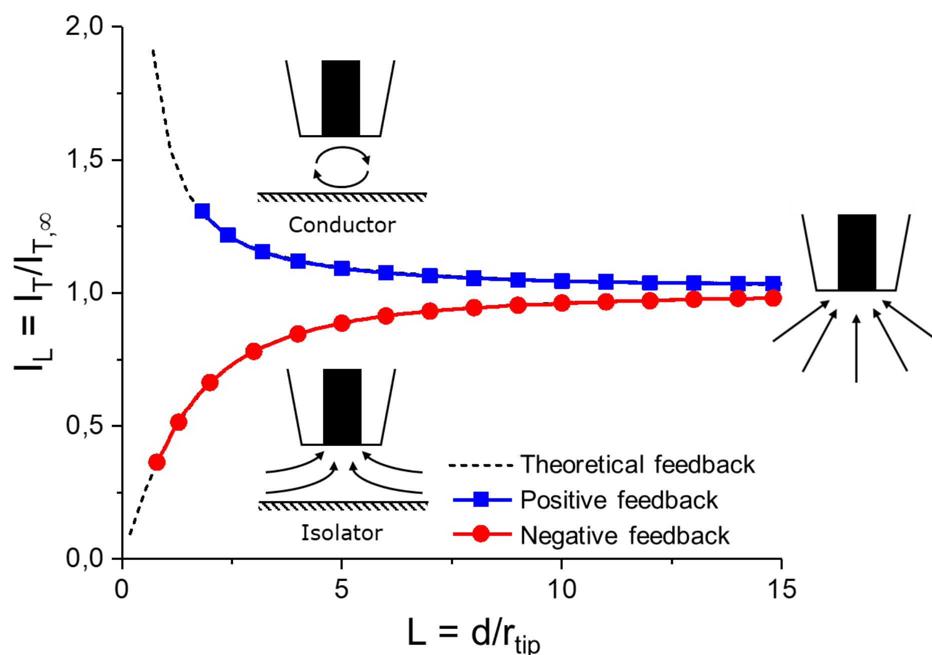

Figure 2.8: Schematic representation of feedback. Steady state current far away from surface due to spherical diffusion at normalized distance L = 15. Positive feedback (blue) in close proximity to a conductive surface due to regeneration of tip-generated species. Negative feedback (red) near insulating surface due to blockage of diffusion. Experimental conditions: 1.5 mM FcMeOH/0.2 M KNO_3 at E_{tip} = 0.4 V with an UME of r_{tip} = 13 µm (RG = 10). Adapted from [17].

2.2.3.2 Generation/Collection modes and Competition mode

In contrast to feedback mode, four electrodes are required for this technique with the UME placed in interaction proximity of the substrate electrode. In the generation/collection modes the electroactive species is in situ generated at one of these electrodes and is collected at the other electrode after diffusion through the tip-substrate-gap. Since both, the substrate and the UME can act as the generator or the collector electrode, two generation/collection modes are existing. In the first case, the substrate is used as the generator electrode and the tip as the collector electrode (SG/TC mode) as illustrated in Fig. 2.9 a). In this technique, the resolution as well as the screening area are limited due to the increasing background current over measurement time by the continuous formation of the active species at the substrate electrode. In the second case the tip is used to generate the active species and the substrate electrode for

collection of this species (TG/SC mode) as depicted in Fig. 2.9 b). The advantage of TG/SC is its small background signal due to the local generation of the active species at the UME tip. Therefore, TG/SC mode is only suited for small substrates since its sensitivity decreases with substrate electrode area [18].

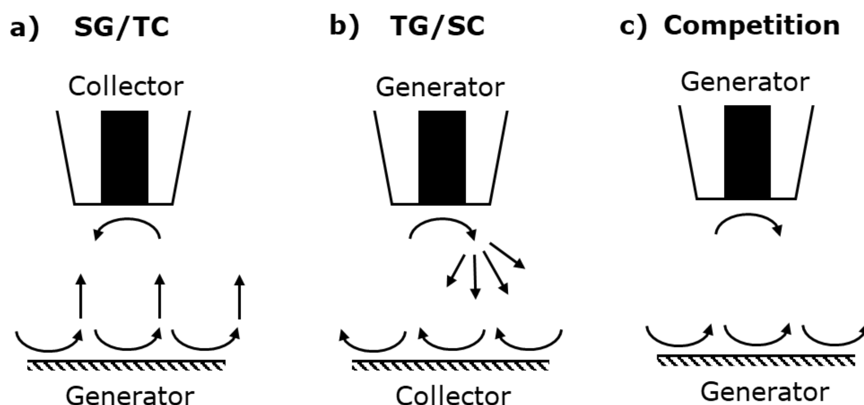

Figure 2.9: Schematic representation of different generation modes. a) Substrate generation/tip collection mode (SG/TC mode), b) tip generation/substrate collection mode (TG/SC mode) and c) both electrodes as generation electrodes (Competition mode).

The collection efficiency η for the generation/collection modes can be quantified by calculating the current ratio between the substrate current I_S and the tip current I_T.

$$\eta = \frac{I_S}{I_T} \tag{26}$$

The efficiency is strongly dependent on the tip-to-substrate distance and is usually approximately $\eta \approx 1$ for TG/SC mode and $\eta \ll 1$ for SG/TC mode. Both modes are applicable methods for studying electrocatalysts, for example in the field of hydrogen evolution reaction (HER) or in oxygen evolution reaction processes [19]. In contrast to the generation/collection modes, substrate and tip electrode are both used as generator electrodes in the competition mode as it can be seen in Fig 2.9 c). Since both electrodes are competing for the same species, the decrease in measured tip current represents the local catalytic activity of the substrate surface. Thus, the sensitivity is not affected by the substrate area in

competition mode in contrast to the TG/SC mode. As a consequence, the resolution can be further increased in competition mode by the usage of smaller UMEs [20].

2.2.4 Imaging process

Imaging describes the process in which the surface is scanned by the tip in the XY plane. Thus, local information about the electrochemical activity and topography of the substrate can be obtained due to surface interaction of the tip in the scanning process. The resolution is dependent on r_{tip}, RG-value, scan speed, and the tip-to-substrate distance. Accordingly, the tip must be brought into working distance before the imaging process [17]. This can be achieved by approaching the UME in feedback mode in a defined mediator solution as described in chapter 2.2.3.1. Two common imaging modes are applicable as it can be seen in Fig 2.10.

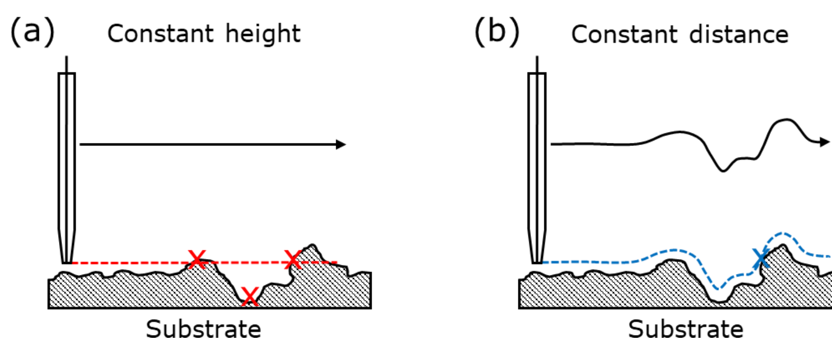

Figure 2.10: Schematic illustration of imaging modes. (a) Constant height and (b) constant distance. Adapted from [21].

In constant height mode the UME is scanned in XY plane at a fixed distance L between tip and substrate. This mode is commonly used for substrates with smooth surfaces and can be utilized in feedback, SG/TC, TG/SC, and competition mode. When scanning in fixed L, problems can arise with surface topography. If the roughness is too large, it is possible that the tip crashes into the substrate at topographic hills or that the surface interaction is lost in topographic valleys (see red crosses in Fig. 2.10). In constant distance mode, the gap between tip and substrate is kept at a constant level by adjusting the z-position of the tip in dependence of the measured tip signal [22]. This mode is limited by the response speed of the distance

control mechanism at strong changes in topography. Since the measured signal in SECM is strongly dependent on the distance between tip and substrate in both modes, local information on topography and electrochemical activity cannot be obtained independently in the imaging process. Accordingly, surface topography can only be obtained in pure negative or pure positive feedback from homogenous materials.

2.3 Electrochemical deposition of copper

2.3.1 Electroplating of copper in semiconductor industry

Electroplating of copper (Cu) was introduced in the semiconductor industry by IBM in 1997 due to good electrical and thermal conductivity as well as the higher resistance to electromigration of copper in comparison to aluminum (Al) [23]. Electrochemical Cu deposition is usually carried out from an acidic Cu electrolyte on a Cu seedlayer (PVD) deposited prior to electroplating.

2.3.1.1 Copper electrolyte

A conventional acidic bath contains inorganic and organic compounds for void free filling of structured surfaces. The inorganic compounds consist of copper(II) sulfate ($CuSO_4$) as Cu source with $c(Cu^{2+}) > 10$ g/l, sulfuric acid (H_2SO_4) for conductivity increment of the solution and to prevent the precipitation of the Cu salt. Further, small amounts of hydrochloric acid (HCl) ($c(Cl^-) < 100$ ppm) are needed to ensure the surface interaction of the organic compounds during the electrochemical deposition process. The organic bath compounds consist usually of three additives which are selectively influencing Cu deposition. The first organic component, the accelerator, is locally enhancing Cu electrodeposition due to its capability to reduce surface potential and to facilitate ion transfer to the surface. Molecules with a thiol-group, for example sulfopropyl-disulfide (SPS) can be used as accelerator. The second organic component, the suppressor, inhibits the Cu deposition locally by the formation of a stable complex with Cu(I) ions and Cl ions at the Cu surface such as polyethylenglycol (PEG). The third organic component, the leveler, facilitates selective filling of trenches and vias due to the accumulation of this additive on edges and corners with high electric field strength. Thus, the local difference between recessed areas and bumps can be balanced.

Usually coloring agents are used as leveler additives, for example Janus Green B (JGB) or polyvinylpyrrolidone (PVP) [24]. Via a suitable concentration ratio of these three additives, it is possible to achieve homogeneous galvanic copper deposition on wafer level scale.

2.3.1.2 Electroplating tool

Electrodeposition from this Cu electrolyte is performed in a two-electrode setup with the structured wafer as cathode and solid copper as anode material. A schematic illustration of a commercial plating tool is depicted in Fig. 2.11.

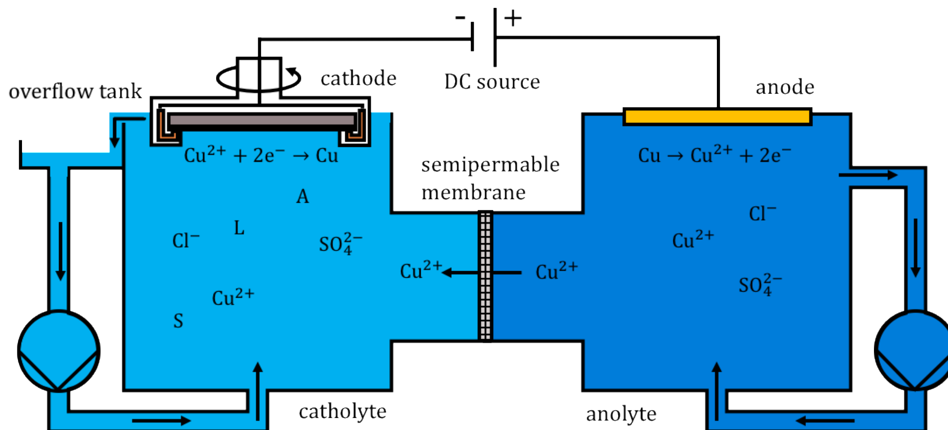

Figure 2.11: Schematic illustration of a commercial plating tool in semiconductor industry. The electrolyte tank is separated in two compartments by a semipermeable membrane. The electrolytes in both chambers are continuously circulated. The anode chamber contains the anode and the anolyte ($CuSO_4$, H_2SO_4, HCl). The cathode chamber is constructed as an overflow tank and includes the rotatable mounting platform for the wafer as well as the catholyte ($CuSO_4$, H_2SO_4, HCl, leveler L, accelerator A, suppressor S).

In order to be able to act as the cathode, the Cu seedlayer on the wafer is electrically contacted and sealed from the edges in a mounting platform prior to immersion in the overflow tank. To stabilize the Cu bath, the interaction of the inorganic compounds with the Cu anode is prevented (US6126798A, [25]). Therefore, the electrolyte tank is divided into two separate individually circulated compartments by a semipermeable membrane. Thus, the cathode chamber contains the catholyte with the inorganic and organic compounds of the electrolyte and the anode chamber includes the anolyte with only the inorganic compounds. The

concentration of Cu in the catholyte is maintained by the diffusion of Cu ions from the anolyte to the catholyte due to the concentration gradient during deposition according to eq. 27 and eq. 28. In order to simulate this wafer scaled deposition process on the laboratory level, a dedicated miniaturized plating cell is utilized for the experimental studies as described in chapter 4.1.

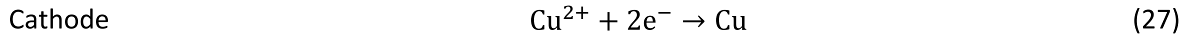

Cathode $$Cu^{2+} + 2e^{-} \rightarrow Cu \tag{27}$$

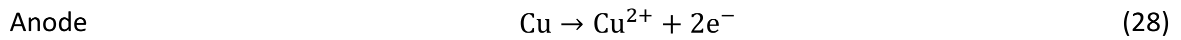

Anode $$Cu \rightarrow Cu^{2+} + 2e^{-} \tag{28}$$

2.3.1.3 Deposition rate of galvanic copper

The galvanic deposition process is carried out in direct current or in a pulsed technique at a predefined deposition rate [24]. This deposition rate is based on Faraday's laws of electrolysis which describe the relationship between flowed charge Q, the valency number of ions z, the Faraday constant F and the amount of substance n. Here, n can be expressed as a function of mass m and molar mass M as depicted in eq. 29.

$$Q = n \cdot z \cdot F = \frac{m}{M} \cdot z \cdot F \tag{29}$$

Utilizing the relationship between Q, the applied current I and the deposition time t in eq. 30, Faraday's law can be expressed as a function of flowed current.

$$Q = I \cdot t \tag{30}$$

Furthermore, implementing the correlation between m, density ρ_D, and volume V, which is the product of deposited area A_{Dep} and thickness d as described by eq. 31, the deposition rate d/t can be expressed as a function of the above-mentioned variables by assuming 100% current efficiency (32):

$$m = \rho \cdot V = \rho \cdot A_{Dep} \cdot d \tag{31}$$

$$\frac{d}{t} = \frac{M}{\rho \cdot z \cdot F} \cdot \frac{I}{A_{Dep}} = const \cdot \frac{I}{A_{Dep}} = const \cdot j \tag{32}$$

As can be seen in eq. 32, d/t is only dependent on the ratio of I and A_{Dep} and therefore on current density j. Consequently, the deposition rate can be adjusted by changing the applied current density in the galvanic Cu deposition process.

2.3.2 Barrier films for copper

Since Al was replaced by Cu metallization as interconnect material [23], barrier films (also referred as liner materials) became mandatory to prevent the diffusion of Cu ($D_{Cu} = 3 \cdot 10^4\, m^2/s$, [26]) into the surrounding dielectrics and Si. It is known that Cu has a strong impact on the function of active elements due to their capability to form silicides like Cu_3Si or deep trap states on the basis of agglomeration. For this reason, the complete encapsulation of Cu structures in a barrier material is necessary. Moreover, these barrier layers have to fulfill several further requirements such as sufficient mechanical stability, good adhesion between dielectric and interconnect, immiscibility with Cu, and the capability to act as etch-stop on top of interconnects. There are a variety of different deposition techniques to achieve the full embedment of Cu in liner materials. Commonly used techniques are physical vapor deposition (PVD) for bottom and side walls, atomic layer deposition (ALD) for conformal deposition in high aspect ratios, chemical vapor deposition (CVD) for contact level, and plasma enhanced chemical vapor deposition (PECVD) for coverage of the top of the interconnects [26]. A schematic cross section of a Cu interconnect with the corresponding barriers films is depicted in Fig. 2.12.

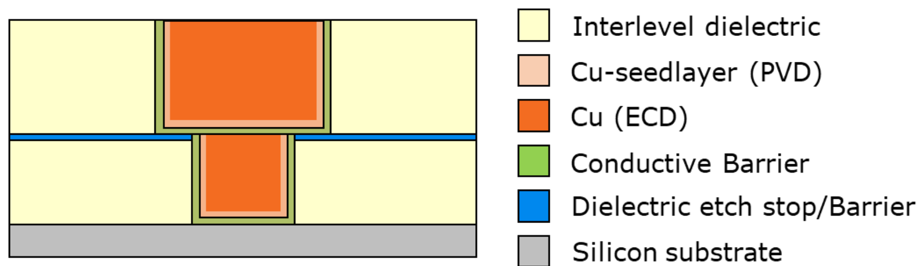

Figure 2.12: Schematic Cu interconnect encapsulated in a barrier thin film surrounded by dielectric material (single damascene process, after subsequent planarization process). Adapted from [26].

The suitability of a material for acting as a liner is given by an empirical rule. This rule states that the activation energy for the diffusion process (mainly grain boundary diffusion) scales with the material melting temperature T_M. Consequently, the property to effectively inhibit diffusion of Cu is given by a high melting point of the material. Therefore, refractory metals with T_M > 2000°C such as Cr, Ti, Mo, W, Ta, Nb as well as their thermodynamically stable compounds are suitable liner candidates. A compilation of common metal-based (Me-X) barrier materials is shown below [26]:

1. Polycrystalline and amorphous Me-N, Me-C, Me-O, Me-B compounds:
   TiN_x, VN_x, ZrN_x, NbN_x, MoN_x, HfN_x, WN_x, TaN_x, WC_x, TaC_x, MoO_x, TaO_x, TiB_2
2. Polycrystalline and amorphous Me-Si compounds:
   $MoSi_x$, WSi_x, $TaSi_x$
3. Polycrystalline and amorphous Me alloys:
   TiW_x, $TaCo_x$, $TaFe_x$, TaW_x, $NiNb_x$, $CuZr_x$

In industrial applications Ta-based, W-based and Ti-based barrier materials are commonly used since they can be deposited by PVD in combination with a Cu seedlayer without breaking the vacuum in order to avoid liner oxidation. The copper interconnect is subsequently enhanced by an electrochemical deposition process of copper from an acidic electrolyte with additives enabling large scale homogenous deposition as described in chapter 2.3.1.

2.3.3 Nucleation process

In this chapter a more detailed description of the nucleation process will be given. Atomistic and thermodynamic models will not be presented as their prediction differs strongly from experimental observations in electrochemical nucleation studies due to the simplified assumptions in the calculation process [27].

2.3.3.1 Definition

Nucleation is defined as the formation of a new crystalline phase from a solution or gas phase. In this process, the molecules and/or atoms are organizing themselves in a thermodynamic stable accumulation phase which can subsequently grow irreversibly into a macroscopic structure. This accumulation phase is defined as nucleus or critical nuclei. The nucleus formation process can be categorized into primary nucleation and secondary nucleation. Primary nucleation refers to the formation process wherein either no crystal (homogeneous nucleation) or a foreign crystal or particle (heterogeneous nucleation) is involved. Consequently, nucleus formation on the crystal of the same substance is denoted as secondary nucleation [28,29].

2.3.3.2 Electrochemical nucleation

Electrochemical nucleation belongs to the category of primary heterogeneous nucleation or secondary nucleation in the case of a type-identical substrate. Since the electrochemical nucleation is based on the conversion of an electroactive species, the nucleation process can be monitored directly by the faradaic current I_F (chapter 2.1.1). As a result, insight into the nucleation and growth process can be obtained by comparing the in situ measured data to theoretical models. These models are based on the description of the kinetics of adatom incorporation on nucleation centers in the early stage of electrocrystallization [30]. The number of nucleation centers N depends on the active sites N_0 of the substrate, the nucleation rate constant A’, and deposition time t.

$$N(t) = N_0 \cdot [1 - \exp(-A' \cdot t)] \tag{33}$$

Based on the equation, electrochemical nucleation can be divided into two limiting cases [10]. If the product in the exponential term is much larger than 1, eq. 33 can be simplified to eq. 34.

$$\text{For } A' \cdot t \gg 1 \qquad N(t) = N_0 \tag{34}$$

This limiting case is called instantaneous nucleation. Accordingly, all nuclei are initially formed at the start of the deposition process. The nuclei are subsequently growing equally with increasing deposition time until coalescence. On the other hand, if the product is much smaller than 1, eq. 33 becomes eq. 35.

$$\text{For } A' \cdot t \ll 1 \qquad N(t) = N_0 \cdot (A' \cdot t) \tag{35}$$

This limiting case is called progressive nucleation. In contrast to instantaneous nucleation, the formation of nucleation centers is continuous with each nucleus growing at an individual rate until all active sites N_0 are depleted [31]. Based on these two nucleation types, different theoretical models were developed to describe the early stage of potential-controlled electrocrystallization as depicted in table 2.4 with the cross-section L^2, coverage θ, and nuclei height h [32]. Consequently, insight in the nucleation process can be obtained by comparing these theoretical models with measured current density transients during potentiostatic deposition.

Table 2.4: Theoretical models for potentiostatic electrocrystallization. Adapted from [32].

Expression	Nucleation type	Growth type	Reaction regime
$j = 2 \cdot z \cdot F \cdot A \cdot L^2 \cdot k \cdot t$	progressive	1D needle	kinetic
$j = (z \cdot F \cdot h \cdot \rho \cdot \pi \cdot \theta^2 \cdot D \cdot A \cdot t)/M$	progressive	2D	diffusion
$j = (2 \cdot z \cdot F \cdot \pi \cdot M \cdot h \cdot N_0 \cdot k^2 \cdot t)/\rho$	instantaneous	2D	kinetic
$j = (z \cdot F \cdot \pi \cdot M \cdot h \cdot A \cdot k^2 \cdot t^2)/\rho$	progressive	2D	kinetic
$j = 2 \cdot z \cdot F \cdot \pi \cdot M^2 \cdot N_0 \cdot k^3 \cdot t^2 \cdot \rho^2$	instantaneous	3D	kinetic
$j = (2 \cdot z \cdot F \cdot \pi \cdot M^2 \cdot h \cdot A \cdot k^3 \cdot t^3)/3/\rho^2$	progressive	3D	kinetic
$j = \left(8 \cdot z \cdot F \cdot N_0 \cdot M^2 \cdot c^3 \cdot D^{3/2} \cdot t^{1/2}\right)/\rho^2$	instantaneous	3D	diffusion
$j = \left(16 \cdot z \cdot F \cdot \pi \cdot A \cdot M^2 \cdot c^3 \cdot D^{3/2} \cdot t^{3/2}\right)/3/\rho^2$	progressive	3D	diffusion

In order to determine the nucleation type without the knowledge of the elusive factor N_0, Scharifker and Hills [33] have developed simplified expressions for this purpose. They are based on diffusion-controlled 3D instantaneous (eq. 36) and progressive nucleation (eq. 37) models, which are considering the overlap of hemispherical diffusion fields during growth and the consequential inhibition of nuclei formation.

$$I(t) = \frac{z \cdot F \cdot D^{1/2} \cdot c}{\pi^{1/2} \cdot t^{1/2}} \cdot \left\{1 - \exp\left[-N_0 \cdot D \cdot t \cdot \left(\frac{8 \cdot \pi \cdot c \cdot M}{\rho}\right)^{1/2}\right]\right\} \quad (36)$$

$$I(t) = \frac{z \cdot F \cdot D^{1/2} \cdot c}{\pi^{1/2} \cdot t^{1/2}} \cdot \left\{1 - \exp\left[-\frac{2}{3} \cdot A \cdot N_0 \cdot \pi \cdot D \cdot t^2 \cdot \left(\frac{8 \cdot \pi \cdot c \cdot M}{\rho}\right)^{1/2}\right]\right\} \quad (37)$$

Normalizing eq. 36 and eq. 37 to the peak current I_{max} and the corresponding time t_{max} results in expressions which are free of N_0 and other constants for instantaneous nucleation (eq. 38) and progressive nucleation (eq. 39) [33].

$$\frac{I^2}{I_{max}^2} = 1.9542 \cdot \left(\frac{t_{max}}{t}\right) \cdot \left[1 - \exp\left(-1.2564 \cdot \frac{t}{t_{max}}\right)\right]^2 \tag{38}$$

$$\frac{I^2}{I_{max}^2} = 1.2254 \cdot \left(\frac{t_{max}}{t}\right) \cdot \left[1 - \exp\left(-2.3367 \cdot \frac{t}{t_{max}}\right)\right]^2 \tag{39}$$

Consequently, the classification of the nucleation type can simply be accomplished by comparing the normalized measured current transients with the previously described expressions. In contrast to that, determination of nucleation type in galvanic deposition is rather complicated. Here, ex situ techniques must be used such as a SEM or AFM based surface characterization methods at defined deposition times [34].

2.3.4 Electrochemical deposition of copper on barrier films

In the process of downscaling device geometry to the sub 30 nm node technology, the filling of nanoscale damascene structures is becoming increasingly difficult. As feature dimensions are comparable with the thickness, a defect-free filling and conformal coating is challenging using conventional deposition methods [35,36]. Consequently, new deposition techniques are investigated to address this topic. A promising approach is the electrochemical deposition of copper on the liner material without using a Cu seedlayer. This strategy is also referred to as direct electroplating, direct electrodeposition or seedless electrodeposition [37]. For defect-free filling of trench structures in direct plating the empirical correlation between the film coalescence at a predefined layer thickness d_{coal} and the nuclei density N_d has to be fulfilled as depicted in eq. 40 [38].

$$d_{coal} = \frac{1}{2\sqrt{N_d}} \quad (40)$$

Therefore, a high initial nucleus density is a prerequisite for the conformal filling of nm-scaled structures. If a conventional acidic electrolyte (chapter 2.3.1) is utilized for direct deposition, the formation of a surface passivation on the liner material in aqueous solution has to be considered. These metal oxides Me-O have a negative influence on nucleation and can completely prevent electrochemical deposition if an insulating layer is formed [35]. Consequently, liner materials which form more unstable oxides than those of Cu should be selected for electroplating with acidic electrolytes. Based on a comparison of Gibbs free energy of formation per nonmetal of the metal oxide ΔG^{a}_{Me-O} and those of Cu ΔG^{a}_{Cu-O} as a criteria (eq. 41), a selection of suitable barriers can be made [39].

$$|\Delta G^{a}_{Me-O}| \leq |\Delta G^{a}_{Cu-O}| \quad (41)$$

Accordingly, the platinum-group metals (PGM) Pt, Pd, Ru, Ir and the metals Rh, Te, Tc, Ag are suitable liners for direct deposition in combination with a standard acidic electrolytes [40]. Alternatively, the bath chemistry and process handling can be modified, if other liner materials (chapter 2.3.2) are utilized for direct plating [37]. Both approaches in direct electrodeposition have been investigated by different working groups since 1995. An overview of the literature sources on direct plating sorted by barrier groups is shown in table 2.5. A detailed description of the procedures is presented in the following chapters based on the associated groups.

Table 2.5: Overview of literature on direct plating of Cu sorted by barrier material

group	barrier material	references
Ti-based	Ti	[42, 45-48]
	TiN	[43,44,49,50-52]
W-based	W	[56-58]
	W_2N	[55]
Ta-based	Ta	[38,59,63-65]
	TaN	[38, 59-62]
PGM-based	Ru	[71-79]
	Ru:Ta(N)	[35, 80-84]
	Ir	[70]
	Os	[34]

2.3.4.1 Titanium-based barrier materials

It is known that Ti based barriers, such as Ti or TiN, are forming a semiconductive oxide TiO_2 in ambient air and also in aqueous solution [41]. Electron transport through TiO_2 is based on pipe tunneling along dislocation cores during electrochemical deposition. Consequently, poor surface coverage and bad adhesion is obtained due to the poor nucleation and the favored grain growth in the plating process on TiO_2 [42–44]. For this reason, it is important to remove the natively formed oxide to achieve a dense Cu deposition with strong adhesion [45]. Here, different methods are known to remove oxide for Ti and TiN. In the case of a Ti barrier, the oxide can simply be removed with a pre-cleaning step in diluted HNO_3 or 1% HF solution [42,46,47]. Afterwards, a standard acidic Cu electrolyte or a complexed Cu electrolyte can be used [48] for the electrochemical deposition. The utilization of a complexed Cu electrolyte is advantageous for thin-film applications due to its large nucleation density in the early stages of deposition according to eq. 40. The electrocrystallization process from complexed Cu baths is characterized by an enhanced nucleation process since grain growth is inhibited due to the blockage of active sites by complexing agents like EDTA or citric acid [45–47]. In contrast to the procedure for Ti interfaces, the TiO_2 removal and electrochemical Cu deposition on TiN can only be carried out by proper plating chemistry and deposition parameters [49–51]. Since TiO_2 is unstable below pH = 8 and potentials lower than E = -1.8 V vs SHE [41],

the reduction to metallic Ti during electrodeposition is possible in complexed Cu electrolytes. These baths usually consist of a significant fraction of citric acid [49–51] or pyrophosphate [52] which leads to the shift of the onset point of Cu reduction towards more negative potentials due to the complexation of Cu ions. The composition of such a complexed Cu bath is shown in table 2.6. The usage of these complexed Cu electrolytes is also suitable for deposition of adherent Cu layer on untreated Ti [46,47].

Table 2.6 Complexed Cu electrolytes for direct electroplating on TiN barriers with references

Components	Molar ratio	pH value	Complexed Copper	Reference
$CuSO_4*5H_2O$, $(NH_4)_2C_6H_7O_7$	1:1	pH = 3.5 to 6.0	copper citrate	[49–51]
$Cu_2P_2O_7$, $K_4P_2O_7$	1:10	pH = 8.5	copper pyrophosphate	[52]

2.3.4.2 Tungsten-based barrier materials

For the deposition of adherent and dense Cu layers on W barriers it is crucial to remove the natively formed oxides of WO_2, WO_3 or W_2O_5 in aqueous solution [41,53,54]. Since WO_2 and W_2O_5 will not be formed under cathodic potentials for pH > 5 and WO_3 being thermodynamically unstable at pH > 4 according to eq. 42, the deposition of Cu on oxide free W can be achieved with a proper bath chemistry.

$$WO_3 + 2OH^- \rightleftharpoons WO_4^{2-} + H_2O \quad (42)$$

Accordingly, a suitable Cu electrolyte for direct electroplating on W must have a pH > 4, contain a source for the generation of OH^- and a complexing agent for Cu ions to prevent Cu precipitation at this pH value. An electrolyte consisting of copper sulfate $CuSO_4$, ammonium citrate $(NH_4)_2HC_6H_5O_7$ and ammonia NH_3 with a molar ratio of $CuSO_4 : (NH_4)_2HC_6H_5O_7 = 1 : 1$ is able to fulfill these requirements. Here, $CuSO_4$ is used as Cu source, $(NH_4)_2HC_6H_5O_7$ is utilized as complexing agent and NH_3 is used to generate OH^- according to eq. 43 and to adjust the pH value.

$$NH_3 + H_2O \rightarrow NH_4^+ + OH^- \quad (43)$$

Using such a bath composition, it is possible to electrochemically deposit Cu with a high nucleation density of $N = 2.0 \cdot 10^{10} \frac{N}{cm^2}$ and good adhesion on W under potential control in comparison to standard acidic Cu baths [55–57]. Moreover, organic bath additives can be used in order to further increase nuclei density and decrease surface roughness [58].

2.3.4.3 Tantalum-based barrier materials

Ta is known for its fast formation of native oxides in ambient air on pure Ta and TaN with the stoichiometry of TaO, TaO_2, Ta_2O_5 and Ta_2O_7. In aqueous solution, only Ta_2O_5 is stable without any dependency on pH value [41]. Accordingly, Ta_2O_5 is the reason for the low adhesion, poor nucleation and inhomogeneity of electroplated Cu on Ta and TaN [38,59,60]. As a result, a pre-cleaning step is required for direct plating. Here, two methods are applicable for oxide removal on Ta-based surfaces. The first method is based on an anodic pre-cleaning step in alkaline solution. On this occasion, the oxide is stripped in potassium hydroxide solution (0.948 M KOH, pH = 13.51) at a high anodic potential for a very short period of time. Time control in this process is crucial as otherwise the Ta barrier is etched which can result in roughening or barrier removal since the thickness of Ta_2O_5 is only d = 2.5 nm [61–63]. After a wet transfer into the Cu electrolyte, electrodeposition of a Cu layer on metallic Ta can be carried out. The drawback of this method is the emergence of large internal stress, which only allows thin layers with a maximum thickness of d = 150 nm to be deposited without crack formation [59,64]. The second method is based on a cathodic removal of Ta_2O_5 in an alkaline solution. In this process, the native oxide is reduced to metallic Ta in a pyrophosphate solution ($K_4P_2O_7$, pH = 10) at a potential near the onset of hydrogen evolution. In order to prevent the formation of a new native oxide layer in aqueous solution, a part of the Cu electrolyte is added to the pre-cleaning solution before the end of the pre-cleaning step. Thus, a complexed Cu electrolyte is mandatory as otherwise Cu will precipitate from the alkaline solution during this process. Due to the addition of the Cu electrolyte, the formation of a large number of nuclei is triggered which can subsequently grow to a dense thin Cu layer as potential is stepped to a less negative value [64,65]. After this “seeding” process, a wet transfer into a Cu electrolyte can be carried out safely to increase the Cu layer. Furthermore, complexed Cu electrolytes are advantageous for electrochemical thin film deposition

on Ta based barriers due to their high nucleus density during the initial deposition phase in comparison to copper sulfate or copper fluoroborate electrolytes according to eq. 40 [38]. Suitable complexed Cu electrolytes for direct plating on Ta based barriers for the aforementioned methods are listed in table 2.7.

Table 2.7: Complexed Cu electrolytes for direct electroplating on Ta based barriers with references

Components	Molar ratio	pH value	Reference
$CuSO_4*5H_2O$, $(NH_4)_2C_6H_7O_7$	1:1	pH = 2.5 to 13.2	[38,51,61–63,66–68]
$Cu_2P_2O_7$, $K_4P_2O_7$	1:10	pH = 8.5 to 10.1	[64,65]
$CuSO_4*5H_2O$, EDTA	1:2	pH = 9.5 to 13.8	[38]

2.3.4.4 Platinum-group metal barrier materials

Platinum-group metals, also referred to as platinoids, are noble and precious metallic elements, which are resistant to corrosion and cannot be easily attacked by acids [69]. As already explained in this chapter, commercial acidic electrolytes can be utilized for direct deposition [34,70–72]. Especially Ru has shown to be an important candidate for direct plating because of its highly adhesive interface with Cu (good electromigration performance) and low solubility in Cu (low impact on Cu resistivity). Furthermore, Ru can be deposited with CVD and ALD techniques, which allows a conformal coverage of high aspect ratio structures. Thus, very thin films, for example d = 5 nm Ru (ALD) can be used for direct electroplating [73]. Since it is known that Ru forms a conductive oxide RuO in ambient air, a pre-cleaning step has to be carried out prior to deposition to prevent the negative influence of the oxide on the nucleation process and layer adhesion [74]. Moreover, this oxide also inhibits the surface interaction of organic bath additives (PEG, SPS) preventing the defect-free filling of structured surfaces [75,76]. As a result, the electrodeposition of copper on Ru should be carried out in a two-step process. In the first step, the native oxide is removed by reducing the oxide to a metallic surface in an acidic medium of H_2SO_4 or HBF_4 at a cathodic potential or under current control. In the second step the substrate is wet-transferred into the Cu electrolyte for deposition [74,75,77]. This process enables the deposition of very thin Cu layers according to eq. 40 due to the high nucleus density. The nucleus density can be further increased by adding a Fe(II)/Fe(III) redox couple (for example: $Fe(II)SO_4*5H_2O/Fe_2(SO_4)_3$) or conducting salts ($K_2SO_4$, Na_2SO_4, $MgSO_4$) to the acidic Cu electrolyte [78,79]. In the case that the Ru layer should simultaneously act as a diffusion barrier and an electroplatable thin film, a polycrystalline metal alloy like RuTa(10%) [35,80–82] can be used instead. The same two-stage procedure is applicable for this alloy [83,84].

References

[1] J. Barek, J. Zima, Eighty years of polarography-History and future, Electroanalysis. 15 (2003) 467–472. doi:10.1002/elan.200390055.

[2] C.H. Hamann, W. Vielstich, Elektrochemie, Wiley-VCH-Verlag, 1998.

[3] A.J. Bard, L.R. Faulkner, J. Leddy, C.G. Zoski, Electrochemical methods: fundamentals and applications, Wiley New York, 1980.

[4] J. Wang, Analytical electrochemistry, John Wiley & Sons, 2006.

[5] I. Montenegro, M.A. Queirós, J.L. Daschbach, Microelectrodes: theory and applications, Springer Science & Business Media, 2012.

[6] R.G. Compton, C.E. Banks, Understanding voltammetry, World Scientific, 2011.

[7] N. Perez, others, Electrochemistry and corrosion science, Springer, 2004.

[8] A. Bard, Electroanalytical chemistry, Electroanal. Chem. 15 (1966).

[9] C. Lefrou, R. Cornut, Analytical expressions for quantitative scanning electrochemical microscopy (SECM), ChemPhysChem. 11 (2010) 547–556. doi:10.1002/cphc.200900600.

[10] H.R. Thirsk, J.A. Harrison, A guide to the study of electrode kinetics, Academic Press, 1972.

[11] A.J. Bard, F.R.F. Fan, J. Kwak, O. Lev, Scanning electrochemical microscopy. Introduction and principles, Anal. Chem. 61 (1989) 132–138. doi:0003-2700/89/0361-0132$01.50/.

[12] M.V. Mirkin, B.R. Horrocks, Electroanalytical measurements using the scanning electrochemical microscope, Anal. Chim. Acta. 406 (2000) 119–146. doi:10.1016/S0003-2670(99)00630-3.

[13] C.G. Zoski, Review—Advances in Scanning Electrochemical Microscopy (SECM), J. Electrochem. Soc. 163 (2016) H3088–H3100. doi:10.1149/2.0141604jes.

[14] R. Cornut, C. Lefrou, A unified new analytical approximation for negative feedback currents with a microdisk SECM tip, J. Electroanal. Chem. 608 (2007) 59–66. doi:10.1016/j.jelechem.2007.05.007.

[15] R. Cornut, C. Lefrou, New analytical approximation of feedback approach curves with a microdisk SECM tip and irreversible kinetic reaction at the substrate, J. Electroanal. Chem. 621 (2008) 178–

184. doi:10.1016/j.jelechem.2007.09.021.

[16] Y. Shao, M. V. Mirkin, Probing Ion Transfer at the Liquid/Liquid Interface by Scanning Electrochemical Microscopy (SECM), J. Phys. Chem. B. 102 (1998) 9915–9921. doi:10.1021/jp9828282.

[17] A.J. Bard, M. V Mirkin, Scanning electrochemical microscopy, CRC Press, 2012.

[18] P. Bertoncello, Advances on scanning electrochemical microscopy (SECM) for energy, Energy Environ. Sci. 3 (2010) 1620. doi:10.1039/c0ee00046a.

[19] A.R. Kucernak, P.B. Chowdhury, C.P. Wilde, G.H. Kelsall, Y.Y. Zhu, D.E. Williams, Scanning electrochemical microscopy of a fuel-cell electrocatalyst deposited onto highly oriented pyrolytic graphite, Electrochim. Acta. 45 (2000) 4483–4491. doi:10.1016/S0013-4686(00)00504-1.

[20] K. Eckhard, X. Chen, F. Turcu, W. Schuhmann, Redox competition mode of scanning electrochemical microscopy (RC-SECM) for visualisation of local catalytic activity, Phys. Chem. Chem. Phys. 8 (2006) 5359–5365.

[21] S. Bergner, P. Vatsyayan, F.-M. Matysik, Recent advances in high resolution scanning electrochemical microscopy of living cells-a review, Anal. Chim. Acta. 775 (2013) 1–13.

[22] M. Nebel, T. Erichsen, W. Schuhmann, Constant-distance mode SECM as a tool to visualize local electrocatalytic activity of oxygen reduction catalysts, Beilstein J. Nanotechnol. 5 (2014) 141.

[23] P.C. Andricacos, C. Uzoh, J.O. Dukovic, J. Horkans, H. Deligianni, Damascene copper electroplating for chip interconnections, IBM J. Res. Dev. 42 (1998) 567–574.

[24] M. Schlesinger, M. Paunovic, Modern electroplating, John Wiley & Sons, 2011.

[25] J.D. Reid, R.J. Contolini, J.O. Dukovic, Electroplating anode including membrane partition system and method of preventing passivation of same, (2000).

[26] M. Baklanov, P.S. Ho, E. Zschech, Advanced interconnects for ULSI technology, John Wiley & Sons, 2012.

[27] B.R. Scharifker, J. Mostany, Electrochemical nucleation and growth, Encycl. Electrochem. Wiley-VCH Verlag GmbH Co. KGaA, Ger. (2007).

[28] A. Milchev, Electrocrystallization: fundamentals of nucleation and growth, Springer Science & Business Media, 2002.

[29] D. Kashchiev, Nucleation, Elsevier, 2000.

[30] A. Bewick, M. Fleischmann, H.R. Thirsk, Kinetics of the electrocrystallization of thin films of calomel, Trans. Faraday Soc. 58 (1962) 2200–2216.

[31] P. Cubillas, M.W. Anderson, Synthesis mechanism: crystal growth and nucleation, Zeolites Catal. Synth. React. Appl. (2010) 1–55.

[32] M. Sun, T.J.O. Keefe, The Effect of Additives on the Nucleation and Growth of Copper onto Stainless Steel Cathodes, Metall. Trans. B. 23 (1992) 591–599. doi:10.1007/BF02649719.

[33] B. Scharifker, G. Hills, Theoretical and experimental studies of multiple nucleation, Electrochim. Acta. 28 (1983) 879–889. doi:10.1016/0013-4686(83)85163-9.

[34] M. Zheng, M. Willey, A.C. West, Electrochemical Nucleation of Copper on Ruthenium Effect of, PEG, and SPS, Electrochem. Solid-State Lett. 8 (2005) C151--C154.

[35] S. Armini, Z. El-Mekki, M. Nagar, A. Radisic, P.M. Vereecken, Wafer Scale Copper Direct Plating on Thin PVD RuTa Layers: A Route to Enable Filling 30 nm Features and Below?, J. Electrochem. Soc. 161 (2014) D564–D570. doi:10.1149/2.1031410jes.

[36] S. Armini, H. Philipsen, Z. El-Mekki, A. Redolfi, A. Van Ammel, A. Radisic, W. Ruythooren, others, Seedless Copper Electrochemical Deposition on Barrier Materials as a Replacement/Enhancement for PVD Cu Seed Layers in HAR TSVs, in: Meet. Abstr., 2010: p. 1280.

[37] B. Pesic, Copper Electrodeposition on Diffusion Barrier Films- A Literature Review, ECS Trans. 2 (2007) 243–256. doi:10.1149/1.2408879.

[38] A. Radisic, Y. Cao, P. Taephaisitphongse, A.C. West, P.C. Searson, Direct Copper Electrodeposition on TaN Barrier Layers, J. Electrochem. Soc. 150 (2003) C362–C367. doi:10.1149/1.1565137.

[39] M.W. Lane, C.E. Murray, F.R. McFeely, P.M. Vereecken, R. Rosenberg, Liner materials for direct electrodeposition of Cu, Appl. Phys. Lett. 83 (2003) 2330–2332. doi:10.1063/1.1610256.

[40] R.C. Weast, M.J. Astle, W.H. Beyer, others, CRC handbook of chemistry and physics, CRC press Boca Raton, FL, 1988.

[41] M. Pourbaix, Atlas of electrochemical equilibria in aqueous solution, NACE. 307 (1974).

[42] H.K. Chang, B.-H. Choe, J.K. Lee, Influence of titanium oxide films on copper nucleation during electrodeposition, Mater. Sci. Eng. A. 409 (2005) 317–328.

[43] L. Magagnin, A. Vicenzo, M. Bain, H.W. Toh, H.S. Gamble, P.L. Cavallotti, Nucleation and growth of ECD Cu on PVD TiN from low acid sulfate electrolyte, Microelectron. Eng. 76 (2004) 131–136. doi:10.1016/j.mee.2004.07.006.

[44] L. Graham, C. Steinbrüchel, D.J. Duquette, Nucleation and Growth of Electrochemically Deposited Copper on TiN and Copper from a Cu NH 3 Bath, J. Electrochem. Soc. 149 (2002) C390–C395. doi:10.1149/1.1487836.

[45] H. Natter, R. Hempelmann, Nanocrystalline copper by pulsed electrodeposition: The effects of organic additives, bath temperature, and pH, J. Phys. Chem. 100 (1996) 19525–19532. doi:10.1021/jp9617837.

[46] B. Im, S. Kim, Surface Morphology Evolution of Cu Thin Films Electrodeposited Directly on Ti Diffusion Barrier in Citric Acid, J. Electrochem. Soc. 162 (2015) D491–D496. doi:10.1149/2.0091510jes.

[47] B. Im, S. Kim, Influence of additives on Cu thin films electrodeposited directly on Ti diffusion barrier in Cl--free electrolytes for Cu interconnect, Microelectron. Eng. 172 (2017) 8–12.

[48] A.J.B. Dutra, T.J. O'Keefe, Copper nucleation on titanium for thin film applications, J. Appl. Electrochem. 29 (1999) 1217–1227. doi:10.1023/A:1003537318303.

[49] S. Kim, D.J. Duquette, Nucleation Characteristics of Directly Electrodeposited Copper on TiN, J. Electrochem. Soc. 153 (2006) C673–C676. doi:10.1149/1.2219712.

[50] S. Kim, D.J. Duquette, Effect of Chemical Composition on Adhesion of Directly Electrodeposited Copper Film on TiN, J. Electrochem. Soc. 153 (2006) C417–C421. doi:10.1149/1.2189971.

[51] S. Kim, D.J. Duquette, Morphology Control of Copper Growth on TiN and TaN Diffusion Barriers in Seedless Copper Electrodeposition, J. Electrochem. Soc. 154 (2007) D195. doi:10.1149/1.2433703.

[52] A. Radisic, J.G. Long, P.M. Hoffmann, P.C. Searson, Nucleation and Growth of Copper on TiN from Pyrophosphate Solution, J. Electrochem. Soc. 148 (2001) C41–C46. doi:10.1149/1.1344539.

[53] C. Wang, J. Lei, S. Rudenja, N. Magtoto, J. Kelber, Seedless electrodeposition of Cu on unmodified tungsten, Electrochem. Solid-State Lett. 5 (2002) C82--C84.

[54] C. Wang, J. Lei, C. Bjelkevig, S. Rudenja, N. Magtoto, J. Kelber, Electrodeposition of adherent copper film on unmodified tungsten, Thin Solid Films. 445 (2003) 72–79.

[55] M.J. Shaw, S. Grunow, D.J. Duquette, “Seedless” electrochemical deposition of copper on physical vapor deposition-W2N liner materials for ultra large scale integration (ULSI) devices, J. Electron. Mater. 30 (2001) 1602–1608. doi:10.1007/s11664-001-0179-8.

[56] B. Im, S. Kim, Nucleation and growth of cu electrodeposited directly on w diffusion barrier in neutral electrolyte, Electrochim. Acta. 130 (2014) 52–59. doi:10.1016/j.electacta.2014.02.154.

[57] K.-S. Park, S. Kim, Seedless Copper Electrodeposition onto Tungsten Diffusion Barrier, J. Electrochem. Soc. 157 (2010) D609–D613. doi:10.1149/1.3491351.

[58] B. Im, S. Kim, Effect of bath additives on copper electrodeposited directly on diffusion barrier for integrated silicon devices, Thin Solid Films. 546 (2013) 263–270.

[59] A. Radisic, G. Oskam, P.C. Searson, Influence of oxide thickness on nucleation and growth of copper on tantalum, J. Electrochem. Soc. 151 (2004) C369--C374.

[60] S.B. Emery, J.L. Hubbley, D. Roy, Voltammetric and amperometric analyses of electrochemical nucleation: electrodeposition of copper on nickel and tantalum, J. Electroanal. Chem. 568 (2004) 121–133.

[61] S. Kim, D.J. Duquette, Quantitative Measurement of Interfacial Adhesion Between Seedless Electrodeposited Copper and Tantalum-Based Diffusion Barriers for Microelectronics, Electrochem. Solid-State Lett. 10 (2007) D6–D9. doi:10.1149/1.2363937.

[62] D.J. Duquette, Materials, Electrochemical Processes for the Production of Copper Interconnects on Non-metallic Barrier Layers, ECS Trans. 25 (2009) 303–314.

[63] S. Kim, Seedless Copper Electrodeposition onto Tantalum Diffusion Barrier by Two-Step Deposition Process, Electrochem. Solid-State Lett. 13 (2010) D83–D86. doi:10.1149/1.3485026.

[64] D. Starosvetsky, N. Sezin, Y. Ein-Eli, Seedless copper electroplating on Ta from an alkaline activated bath, Electrochim. Acta. 82 (2012) 367–371. doi:10.1016/j.electacta.2012.03.033.

[65] D. Starosvetsky, N. Sezin, Y. Ein-eli, Seedless copper electroplating on Ta from a “ single ” electrolytic bath, Electrochim. Acta. 55 (2010) 1656–1663. doi:10.1016/j.electacta.2009.10.044.

[66] S. Kim, D.J. Duquette, Growth of conformal copper films on TaN by electrochemical deposition for ULSI interconnects, Surf. Coatings Technol. 201 (2006) 2712–2716. doi:10.1016/j.surfcoat.2006.05.022.

[67] S. Kim, D.J. Duquette, Multiple bath usage for adhesion enhancement of directly electrodeposited copper on TaN, Electrochem. Solid-State Lett. 9 (2006) C38--C40.

[68] N.E. Lay, D.J. Duquette, “Seedless” Copper Electrochemical Deposition on Air Exposed TaN Barrier Layers with Pd Adhesion Promoters, ECS Trans. 3 (2007) 153–160.

[69] N. Wiberg, K. Dehnicke, Hollemann-Wiberg, Lehrbuch der Anorganischen Chemie, Angew. Chemie-German Ed. 108 (1996) 2696.

[70] D. Josell, J.E. Bonevich, T.P. Moffat, T. Aaltonen, M. Ritala, M. Leskelä, Osmium Barriers for Direct Copper Electrodeposition in Damascene Processing, Electrochem. Solid-State Lett. 9 (2006) C48-50. doi:10.1149/1.2179770.

[71] D. Josell, J.E. Bonevich, T.P. Moffat, T. Aaltonen, M. Ritala, M. Leskelä, Iridium Barriers for Direct Copper Electrodeposition in Damascene Processing, Electrochem. Solid-State Lett. 9 (2006) C48–C50. doi:10.1149/1.2179770.

[72] D. Josell, D. Wheeler, C. Witt, T.P. Moffat, Seedless Superfill: Copper Electrodeposition in Trenches with Ruthenium Barriers, Electrochem. Solid-State Lett. 6 (2003) C143–C145. doi:10.1149/1.1605271.

[73] B. Im, S. Kim, S.-H. Kim, Influence of additives upon Cu thin film growth on atomic-layer-deposited Ru layer and trench-filling by direct electrodeposition, Thin Solid Films. 636 (2017) 251–256.

[74] U. Emekli, A.C. West, Effect of additives and pulse plating on copper nucleation onto Ru, Electrochim. Acta. 54 (2009) 1177–1183. doi:10.1016/j.electacta.2008.08.065.

[75] T.P. Moffat, M. Walker, P.J. Chen, J.E. Bonevich, W.F. Egelhoff, L. Richter, C. Witt, T. Aaltonen, M. Ritala, M. Leskelä, D. Josell, Electrodeposition of Cu on Ru Barrier Layers for Damascene Processing, J. Electrochem. Soc. 153 (2006) C37. doi:10.1149/1.2131826.

[76] M.L. Walker, L.J. Richter, D. Josell, T.P. Moffat, An in situ ellipsometric study of Cl- induced adsorption of PEG on Ru and on underpotential deposited Cu on Ru, J. Electrochem. Soc. 153 (2006) C235--C241.

[77] T.N. Arunagiri, Y. Zhang, O. Chyan, M. El-Bouanani, M.J. Kim, K.H. Chen, C.T. Wu, L.C. Chen, 5 nm ruthenium thin film as a directly plateable copper diffusion barrier, Appl. Phys. Lett. 86 (2005) 83104.

[78] F. Qiao, A.C. West, The impact of cations on nucleus density during copper electrodeposition, Electrochim. Acta. 150 (2014) 8–14. doi:10.1016/j.electacta.2014.10.135.

[79] F. Qiao, B.B. O'Brien, K. a. Dunn, A.C. West, The Effect of Fe(III)/Fe(II) Redox Couple on Nucleus Density during Cu Electrodeposition Process, J. Electrochem. Soc. 160 (2013) D271–D278. doi:10.1149/2.142306jes.

[80] M. Nagar, A. Radisic, K. Strubbe, P.M. Vereecken, The effect of polyether suppressors on the nucleation and growth of copper on RuTa seeded substrate for direct copper plating, Electrochim. Acta. 127 (2014) 315–326.

[81] S. Kumar, D. Greenslit, E. Eisenbraun, Development of manufacturable solutions for the direct plating of copper on robust ALD-grown barriers, ECS Trans. 6 (2007) 77–88.

[82] M. Nagar, A. Radisic, K. Strubbe, P.M. Vereecken, The effect of cupric ion concentration on the nucleation and growth of copper on RuTa seeded substrates, Electrochim. Acta. 92 (2013) 474–483.

[83] M. Nagar, A. Radisic, K. Strubbe, P.M. Vereecken, The Effect of the Substrate Characteristics on the Electrochemical Nucleation and Growth of Copper, J. Electrochem. Soc. 163 (2016) D3053--D3061.

[84] A. Radisic, M. Nagar, K. Strubbe, S. Armini, Z. El-Mekki, H. Volders, W. Ruythooren, P.M. Vereecken, Copper Plating on Resistive Substrates, Diffusion Barrier and Alternative Seed Layers, ECS Trans. 25 (2010) 175–184. doi:10.1149/1.3318516.

3 Experimental

In this section, a general introduction to the chemicals, materials and instruments which were used in this research will be given. In some cases, tailored solutions were employed. The description of these cases can be found in the corresponding experimental section of each chapter in the result and discussion part of chapter 4.

3.1 Materials

Chemicals and Probes

Ammonia 28% (NH_3)	Analytical grade, BASF (Ludwigshafen, Germany)
Ammonium citrate ($(NH_4)_3C_6H_5O_7$)	Analytical grade, VWR Chemicals (Radnor, Pennsylvania)
Ammonium sulfate ($(NH_4)_2SO_4$)	Analytical grade, Merck (Darmstadt, Germany)
Citric acid ($C_6H_8O_7$)	Analytical grade, Sigma-Aldrich (St. Louis, Missouri)
Copper sulfate pentahydrate ($CuSO_4*5H_2O$)	Analytical grade, Merck (Darmstadt, Germany)
Different thin films on silicon 8-inch wafer	Infineon Technologies AG (Regensburg, Germany)
Ferrocenemethanol (FcMeOH)	99%, ABCR (Karlsruhe, Germany)
Hexaammineruthenium(III) chloride ($Ru(NH_3)_6Cl_3$)	98%, Sigma-Aldrich (St. Louis, Missouri)
Hydrochloric acid 0.1M (HCl)	Analytical grade, Merck (Darmstadt, Germany)
Potassium hydroxide (KOH)	Analytical grade, Honeywell Chemicals (Morristown, New Jersey)
Potassium nitrate (KNO_3)	Analytical grade, Merck (Darmstadt, Germany)
Potassium octacyanotungstate(IV) dihydrate ($K_4W(CN)_8)*2H_2O$)	In-house production
Sulfuric acid 1M (H_2SO_4)	Analytical grade, Merck (Darmstadt, Germany)
Ultrapure water (resistivity > 18MΩ/cm)	Milli- Q Advantage A10 system, Merck Millipore, (Darmstadt, Germany)

Consumable materials

Copper cable	Leonische Drahtwerke AG (Nürnberg, Germany)
Lapping foils (30, 10, 3, 0.3 micron)	Sigma-Aldrich (Seelze, Germany)
PDMS kit Sylgrad® 184	Sigma-Aldrich (Seelze, Germany)
Plastic paraffin film Parafilm M	Pechiney Plastic Packaging Inc. (Chicago, Illinois)
Platinum wire (d = 25 µm)	Goodfellow (Cambridge, Great Britain)
PTFE syringe filter (poresize: 0.05 micron)	Carl Roth, GmbH & Co. KG (Karlsruhe, Germany)
Soda lime glass capillaries (d_{inner} = 1.1 mm, d_{outer} = 1.8 mm)	Glaswerke Ilmenau (Ilmenau, Germany)
Various syringes	B. Braun Injekt (Melsungen, Germany)
Two-component epoxide adhesive glue	Uhu (Bühl, Germany)

Instrumentation

Autolab PGST302N	Metrohm (Herisau, Switzerland)
Bullseye level (model 1034, diameter 14 mm, sensitivity: 5’)	Glas- und Meßtechnik GmbH (Wächtersbach, Germany)
LEXT OLS4000 3D laser measuring microscope	Olympus (Tokyo, Japan)
pH-meter 827 pH Lab Meter	Metrohm (Herisau, Switzerland)
Reference electrode Ag/AgCl/3M KCl (model 6.0728.130)	Metrohm (Herisau, Switzerland)
Scanning electron microscope Zeiss Gemini Ultra 55	Zeiss (Oberkochen, Germany)
Smart cell 1000w plating tool	Yamamoto MS (Tokyo, Japan)
Soldering equipment WE CP-20	Weller, Wetzlar, Germany
Wide stand microscope x100	PEAK (Bornheim-Roisdorf, Germany)
Faradaic cage	laboratory constructed

Software

Origin 2017	OriginLab Corporation, Inc. (Northampton, Massachusetts)
LEXT OLS4000 software	Olympus (Tokyo, Japan)
Microsoft Office 2016	Microsoft (Redmond, Washington)
SECM software CHI920C	CH Instruments (Austin, Texas)
DIPS	Point electronic (Halle, Germany)
ImageJ	open source
NOVA 2.0	Metrohm (Herisau, Switzerland)

3.2 Mediators

Three different mediators and one mediator-free solution were used in the studies. The composition of the solutions is shown in table 3.1. For the preparation of stable mediators, the deionized water was deaerated at T = 80 °C by nitrogen bubbling for 1 hour prior to the fabrication process. After cooling, the mediator species and the conducting salt were dissolved at T = 45 °C under sonication for 30 min in a 50 ml conical flask. To prevent the dissolution of oxygen from ambient air in the prepared solutions, the flasks were sealed using a parafilm sealing film. After cooling, the solutions were stored for 24 h at room temperature to reach equilibrium state. The solutions were filtered twice after cooling with a PTFE syringe filter with a pore size of 0.05 micron to remove precipitates. The stability of the mediator was tested by recording cyclic voltammograms with an ultramicroelectrode in a three-electrode configuration. A mediator was defined as stable when the measured cycles were reproducible.

Table 3.1: Mediator composition

Mediator	Active species	Supporting electrolyte
Ferrocenemethanol	1.5 mM FcMeOH	0.2 M KNO_3
Potassium octacyanotungstate(IV) dihydrate	1.5 mM $(K_4W(CN)_8)*2H_2O$	0.2 M KNO_3
Hexaammineruthenium(III) chloride	1 mM $Ru(NH_3)_6Cl_3$	0.2 M KNO_3
Mediator-free	-	0.2 M KNO_3, 1.4 mM HCl

3.3 Copper electrolytes

Different electrolytes were used to deposit copper potentiostatically or under current control on selected barrier films with good adhesion. The choice of bath composition is based on chapter 2.3.4. Four different Cu electrolytes were used for the direct deposition studies. Their composition is shown in table 3.2. All electrolytes were prepared by dissolving the components in deionized water. The pH value was adjusted with H_2SO_4 or NH_3 if required. The virgin-make up solution electrolyte (VMS) was used for potentiostatic or galvanic deposition on Ru and Pt. The complexed bath was used for direct plating on TiN under potential control. The alkaline bath was applied for Cu deposition on TaN following a special protocol described in chapter 4.3.2. The low acidic bath has been employed for galvanic deposition on Ru.

Table 3.2: Cu electrolyte composition for direct electroplating on barrier with references

Type	Copper source	Supporting electrolyte	pH value	Barrier
VMS bath [1]	0.63M $CuSO_4$	0.3M H2SO4, 1.4 mM HCl	pH < 1	Ru, Pt
Complexed bath [2]	0.08 M $CuSO_4$	0.1M $(NH_3)_3C_6H_5O_7$	5 < pH < 6	TiN
Alkaline bath [3]	0.08 M $CuSO_4$	0.4M $(NH_3)_3C_6H_5O_7$	pH > 10	TaN
Low acidic bath [4]	0.4 M $CuSO_4$	0.38M $(NH_4)_2SO_4$, 0.03 $C_6H_8O_7$	1.9 < pH < 2.5	Ru

3.4 SECM probe fabrication and characterization

3.4.1 Fabrication of ultramicroelectrodes

Pt-ultramicroelectrodes were prepared based on the protocol of Lee et al. [5]. A schematic overview of the process steps is represented in Fig. 3.1.

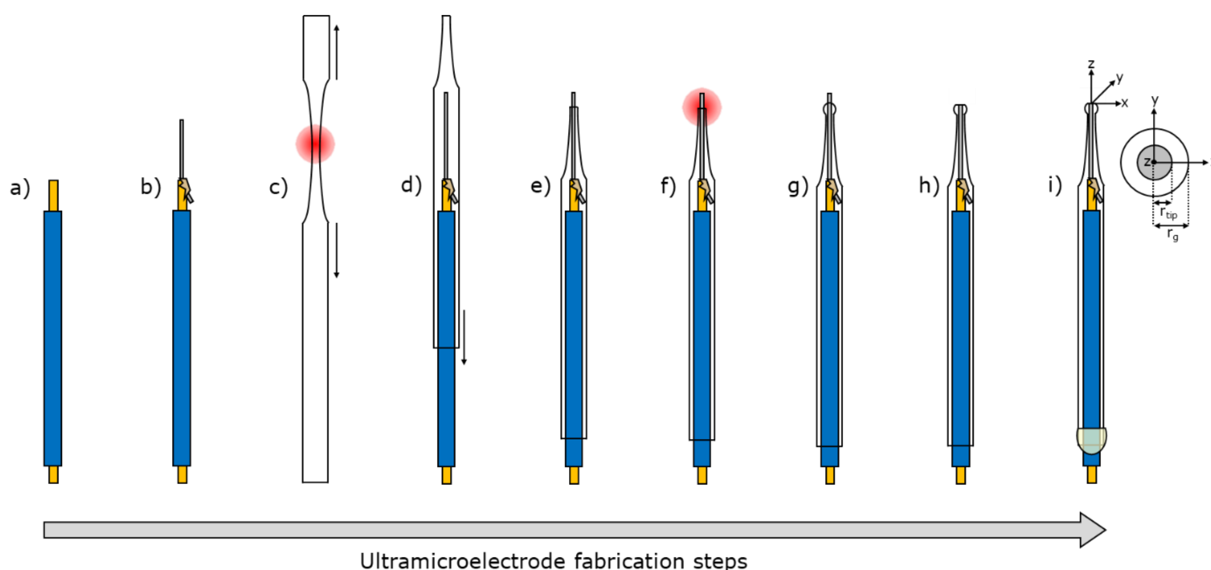

Figure 3.1: Fabrication process of an ultramicroelectrode. (a) removal of isolation of Cu wire, (b) soldering of Pt wire on Cu wire, (c) fabrication of tapering from a soda lime glass by local heating, (d) insertion of wire into glass capillary, (e) positioning of Pt wire in the clipped glass capillary, (f) local heating of capillary tip, (g) sealed Pt wire in glass capillary, (h) tip polishing with abrasive paper, (i) fixation of Cu wire in glass capillary with two-component glue and characterization of the electrode tip.

In the first step, the insulation of a 4 cm long Cu wire was removed at both ends for subsequent processing. Afterwards, a 5 mm long Pt wire was soldered on one end of the exposed Cu wire. The radius of the used Pt wire does correspond to the final electrode size. Here, commercially available Pt wires with r_{Pt} = 12.5 µm or r_{Pt} = 6.25 µm were used for fabrication of standard UME's of r_{tip} = 12.5 µm or r_{tip} = 6.25 µm, respectively. For smaller electrode diameters the Pt-wires were electrochemically etched to obtain sharpened wires [6]. In this process, the tip of the Pt wire has to be immersed in a solution of 60% $CaCl_2$ and 4% HCl and etched

by applying potential pulses of ± 2 V at a frequency of 50 Hz in a two-electrode configuration with a Pt-wire as RE/CE. In the next step of the fabrication procedure, the Cu wire with the attached Pt wire is inserted into a previously pulled and cropped soda lime glass capillary with the Pt tip protruding from the conical end of the capillary. Afterwards, the Pt wire was sealed and mechanically stabilized by locally melting the tip of the soda lime glass capillary at $T \approx 1200$ K with a torch or heating coil. Followingly, the melted tip was carefully polished with lapping foils of different grain sizes until the electrode area with a defined RG value was exposed. In the last step, the Cu wire was fixed inside the glass capillary to relieve the Pt-wire mechanically by a small droplet of a two-component glue at the upper end of the glass capillary.

3.4.2 Characterization of ultramicroelectrodes

The sealing of the glass mantle was checked utilizing steady-state voltammograms in a mediator of 1.5 mM FcMeOH and 0.2 M KNO_3 in a three-electrode configuration with a Pt wire as counter electrode and an Ag/AgCl/3M KCl reference electrode. Potential controlled cycling was carried out between 0 V and 0.5 V with a scan rate of 50 mV/s. A dense sealing is expressed by reproducible cycles and almost no offset between the forward and the reverse scan. The characteristic sizes of the UME were determined from negative feedback curves towards a planar Teflon surface in the previously described setup. The probe scan curves were recorded at a scan rate of 2.5 µm/s (z_{incr} = 0.5 µm, t_{incr} = 0.2 s) at E_{tip} = 0.45 V. The measured curves can be correlated with the analytical expression of eq. 21, whereby the determination of r_{tip} and the RG value can be achieved with a software based numerical method. However, since the distance between the tip and the substrate d is unknown during probe approach, a correlation factor z' between d and step length z is required for fitting as can be seen in Fig. 3.2 a). Consequently, using this correlation factor z', eq. 20 is modified to eq. 44.

$$L = \frac{d}{r_{tip}} = \frac{z' - z}{r_{tip}} \quad (44)$$

Utilizing eq. 21, the measured tip current I_T can be expressed independently of L:

$$I_T = \frac{\left(\frac{2.08}{\left(\frac{r_g}{r_{tip}}\right)^{0.358}} \cdot \left(\frac{z'-z}{r_{tip}} - \frac{0.145}{\left(\frac{r_g}{r_{tip}}\right)}\right) + 1.585\right) \cdot I_{T,\infty}}{\frac{2.08}{\left(\frac{r_g}{r_{tip}}\right)^{0.358}} \cdot \left(\frac{z'-z}{r_{tip}} + 0.0023 \cdot \left(\frac{r_g}{r_{tip}}\right)\right) + 1.57 + \frac{\ln\left(\left(\frac{r_g}{r_{tip}}\right)\right)}{\left(\frac{z'-z}{r_{tip}}\right)} + \frac{2}{\pi \cdot \left(\frac{r_g}{r_{tip}}\right)} \cdot \ln\left(1 + \frac{\pi \cdot \left(\frac{r_g}{r_{tip}}\right)}{2 \cdot \left(\frac{z'-z}{r_{tip}}\right)}\right)} \quad (45)$$

With the help of a nonlinear fitting algorithm, such as the Levenberg Marquardt iteration algorithm the characteristic paramaters r_{tip}, r_g, $I_{T,\infty}$ and z' can be determined simultaneously from one single measurement curve. In this thesis, the software Origin 2017 was selected for computation. The software-based characterization matches the optical inspection well as can be seen by comparing the results of Fig 3.2 a) and Fig. 3.2 c).

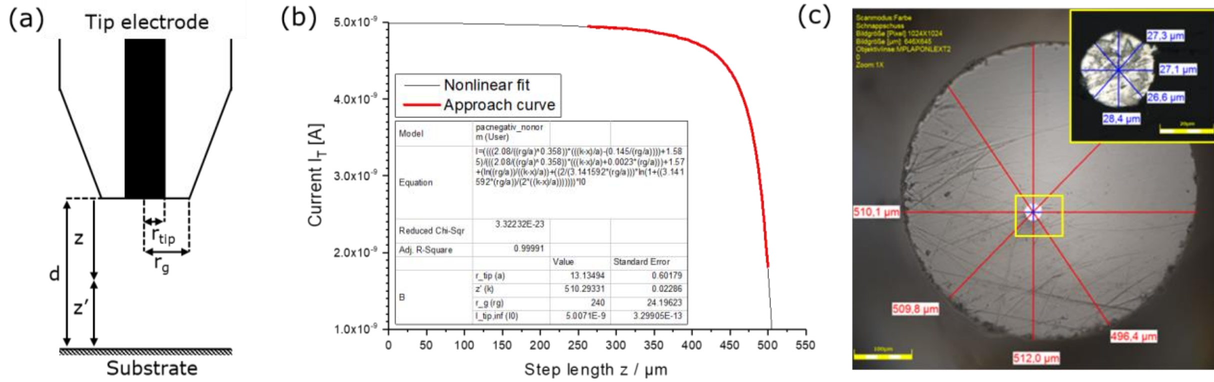

Figure 3.2: Determination of characteristic sizes of an ultramicroelectrode. (a) Schematic diagram of the relationship between correlation factor z', tip-to-substrate distance d and step length z, (b) characterization of an UME by fitting of eq. 45 into raw data of a probe approach curve (r_{tip} = 13.3 µm, RG = 18.3) and (c) characterization of the same UME with a microscope image (r_{tip} = 13.7 µm, RG = 18.5).

3.5 Multipurpose cell

A special cell for thin-film materials on silicon substrates was developed for electrochemical surface characterization and surface modification studies presented in this work. Accordingly, the electrical connection had to be located directly on the thin film, due to the fact that silicon is a semiconductor. Furthermore, the requirements listed below should also be fulfilled:

- Defined exposed area
- Homogenous current and potential distribution across exposed area with negligible ohmic drop
- Simple wafer specimen transfer without further preparation steps
- No contact of the electrical connection points of the cell with the solution
- Suitable for various applications

Based on these requirements, a special mounting platform for wafer-based samples was developed and constructed. In the following, this platform is referred to as multipurpose cell. A schematic illustration of this multipurpose cell is depicted in Fig. 3.3.

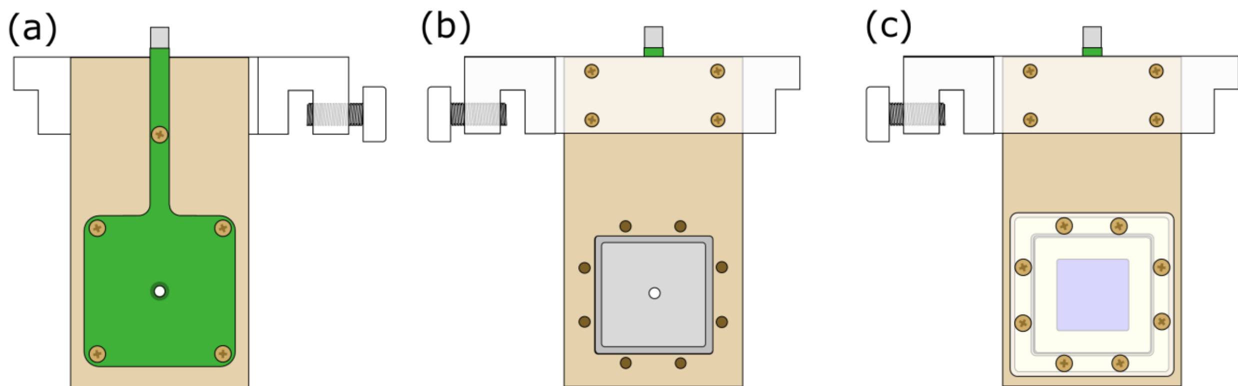

Figure 3.3: Schematic representation of the multipurpose cell. (a) frontside, (b) backside without back plate and (c) backside with sealed wafer specimen.

Fig. 3.3 a) shows that the multipurpose cell consists of a structured metal plate with a small circular opening (r = 4.26 mm) inserted and sealed into a peek body. The electrical contact and a clamping screw for attachment of the cell are located on the top side. The frontside of the metal plate is coated with a

polymeric Teflon-like coating in order to inhibit the interaction of the surface with the surrounding solution. The metal plate has a cavity where a sample of size 4 cm x 4 cm can be placed as it can be seen in Fig 3.3 b). This silicon wafer specimen is placed in the multipurpose cell from the backside, with the thin film pointing in the direction of the metal plate to ensure electrical contact. Sample attachment and sealing is carried out simultaneously using two silicon sealing rings, a back plate and 8 PEEK screws. The described mounting procedure for the silicon specimen is vividly illustrated and explained in Fig. 3.4. As shown in Fig. 3.4 d), the thin film is only exposed to the solution in the circular opening of the metal plate. The presented multipurpose cell was the basis for all experiments carried out in this work. The obtained results are explained and discussed in the following chapter.

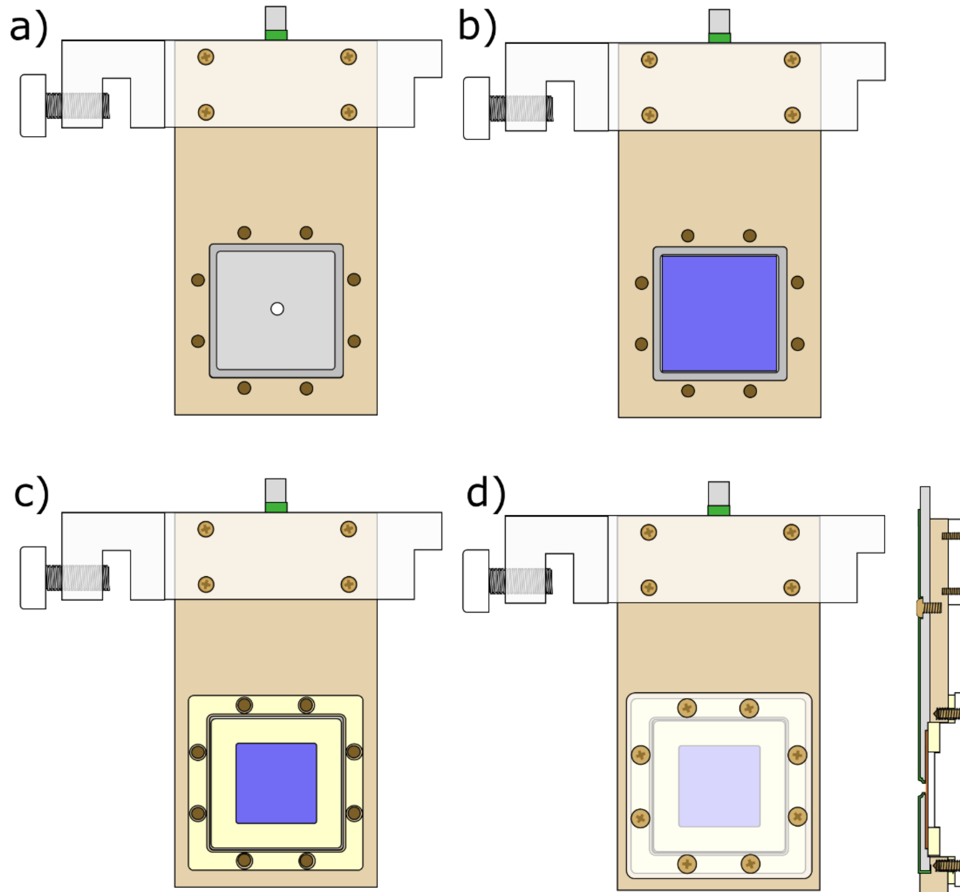

Figure 3.4: Mounting steps of thin film materials on a silicon specimen in the multipurpose cell. (a) Cell without sample, (b) silicon specimen is placed into the cavity of the metal plate, (c) silicon sealing rings are placed above the wafer specimen and on the sealing section of the PEEK plate and (d) wafer specimen is fixed and sealed by a back plate and 8 peek screws (left backside, right cross-section).

References

[1] A. Radisic, O. Lühn, H.G.G. Philipsen, Z. El-Mekki, M. Honore, S. Rodet, S. Armini, C. Drijbooms, H. Bender, W. Ruythooren, Copper plating for 3D interconnects, Microelectron. Eng. 88 (2011) 701–704. doi:10.1016/j.mee.2010.06.030.

[2] S. Kim, D.J. Duquette, Effect of Chemical Composition on Adhesion of Directly Electrodeposited Copper Film on TiN, J. Electrochem. Soc. 153 (2006) C417–C421. doi:10.1149/1.2189971.

[3] D. Starosvetsky, N. Sezin, Y. Ein-eli, Seedless copper electroplating on Ta from a " single " electrolytic bath, Electrochim. Acta. 55 (2010) 1656–1663. doi:10.1016/j.electacta.2009.10.044.

[4] S.D. Kang, J. Joon Yoo, H.-K. Lyeo, J. Yong Song, S. Lee, J. Yu, Assessing the thermal conductivity of non-uniform thin-films: Nanocrystalline Cu composites incorporating carbon nanotubes, J. Appl. Phys. 110 (2011) 23506.

[5] C. Lee, C.J. Miller, A.J. Bard, Scanning electrochemical microscopy: preparation of submicrometer electrodes, Anal. Chem. 63 (1991) 78–83. doi:10.1021/ac00001a016.

[6] S. Bergner, P. Palatzky, J. Wegener, F.-M. Matysik, High-Resolution Imaging of Nanostructured Si/SiO2 Substrates and Cell Monolayers Using Scanning Electrochemical Microscopy, Electroanalysis. 23 (2011) 196–200.

4 Results and discussion

4.1 Development and application of a multipurpose electrodeposition cell configuration

Patrick Hanekamp, Werner Robl and Frank-Michael Matysik,

Applied Electrochemistry 47 (2017): 1305-1312.

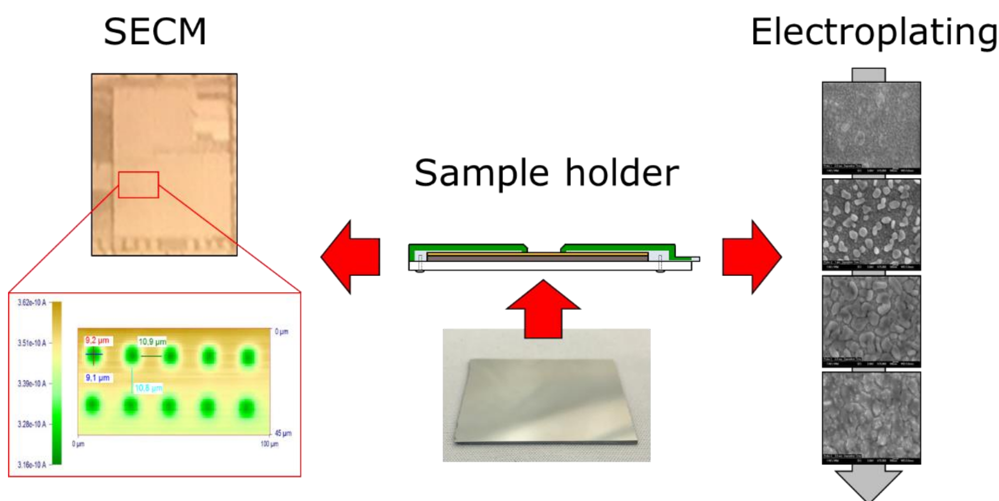

Copyright © 2017 Springer Nature

Abstract

In this report a versatile experimental concept for electrochemical deposition and subsequent surface characterization studies is presented. This concept can be utilized to perform semiconductor plating processes at laboratory scale followed by scanning electrochemical microscopy (SECM). The same sample holder used for electroplating experiments could be integrated into the SECM instrument. Conductive thin-film barrier materials were deposited on planar silicon wafers. The substrate samples were fixed in the multipurpose sample holder ensuring a large electrical contact area to minimize ohmic drop across the sample surface with a small circular area of the substrate material of 16 mm^2 exposed to electrolyte solution. In order to investigate the capabilities of the electrochemical cell configuration, a potentiostatic copper deposition on ruthenium was carried out. Thus, information on film coalescences, grainsize and growth mode could be derived. SECM was used to study the effect of biasing during probe approach curves on a titanium surface. Furthermore, microstructured copper layers were imaged using ferrocenemethanol (FcMeOH) as mediator. The results show that biasing the substrate is essential for nondestructive and

interaction-free measurements of semiprecious thin-film materials and copper structures, if FcMeOH is used as electrochemical mediator.

4.1.1 Introduction

Copper (Cu) plating plays an essential role in the semiconductor industry. The Cu metallization on wafer level is usually done by electrochemical deposition from an acidic copper electrolyte containing various additives on a Cu seed layer. The Cu seed layer, commonly deposited by physical vapor deposition (PVD), atomic layer deposition (ALD) or chemical vapor deposition (CVD), acts as the starting layer for the electrolytic deposition due to its good conductivity. In order to prevent the diffusion of the deposited Cu into the dielectric, a thin barrier layer of tantalum (Ta), tantalum nitride (TaN), titanium nitride (TiN) or tungsten nitride (WN) is deposited prior to the Cu seed layer formation [1]. As feature sizes continue to shrink, the deposition of a thin conformal and void-free Cu seed layer in the trenches and vias is challenging. Hence, new approaches are investigated in order to deposit the Cu metallization layer directly onto the barrier material like ruthenium (Ru) [2–5], TaN [6, 7], TiN [8–10], tungsten nitride (W_2N) [11], osmium (Os) [12] or iridium (Ir) [13]. Ru based barriers are the most promising materials for direct plating due to their good conductivity and strong adhesion of the electrodeposited Cu layer [14]. Furthermore the Cu deposition from a standard acidic Cu plating bath is possible which is advantageous in terms of process integration in semiconductor industry on wafer scale [4, 15]. In order to study the nucleation and the growth of these directly plated Cu layers, special plating equipment with high laminar agitation is needed to simulate the wafer scale process on a miniaturized laboratory level. For deposition experiments a front side contacting is required since the Cu is deposited on the metallized silicon substrate surface. Hence, an areal electrical contact is advantageous in order to reduce the ohmic drop associated with the thin-film layers on the silicon surface. Ohmic drop effects on thin-film substrates can lead to varying results on different locations of the sample [2, 7]. The above-mentioned requirements should be feasible without any sample preparation in order to prevent the disruption of a subsequent process step, for example an annealing process or the deposition of a passivation layer. In addition, it should be possible to obtain time-resolved information during deposition [16] and to couple the deposition cell with different devices in order to examine the sample surface. Scanning electrochemical microscopy (SECM), for example has proven to be a promising electroanalytical tool for the application in semiconductor industry due to the possibilities to study not only the nucleation [17], corrosion [18–20] and dissolution of metals [21], but

also the chemical stability of inhibitor films [22–28]. In this paper we introduce a versatile experimental concept for electrochemical deposition which can be coupled to SECM and other characterization techniques. First results of electrochemical nucleation studies and SECM investigations with commonly used semiconductor materials are presented.

4.1.2 Experimental

4.1.2.1 Reagents and Materials

All experiments were performed using 4 x 4 cm² silicon wafer specimens with a thermally grown silicon oxide (SiO_2). For copper nucleation experiments and SECM measurements thin layers of Ru (50 nm, PVD), Ti (50 nm, PVD), SiN (50 nm, CVD) and Cu (300 nm with 50 nm TiW adhesion layer, PVD) were deposited on these substrates. For SECM imaging experiments structures of a chemically polished dual damascene metallization layer were chosen. Thus, the Cu structures are embedded planar into a SiO_2 matrix with a very smooth surface. This enables the comparison of SECM based measurements with microscope images taken with a LEXT OLS4000 3D laser measuring microscope (Olympus, Tokyo, Japan). For electrochemical deposition studies an electrolyte consisting of 0.63 M $CuSO_4$, 0.3 M H_2SO_4, and 1.4 mM HCl with pH < 1 was used. The specified electrolyte is commonly known as virgin make up solution in semiconductor application and is subsequently denoted as VMS [29]. No further additives were added to this bath composition. SECM experiments were performed with a mediator consisting of 1.5 mM ferrocenemethanol (99%, ABCR, Karlsruhe, Germany) and 0.2 M KNO_3 (analytical grade, Merck, Darmstadt, Germany). The aqueous solution was prepared with ultrapure water with a resistivity higher than 18 MΩ/cm. All potentials of the electrochemical deposition experiments as well as the SECM studies refer to an Ag/AgCl/3 M KCl reference electrode. The ultramicroelectrodes were fabricated using a 25 µm Pt-wire (99.99%, Goodfellow, Huntingdon, England) and a soda-lime glass capillary (Technische Glaswerke Illmenau, Illmenau, Germany) following a previously described protocol [30]. The Pt wires were sharpened with the method of Zhang et al. [31] and were sealed and polished with the procedure adapted from Lee et al. [32]. The electrode dimensions were determined afterwards from steady-state voltammograms and negative feedback approach curves on a Teflon surface for the imaging experiments with SECM.

4.1.2.2 Sample holder and sample preparation

The sample holder for silicon wafer based specimen was developed and adapted according to previous reports [8, 33, 34]. The mounting device enables the areal electrical contact of a thin film material deposited on a semiconductor substrate with an exposed circular opening (diameter d = 4.5 mm). Thus, in comparison to a single point electrical contact, the ohmic drop across the surface is reduced, leading to a more homogenous potential and current distribution of the exposed surface area. This enables a well-controlled electrochemical deposition on the active electrode surface. In order to inhibit any contact of the electrical connection with the solution, the surface of the holder is coated with a passivating polymeric film. The 4 x 4 cm^2 silicon wafer specimen with the deposited thin layer is placed from the backside into the sample holder with the surface of interest pressed onto the electrical contact plate with the circular opening. The samples are subsequently sealed and fixed with a back plate and 8 PEEK screws in order to prevent any contact of the solution except of the exposed area. After this procedure no further sample preparation is required. The sample holder with the sealed silicon wafer specimen can be transferred between the electroplating cell and the SECM system without any risk of damaging the thin film and electrodeposited structures due to further sample preparation steps. Furthermore, no additional process step in SECM integration is necessary since a customized mounting platform was specially developed for this sample holder.

4.1.2.3 Electroplating experiments

The electrochemical experiments were performed using a modified Smart Cell 1000w (Yamamoto MS, Tokyo, Japan) laboratory plating cell. A schematic drawing of the plating setup is shown in Fig. 4.1a. The convection inside the deposition cell is generated by the overflow function through stirring with a magnetic stirrer. It can be further increased with a rocking paddle positioned close to the cathode surface. Furthermore, in order to prevent the interaction of the additives with the counter electrode, the anodic compartment can be separated from the plating bath utilizing a Nafion® N424 membrane. A three electrode setup is used for deposition experiments consisting of the sample holder, an Ag/AgCl/3 M KCl reference electrode and a phosphorous Cu plate as counter electrode. The electroplating experiments were performed with a potentiostat Autolab PGST302N (Metrohm, Herisau, Switzerland). The additive-free VMS electrolyte was used as received. A separation of the anode by a Nafion® membrane was not

required. It is assumed that no passivation layer is formed under the applied conditions and that no pretreatment is required as the measured open circuit potential of the Ru coated specimen in the plating bath is -2 mV. The deposition potential for nucleation studies was derived from a preliminary test with linear sweep voltammetry starting at the open circuit potential and sweeping with a scan rate of 50 mV/s to a final potential of -0.7 V. A suitable potential with a slow Cu deposition rate was found at -0.02 V. Potentiostatic Cu deposition at fixed times of 0.5 s, 1.0 s, 2.5 s, 3.5 s, 5.0 s, and 10 s was carried out and Cu nucleation was examined with a scanning electron microscope Zeiss Gemini Ultra 55 (Zeiss, Oberkochen, Germany) after carefully cleaning of the samples with isopropanol and drying them with nitrogen.

4.1.2.4 Scanning electrochemical microscopy studies

For SECM studies the sample holder was used in combination with a commercially available SECM, CH Instruments CHI920C (Austin, Texas) in a homemade Faraday cage which is placed on a damped working bench. The sample holder is horizontally placed and fixed on a customized mounting platform for levelling in the SECM setup without any further preparation step of the integrated wafer specimens. The measuring cell for SECM studies consists of a 4 mL homemade Teflon cell placed on top of the exposed sample area. Separate drillings are integrated to keep for the reference- and counter electrodes in place. The bottom of the Teflon cell body which is in contact with the sample holder is coated with a thin silicone film preventing leakage of internal solution. A schematic drawing is depicted in Fig. 1b. The holder with the wafer specimen was leveled with the help of an integrated circular level prior to each experiment. The SECM was operated in a four electrode configuration with a Pt-wire as counter-, the UME as probe, the sample holder as substrate- and an Ag/AgCl/3 M KCl as reference electrode. A potential of 0.5 V was applied to the UME for the probe approach curves (PACs). They were recorded with an approach rate of 0.5 µm/s (20 nm/0.04 s) without and with biasing (-0.5 V) of the substrate, respectively. Surface imaging was performed at a scan speed of 5 µm/s (1 µm/0.2 s) with a tip-to-surface distance corresponding to a current increase between 130% and 140% compared to the measured current in bulk solution.

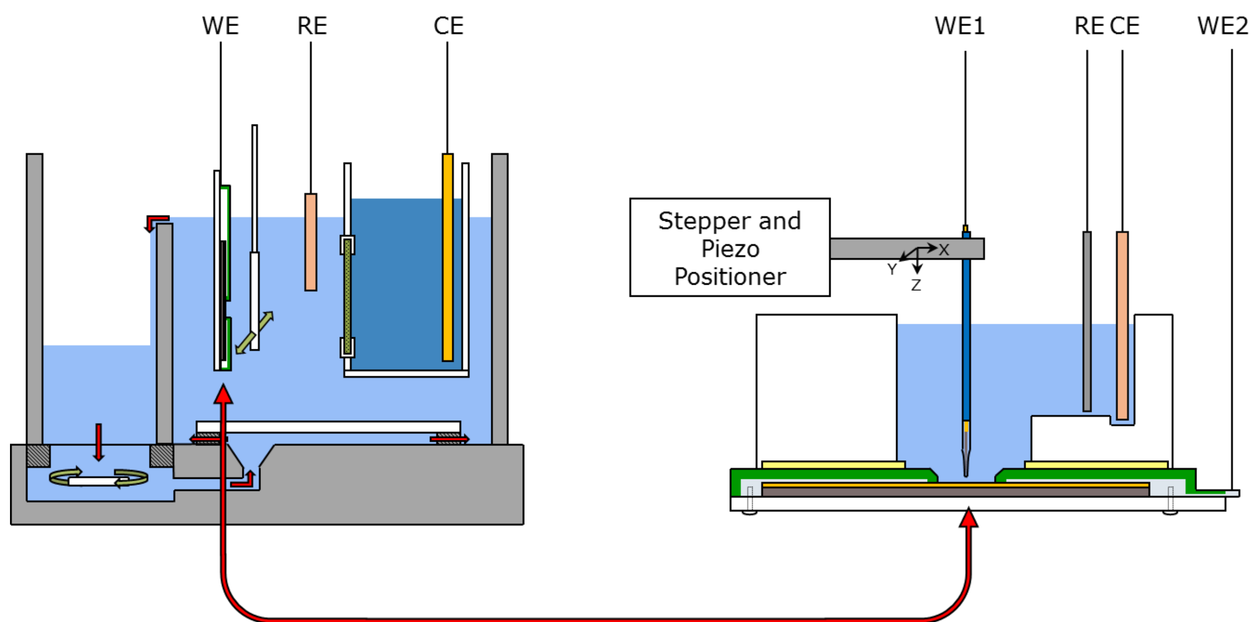

Figure 4.1: Schematic drawing of (a) three-electrode electrodeposition setup. The anodic compartment can be separated with a membrane from the cathodic one to prevent interaction of additives; convection is generated by overflow through magnetic stirring and can be furthermore increased with a rocking paddle near the cathode surface and (b) SECM with 4-electrode setup with detailed view of shield type sample holder with the passivating polymeric coating (green) and the Teflon cell (white) placed above the holder using a PDMS sealing film (yellow).

4.1.3 Result and discussion

4.1.3.1 Application of the electrodeposition cell to nucleation studies of copper on silicon samples with thin layers of ruthenium

In order to characterize the performance of electroplating experiments based on the use of the shield type substrate holder, the nucleation of Cu on Ru was chosen as a model system as it was previously studied by different working groups [2, 3]. The copper deposition and surface examination was carried out as described in the experimental section. Fig. 4.2 shows that Cu nucleation on the untreated Ru surface is characterized by a Volmer-Webber (3D) island growth.

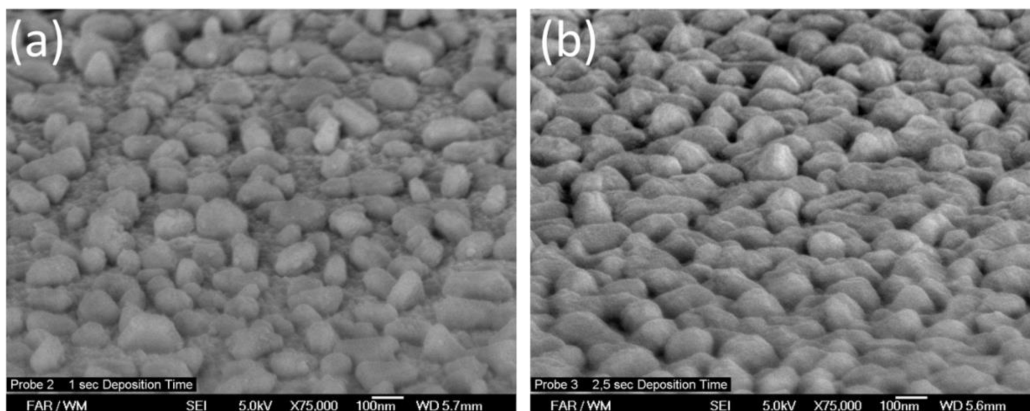

Figure 4.2: Tilted view (angle 70°) of deposited Cu after (a) 1 s and (b) 2.5 s deposition time at -0.02 V vs Ag/AgCl/3 M KCl. Three dimensional grain growth and coalescence can be observed. No closed Cu layer is formed as there are still exposed surface regions of ruthenium.

At the beginning of the deposition Cu nuclei of 100 nm in diameter have emerged, which subsequently grew showing a hemispherical shape. During the grain growth further Cu seeds are continuously formed until a closed Cu layer has developed by coalescence after about 5 seconds deposition time under the applied experimental conditions. After coalescence, the deposition of the Cu layer is dominated by a two dimensional layer growth (Fig. 4.3). Thus, the growth of Cu nuclei can be described as a mixed form of instantaneous and progressive growth. The adhesion of the Cu layer on the sputtered Ru was examined performing a tape test with the sample after 10 seconds deposition time. No peeling was observed which is in good agreement with comparable protocols described in literature [14]. The characteristics of the copper deposition were very uniform and homogeneous across the exposed electrode area of the wafer specimen fixed in the novel sample holder.

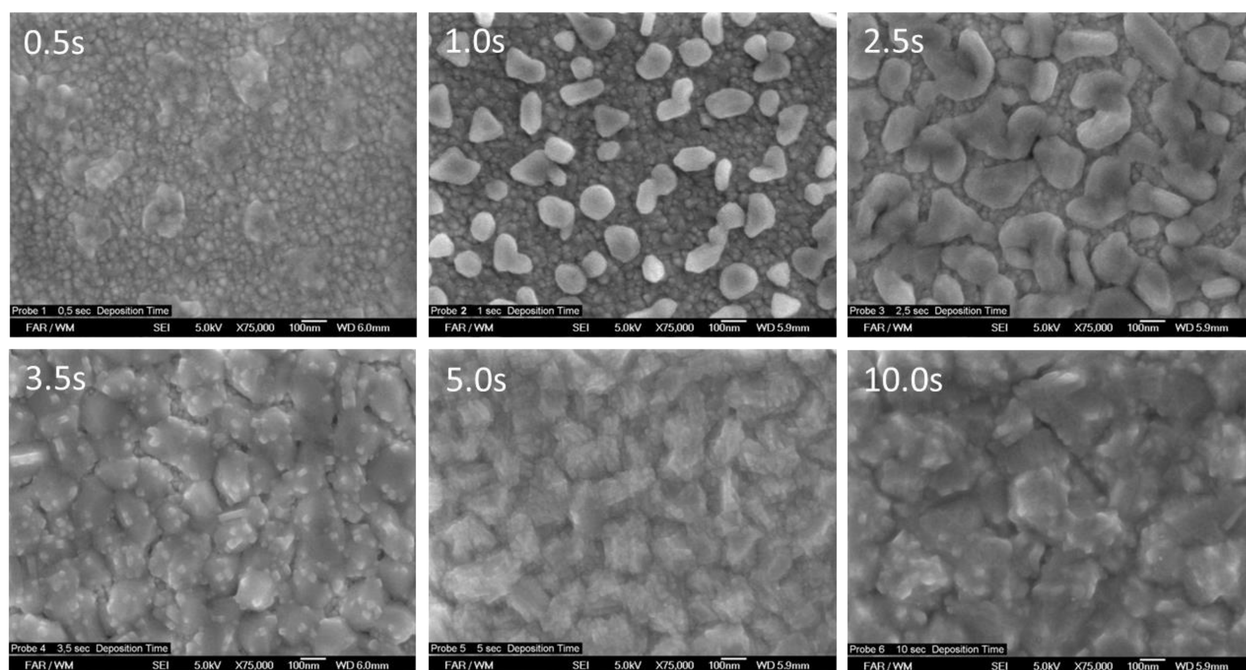

Figure 4.3: Potentiostatic deposition at -0.02 V vs Ag/AgCl/3 M KCl of Cu from VMS electrolyte on thin layers of Ru on silicon at fixed deposition times. Coalescence of the Cu layer can be observed. All images have the same magnification.

4.1.3.2 Scanning electrochemical microscopy - approach curves on thin layer films

In order to examine the versatility of the experimental setup various thin layer materials typically used in semiconductor manufacturing were chosen for SECM studies. Thereby, Cu und Ti were used as conductive and SiN as non-conductive thin layer materials for the recording of PACs. The parameters for the PACs can be found in the experimental section. The probe dimensions of the UME were determined from the negative feedback of the approach curve on SiN in 1.5 mM FcMeOH solution based on the theoretical negative feedback model developed by Galceran et al. [35]. In this study the tip radius r_{tip} of the platinum microdisk and the RG value (ratio between r_{tip} and the radius of glass mantle) were calculated by fitting the theoretical negative feedback into the measured feedback curve. The determined electrode dimensions (r_{tip} = 14 µm and RG = 5.3) were subsequently used to calculate the positive feedback with a parameter setting of RG = 5.1 according to [36]. Since an interaction of the unbiased metal surfaces and the mediator is possible [37] the Cu and Ti substrates were biased at -0.5 V in order to prevent a local surface modification of the thin layer material. Fig. 4.4 shows that the theoretically calculated positive

feedback is in good agreement with the normalized approach curves on the biased semiprecious metals. Since no difference between the positive approach curves and the theoretical model was found, it is assumed that no “pure material contrast” between Cu and Ti will be observable in the SECM imaging mode. In order to investigate the interaction of the mediator and the metal interface, a second approach curve on the same spot of the Ti without biasing was recorded after the tip was retracted to a tip-to-substrate distance of 350 µm. A weak positive feedback response was recorded during the initial period of the approach procedure (see Fig. 4.4b) which then turns to a negative feedback as the tip-to-substrate distance reaches the tip dimensions of d = 20 µm (insert of Fig. 4.4b). This behavior can be explained by the formation of an insulating titanium oxide (TiO_2) layer, which is the result of the local oxidation of the Ti surface by the oxidized FcMeOH ($FcMeOH^+$) species generated at the tip. The oxidation of the surface is thereby triggered locally as the tip-to-substrate distance reaches tip dimensions and the local surface potential is shifted to a more positive potential. Alternatively, the change of the feedback behavior could also be explained by the presence of an ensemble of active regions dispersed on a conductive but non-active surface. In addition, effects of kinetically controlled regeneration of $FcMeOH^+$ at the substrate might play a role.

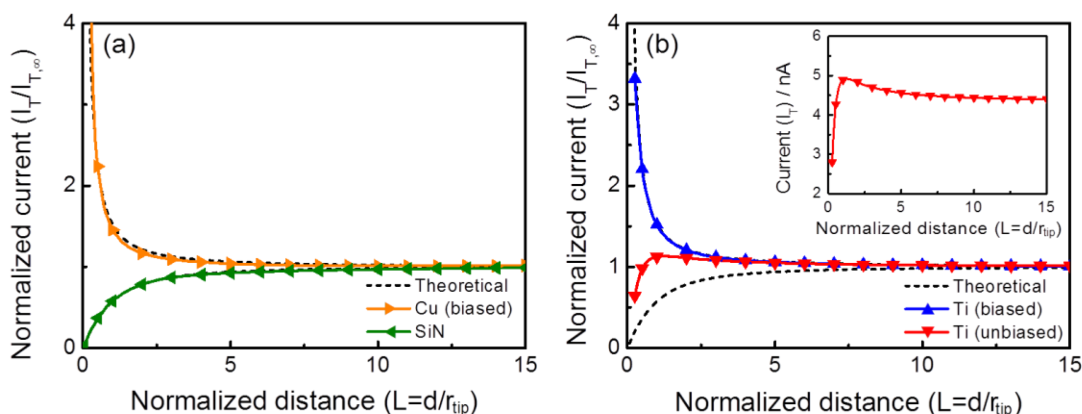

Figure 4.4: Approach curves with an ultramicroelectrode (r_{tip}=14 µm, RG=5.3) moved towards the surface of thin layers of Cu, SiN, and Ti on silicon substrates. Experimental conditions: mediator solution, 1.5 mM ferrocenemethanol/0.2 M KNO_3 on (a) unbiased SiN (◀) and biased Cu (▶) at -0.5 V vs Ag/AgCl/3 M KCl and (b) on biased (▲) -0.5 V and unbiased (▼) Ti surface. The theoretical (positive and negative) feedback responses are plotted as dashed curves. Insert graphic in Figure b shows the approach curve for an unbiased Ti surface without current normalization.

4.1.3.3 Scanning electrochemical microscopy - imaging of structured thin copper layer

Imaging experiments were performed as described in the experimental section with a sample of a dual damascene metallization layer in order to test the applicability of SECM as a non-destructive electrochemical characterization method on microstructured samples. It is well known from literature that surface etching of the thin film of copper by the tip-generated oxidized species will occur at open circuit potential, however, for the use of other mediator systems than in the present work [37, 38]. Thus, the structured dual damascene metallization layer was imaged without and with biasing at -0.5 V, in order to study the impact of surface etching during SECM measurements. Microscopic images of the scanned area were taken after the measurements to compare them with the SECM images. The surface imaging at a tip-to-substrate distance corresponding to 130% current increase is illustrated in Fig. 4.5. From the SECM measurement shown in Fig. 4.5b, it can be observed that the mediator is regenerated at the Cu surface leading to a positive feedback on the Cu structures. As expected the Cu surface was locally etched during SECM measurements by $FcMeOH^+$ species generated at the ultramicroelectrode tip and the microstructure was partially destroyed exposing the silicon interface (Figure 5a).

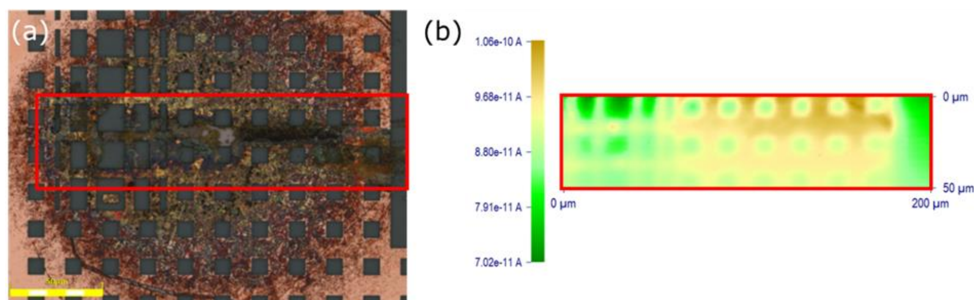

Figure 4.5: (a) Optical micrograph of a Cu microstructure after imaging with SECM without biasing of the sample, (b) SECM image in feedback mode using ferrocenemethanol as mediator and an ultramicroelectrode with r_{tip} = 2.5 µm, RG = 13, $I_T/I_{T,\infty}$ = 130%. Cu structures show a positive feedback in contrast to the negative feedback of SiO_2.

In contrast to the unbiased sample the biased surface with an applied potential of -0.5 V did not show any damage during SECM imaging. Fig. 6a illustrates an optical micrograph after SECM imaging of a biased sample and Fig. 6b shows a well-defined SECM image recorded at a distance corresponding to a current

increase of 140%. The imaged surface of the embedded copper structures in the SiO_2 matrix as obtained in the SECM measurements was in good agreement with the microscopic picture (Figure 6b).

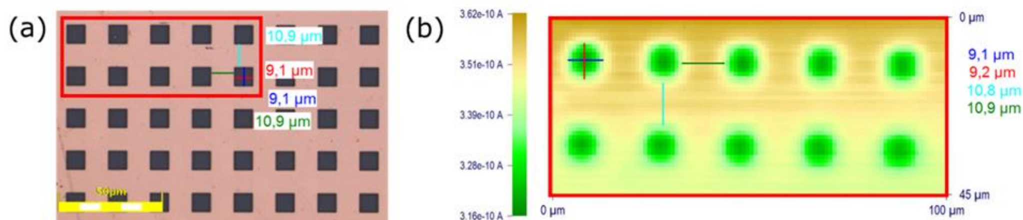

Figure 4.6(a) Optical micrograph of a Cu structure after SECM imaging with biasing of the substrate at -0.5 V vs Ag/AgCl /3 M KCl. (b) SECM image in feedback mode using ferrocenemethanol as mediator and an ultramicroelectrode with r_{tip} = 2.0 µm, RG = 22, $I_T/I_{T,\infty}$ = 140%, the structured Cu substrate was biased at -0.5 V.

With the biased sample a stable positive feedback behavior was found over copper structures and etching of copper could be avoided. In contrast to optical microscopy SECM has the potential to indicate surface deactivation due to adsorbed films. It can be concluded that no insulating film has formed on the copper structures since no change in surface reactivity has been observed in the imaged area. On the other hand, the regeneration of mediator at the insulating SiO_2 matrix is not possible leading to a decrease in current over the quadratic structures (negative feedback). The resolution of the square geometry of the SiO_2 surface was limited due to diffusive broadening but could be improved by using probes with smaller tip radii.

4.1.4 Conclusion

A versatile experimental concept for electrochemical deposition studies is presented. The multipurpose cell configuration can be utilized to perform semiconductor plating processes at laboratory scale as well as film characterizations with SECM or other techniques. The electrochemical cell enabled the study of nucleation phenomena of Cu on a Ru thin film on a silicon substrate whereas the deposition parameters and the convection inside the cell could be varied in a broad range without any complex sample

preparation. The sample holder of the electrodeposition cell can easily be implemented in a correspondingly modified SECM cell configuration for further surface characterization. The SECM studies presented in this work have shown that in the case of semi-precious metals and using FcMeOH as mediator it is important to bias the substrate. Applying a suitable potential to the substrate surface prevents the interaction of the oxidized mediator species generated at the UME tip with the substrate material by inhibiting the local oxide formation and etching. The presented experimental concept facilitates both, a versatile operation of electrodeposition experiments using relevant wafer specimen from the semiconductor industry and a straightforward complementary characterization of electrodeposited films by SECM.

References

1. Baklanov M, Ho PS, Zschech E (2012) Advanced interconnects for ULSI technology. John Wiley & Sons

2. Moffat TP, Walker M, Chen PJ, Bonevich JE, Egelhoff WF, Richter L, Witt C, Aaltonen T, Ritala M, Leskelä M, Josell D (2006) Electrodeposition of Cu on Ru Barrier Layers for Damascene Processing. J Electrochem Soc 153:C37. doi: 10.1149/1.2131826

3. Emekli U, West AC (2009) Effect of additives and pulse plating on copper nucleation onto Ru. Electrochim Acta 54:1177–1183. doi: 10.1016/j.electacta.2008.08.065

4. Armini S, El-Mekki Z, Nagar M, Radisic A, Vereecken PM (2014) Wafer Scale Copper Direct Plating on Thin PVD RuTa Layers: A Route to Enable Filling 30 nm Features and Below? J Electrochem Soc 161:D564–D570. doi: 10.1149/2.1031410jes

5. Nagar M, Radisic A, Strubbe K, Vereecken PM (2016) The Effect of the Substrate Characteristics on the Electrochemical Nucleation and Growth of Copper. J Electrochem Soc 163:D3053--D3061.

6. Kim S, Duquette DJ (2006) Growth of conformal copper films on TaN by electrochemical deposition for ULSI interconnects. Surf Coatings Technol 201:2712–2716. doi: 10.1016/j.surfcoat.2006.05.022

7. Radisic A, Cao Y, Taephaisitphongse P, West AC, Searson PC (2003) Direct Copper Electrodeposition on TaN Barrier Layers. J Electrochem Soc 150:C362–C367. doi:

10.1149/1.1565137

8. Graham L, Steinbrüchel C, Duquette DJ (2002) Nucleation and Growth of Electrochemically Deposited Copper on TiN and Copper from a Cu NH 3 Bath. J Electrochem Soc 149:C390–C395. doi: 10.1149/1.1487836

9. Kim S, Duquette DJ (2006) Nucleation Characteristics of Directly Electrodeposited Copper on TiN. J Electrochem Soc 153:C673–C676. doi: 10.1149/1.2219712

10. Oskam G, Vereecken PM, Searson PC (1999) Electrochemical Deposition of Copper on n-Si/TiN. J Electrochem Soc 146:1436–1441. doi: 10.1149/1.1391782

11. Shaw MJ, Grunow S, Duquette DJ (2001) “Seedless” electrochemical deposition of copper on physical vapor deposition-W2N liner materials for ultra large scale integration (ULSI) devices. J Electron Mater 30:1602–1608. doi: 10.1007/s11664-001-0179-8

12. Josell D, Bonevich JE, Moffat TP, Aaltonen T, Ritala M, Leskelä M (2006) Osmium Barriers for Direct Copper Electrodeposition in Damascene Processing. Electrochem Solid-State Lett 9:C48-50. doi: 10.1149/1.2179770

13. Josell D, Bonevich JE, Moffat TP, Aaltonen T, Ritala M, Leskelä M (2006) Iridium Barriers for Direct Copper Electrodeposition in Damascene Processing. Electrochem Solid-State Lett 9:C48–C50. doi: 10.1149/1.2179770

14. Chyan O, Arunagiri TN, Ponnuswamy T (2003) Electrodeposition of Copper Thin Film on Ruthenium. J Electrochem Soc 150:C347. doi: 10.1149/1.1565138

15. Lane MW, Murray CE, McFeely FR, Vereecken PM, Rosenberg R (2003) Liner materials for direct electrodeposition of Cu. Appl Phys Lett 83:2330–2332. doi: 10.1063/1.1610256

16. Scharifker B, Hills G (1983) Theoretical and experimental studies of multiple nucleation. Electrochim Acta 28:879–889. doi: 10.1016/0013-4686(83)85163-9

17. Kim J, Renault C, Nioradze N, Arroyo-Currás N, Leonard KC, Bard AJ (2016) Electrocatalytic Activity of Individual Pt Nanoparticles Studied by Nanoscale Scanning Electrochemical Microscopy. J Am Chem Soc 138:8560–8568. doi: 10.1021/jacs.6b03980

18. Gabrielli C, Ostermann E, Perrot H, Vivier V, Beitone L, Mace C (2005) Concentration mapping

around copper microelectrodes studied by scanning electrochemical microscopy. Electrochem commun 7:962–968. doi: 10.1016/j.elecom.2005.06.018

19. Izquierdo J, Eifert A, Kranz C, Souto RM (2017) In situ investigation of copper corrosion in acidic chloride solution using atomic force- scanning electrochemical microscopy. Electrochim Acta 247:588–599. doi: 10.1016/j.electacta.2017.07.042

20. Asserghine A, Filotás D, Nagy L, Nagy G (2017) Scanning electrochemical microscopy investigation of the rate of formation of a passivating TiO 2 layer on a Ti G4 dental implant. Electrochem commun. doi: 10.1016/j.elecom.2017.08.018

21. Izquierdo J, Fernández-Pérez BM, Eifert A, Souto RM, Kranz C (2015) Simultaneous Atomic Force-Scanning Electrochemical Microscopy (Afm-Secm) Imaging of Copper Dissolution. Electrochim Acta 201:320–332. doi: 10.1016/j.electacta.2015.12.160

22. Izquierdo J, Santana JJ, González S, Souto RM (2010) Uses of scanning electrochemical microscopy for the characterization of thin inhibitor films on reactive metals: The protection of copper surfaces by benzotriazole. Electrochim Acta 55:8791–8800. doi: 10.1016/j.electacta.2010.08.020

23. Izquierdo J, Santana JJ, González S, Souto RM (2012) Scanning microelectrochemical characterization of the anti-corrosion performance of inhibitor films formed by 2-mercaptobenzimidazole on copper. Prog Org Coatings 74:526–533. doi: 10.1016/j.porgcoat.2012.01.019

24. Li C, Li L, Wang C (2014) Study of the inhibitive effect of mixed self-assembled monolayers on copper with SECM. Electrochim Acta 115:531–536. doi: 10.1016/j.electacta.2013.11.029

25. Mansikkamäki K, Ahonen P, Fabricius G, Murtomäki L, Kontturi K (2005) Inhibitive Effect of Benzotriazole on Copper Surfaces Studied by SECM. J Electrochem Soc 152:B12–B16. doi: 10.1149/1.1829413

26. Pähler M, Santana JJ, Schuhmann W, Souto RM (2011) Application of AC-SECM in corrosion science: Local visualisation of inhibitor films on active metals for corrosion protection. Chem - A Eur J 17:905–911. doi: 10.1002/chem.201000689

27. Santana JJ, Pähler M, Schuhmann W, Souto RM (2012) Investigation of copper corrosion inhibition with frequency-dependent alternating-current scanning electrochemical microscopy.

Chempluschem 77:707–712. doi: 10.1002/cplu.201200091

28. Ramírez-Cano JA, Veleva L, Souto RM, Fernández-Pérez BM (2017) SECM study of the pH distribution over Cu samples treated with 2-mercaptobenzothiazole in NaCl solution. Electrochem commun 78:60–63. doi: 10.1016/j.elecom.2017.04.005

29. Radisic A, Lühn O, Philipsen HGG, El-Mekki Z, Honore M, Rodet S, Armini S, Drijbooms C, Bender H, Ruythooren W (2011) Copper plating for 3D interconnects. Microelectron Eng 88:701–704. doi: 10.1016/j.mee.2010.06.030

30. Iffelsberger C, Vatsyayan P, Matysik F-M (2017) Scanning Electrochemical Microscopy with Forced Convection Introduced by High-Precision Stirring. Anal Chem 89:1658–1664. doi: 10.1021/acs.analchem.6b03764

31. Zhang B, Galusha J, Shiozawa PG, Wang G, Bergren AJ, Jones RM, White RJ, Ervin EN, Cauley CC, White HS (2007) Bench-top method for fabricating glass-sealed nanodisk electrodes, glass nanopore electrodes, and glass nanopore membranes of controlled size. Anal Chem 79:4778–4787. doi: 10.1021/ac070609j

32. Lee C, Miller CJ, Bard AJ (1991) Scanning electrochemical microscopy: preparation of submicrometer electrodes. Anal Chem 63:78–83. doi: 10.1021/ac00001a016

33. Park K-S, Kim S (2010) Seedless Copper Electrodeposition onto Tungsten Diffusion Barrier. J Electrochem Soc 157:D609–D613. doi: 10.1149/1.3491351

34. Vargas Llona LD, Jansen HV, Elwenspoek MC (2006) Seedless electroplating on patterned silicon. J Micromech Microeng 16:S1–S6. doi: 10.1088/0960-1317/16/6/s01

35. Galceran J, Cecı J, Puy J (2000) Analytical Expressions for Feedback Currents at the Scanning Electrochemical Microscope. J Phys Chem B 104:7993–8000. doi: 10.1021/jp001564s

36. Mirkin M V., Wang Y (2012) 5.2 Feedback Mode of SECM Operation. In: Bard AJ, Mirkin M (eds) Scanning electrochemical microscopy. CRC Press, pp 76–96

37. Sheffer M, Mandler D (2008) Why is copper locally etched by scanning electrochemical microscopy? J Electroanal Chem 622:115–120. doi: 10.1016/j.jelechem.2008.05.005

4.2 Probe approach curves on barrier films on semiconductor substrates

4.2.1 Introduction

Since the introduction of the damascene process by IBM in 1997, copper (Cu) plating has become an integral part for the production of metallization layers in semiconductor industry. These conductive layers are formed by electrodeposition from an acidic Cu electrolyte containing various organic additives on a previously deposited Cu seed layer as starting layer. The seed layer is usually deposited in combination with a thin barrier layer by physical vapor deposition (PVD), chemical vapor deposition (CVD) or atomic layer deposition (ALD). This barrier layer of tantalum (Ta), tantalum nitride (TaN), tungsten nitride (W_xN) or titanium nitride (TiN) has the protective function of inhibiting the Cu diffusion into the surrounding dielectric and oxides [1]. With the continuous process of miniaturization of feature sizes, it is more and more difficult to obtain a defect-free and homogenous seed layer in trenches or vias with the aforementioned techniques [2]. Hence, new methods are developed to address this topic. One promising approach is the direct electrodeposition of Cu on the barrier thin film. In order to gain insight into the early stages of this of electrocrystallization process, current transients are evaluated [3]. The disadvantage of this procedure is that only areal electrochemical information of the growth process can be obtained. In this context, it was successfully demonstrated that scanning electrochemical microscopy (SECM) is a promising electroanalytical tool for the local characterization of semiconductor industry relevant materials [4]. In order to assess the capability of this technique for such an application, suitable thin film barrier materials for direct plating and commonly used substrates in SECM are being examined. First results on electrochemical surface characterization with different mediator systems in conventional feedback mode are presented.

4.2.2 Experimental

4.2.2.1 Reagents and materials

All the experiments were carried out using 4 x 4 cm^2 silicon wafer specimen with a thermal grown oxide (SiO_2). Thin films of Pt (50 nm with 30 nm Ti adhesion layer, PVD), Ru (50 nm, PVD), TaN (50 nm, PVD), W (50 nm, CVD), Cu (300 nm with 50 nm TiW adhesion layer, PVD) and TiN (50 nm, PVD) were deposited on the substrates. SECM measurements were performed with three different mediators systems: 1.5 mM ferrocenemethanol (FcMeOH, 99%, ABCR, Karlsruhe, Germany) with 0.2 M potassium nitrate (KNO_3, Analytical grade, Merck, Darmstadt, Germany), 1 mM hexaammineruthenium(III) chloride ($Ru(NH_3)_6Cl_3$, 98%, Sigma-Aldrich, St. Louis, Missouri, USA) with 0.2 M KNO_3, and 1.5 mM potassium octacyanotungstate(IV) dihydrate (($K_4W(CN)_8$)*$2H_2O$, self-synthesis, University Regensburg, Germany) with 0.2 M KNO_3. The aqueous solutions were prepared using deaerated ultrapure water with a resistivity > 18 MΩ·cm. All experimental potentials refer to an Ag/AgCl/3 M KCl reference electrode. The ultramicroelectrodes (UME) with an electrode diameter of 25 µm and RG = 10 were fabricated from Pt wires with the same size (99.99%, Goodfellow, Huntingdon, England) and soda lime glass capillaries following the method described in [5]. Electrode dimensions were determined from negative feedback curves towards a glass slide utilizing the theoretical feedback model of [6].

4.2.2.2 Recording of approach curves

SECM studies were performed with a special multipurpose cell for wafer-based samples with a Teflon cup placed above its opening in combination with a commercial SECM CH Instruments CHI920C (Austin, Texas). The measurements were carried out in a four-electrode configuration with the UME as probe, an Ag/AgCl/3 M KCl as reference electrode, a Pt wire as counter electrode and the multipurpose cell containing the thin film as substrate electrode as published in [4]. The setup was placed in a laboratory constructed Faraday cage. Before each measurement session, the substrate electrode was levelled with an integrated circular bubble. For the acquisition of reproducible approach curves, a defined scan length was set by carefully placing the UME on the substrate and retracting the UME by 400 µm in z-direction before placing the mediator in the cell. Since the interaction between the mediator and the surface of the thin films on the silicon wafer specimen was unknown, the approach curves were recorded with a constant

scan rate of 2.5 µm/s (z_{incr} = 0.5 µm, t_{incr} = 0.2 s). All measurements were carried out without substrate biasing with E_{tip} = 0.45 V in FcMeOH mediator, E_{tip} = 0.5 V in $Ru(NH_3)_6Cl_3$ mediator and E_{tip} = -0.2 V in $(K_4W(CN)_8)*2H_2O$ mediator. Each measurement was carried out with a new substrate in order to reduce the risk of a mediator-based modification of the surface influencing the measurement results and was repeated two times. The tip-to-substrate distance was calculated from the signal change arising from the contact of the tip with the substrate.

4.2.3 Result and discussion

Approach curves towards thin films of Pt, Ru, TaN, W, Cu, TiW, TiN and SiO_2 thin films on Si wafer specimen were recorded in FcMeOH, $Ru(NH_3)_6Cl_3$ and $(K_4W(CN)_8)*2H_2O$ mediator. These three mediators were selected due to their different interaction with the surface. During this process, the tip-generated oxidized species of FcMeOH and $(K_4W(CN)_8)*2H_2O$ are reduced and the tip-generated reduced species of $Ru(NH_3)_6Cl_3$ is oxidized on the conductive thin film surface. The normalized approach curves and theoretical negative [6] and positive [7] feedback curve (r_{tip} = 12.5 µm, RG = 10) are plotted in Fig. 4.7.

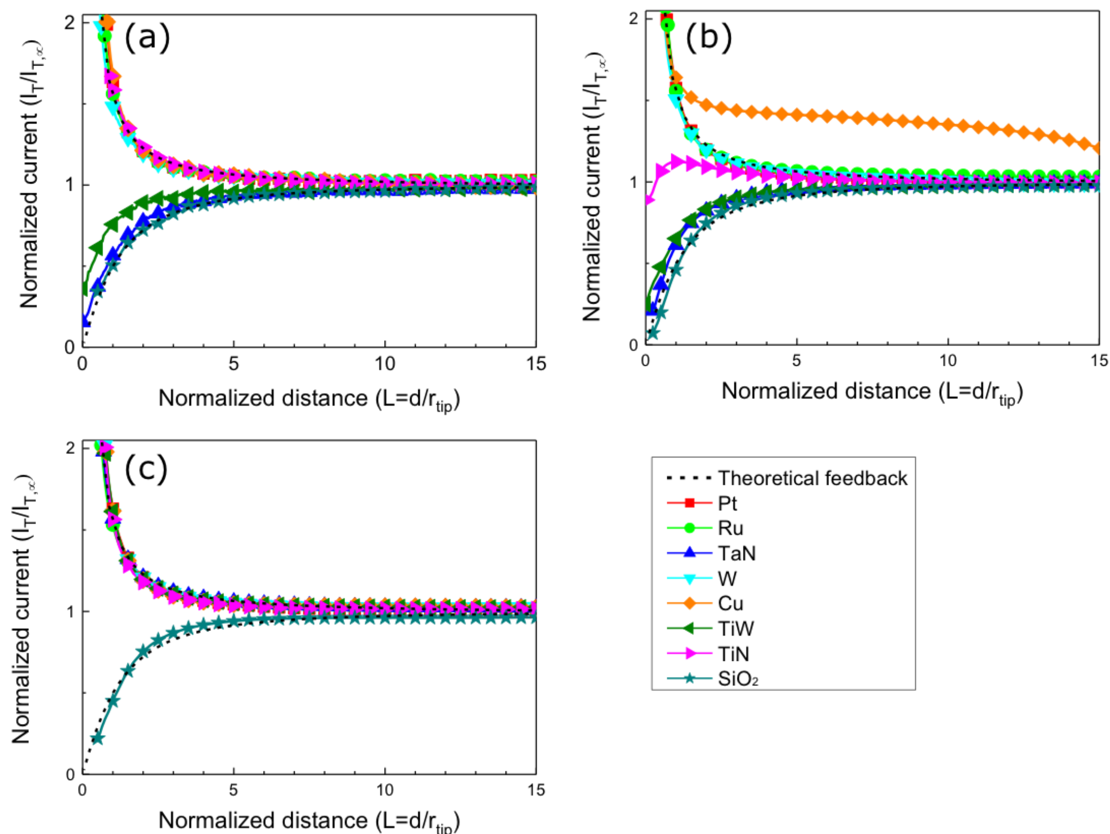

Figure 4.7: Approach curves towards the surface of various thin films on a Si substrate recorded with an ultramicroelectrode (r_{tip} = 12.5 µm, RG = 10) using different mediator solutions. Thin films: Pt (red), Ru (green), TaN (blue), W (pale blue), Cu (orange), TiW (dark green), TiN (pink) and SiO_2 (cobalt). Experimental conditions: (a) 1.5 mM FcMeOH/0.2 M KNO_3 (E_{tip} = 0.45 V), (b) 1.5 mM $K_4[W(CN)_8]$/0.2 M KNO_3 (E_{tip} = 0.5 V) and (c) 1 mM $Ru(NH_3)_6Cl_3$/0.2 M KNO_3 (E_{tip} = -0.2 V) The theoretical (positive and negative) feedback are plotted in black.

As it is observable from the approach curves, the obtained feedback responses on the thin film materials differ significantly between the utilized mediators. In order to be able to distinguish between the electrochemical information and measuring-related surface interactions in feedback mode, a systematic classification of the measured current responses was performed. On this occasion, the current curves are categorized into positive (pos) and negative (neg) feedback responses for current increase and current decrease towards the surface, respectively. Furthermore, a classification into diffusion-controlled (dif) and kinetically controlled (kin) reaction regimes was carried out. Here, a kinetically controlled interaction of the mediator is given, when the measured approach curve is deviating from the calculated approach curve

for diffusion-controlled feedback. The classification is illustrated in table 4.1. The results will be discussed separately for each thin film material.

Table 4.1: Categorization of measured current responses on various thin films for different mediators. The obtained feedback of the FcMeOH, $K_3[W(CN)_8]$ and $Ru(NH_3)_6Cl_3$ mediators on Pt, Ru, TaN, W, Cu, TiW, TiN and SiO_2 of Fig. 4.7 were classified into positive (pos) or negative (neg) feedback and were divided in diffusion (dif) or kinetically (kin) controlled reaction regime.

Material	FcMeOH	$K_4[W(CN)_8]$	$Ru(NH_3)_6Cl_3$
Pt	pos, dif	pos, dif	pos, dif
Ru	pos, dif	pos, dif	pos, dif
TaN	neg, dif	neg, dif	pos, dif
W	pos, dif	pos, dif	pos, dif
Cu	pos, dif	pos, kin	pos, dif
TiW	neg, kin	neg, kin	pos, dif
TiN	pos, dif	pos, kin	pos, dif
SiO_2	neg, dif	neg, dif	neg, dif

Platinum and silicone oxide

Pt and SiO_2 thin films were chosen as conductive and isolating reference materials in this study. Accordingly, the approach curves match the calculated positive and negative feedback for all mediators due to the excellent inert properties of both materials.

Ruthenium

The obtained current responses on Ru thin film are in good correspondence with the theoretically calculated positive feedback independent of the utilized mediator. The formation of a native conductive oxide RuO [8,9] does not have an influence on the observed feedback. Consequently, it can be said that the regeneration of the mediator at the surface is diffusion controlled on thin film Ru.

Tantalum nitride

Comparing the current responses between the mediators on TaN thin film in Table 4.1, it is observable that a diffusion controlled negative feedback is achieved for FcMeOH and $K_4[W(CN)_8]$. This measured feedback response does not match with the high conductivity of TaN films. The observed effect can be attributed to the formation of a native insulating oxide Ta_2O_5 in aqueous solution [10,11]. Accordingly, the mediators cannot be regenerated at the substrate surface, which leads to the observed negative feedback. Contrary to FcMeOH and $K_4[W(CN)_8]$, a diffusion controlled positive feedback is obtained for $Ru(NH_3)_6Cl_3$. In this case, the tip-generated reduced species can be regenerated by oxidation at the substrate due to the local reduction of the formed Ta_2O_5 layer.

Tungsten

The feedback responses on W are in good correspondence with the calculated theoretical positive feedback independent of the active mediator species. The formation of a native WO_2 oxide in aqueous solution in the pH range of 2 to 6 [9,12] at open circuit potential has no impact on the measurement due to its good conductivity. As a result, the mediators can be regenerated at the substrate interface in contrast to the case of the insulating Ta_2O_5 surface on TaN thin films.

Copper

The current responses measured in FcMeOH and $Ru(NH_3)_6Cl_3$ on thin film Cu are in good correspondence with the theoretical positive feedback under diffusion control. In this process, it cannot be completely ruled out that the Cu surface may be locally etched by the regeneration of the tip-generated oxidized FcMeOH species as already observed in a previous work [4]. In contrast, the measured current for $K_3[W(CN)_8]$ is much larger than predicted by the theoretical model and does not fit to a kinetically or diffusion-controlled reaction regime. This deviation already starts at a distance of $L = 20$, where no interaction of the mediator with the surface is expected by the theoretical model as shown in Fig. 4.8 a). It can be noted that this effect is associated with a strong areal corrosion of the Cu surface which is depicted in the inlet of Fig. 4.8 b). This effect is not fully understood and a more focused study concerning this topic is required. Therefore, it is not recommended to use $K_4[W(CN)_8]$ for imaging of Cu containing surfaces at open circuit potential due to its strong oxidative properties.

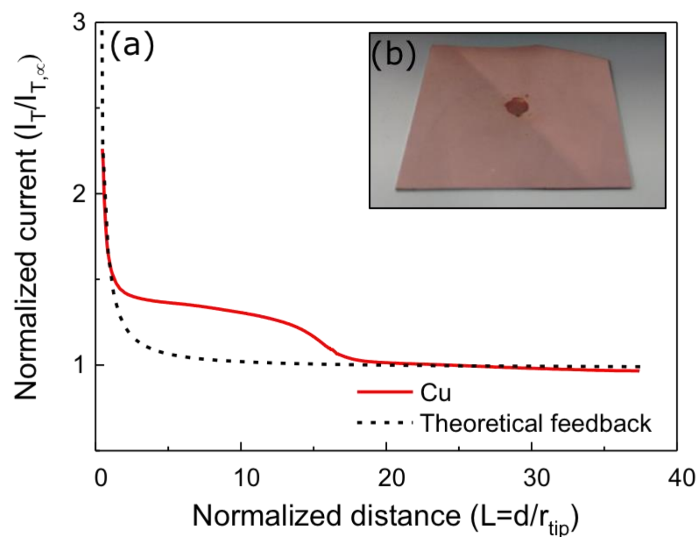

Figure 4.8: (a) Normalized approach curve in $K_3[W(CN)_8$ towards thin film of Cu on a silicon substrate. Experimental parameters: E_{tip} = 0.5 V, $E_{substrate}$ = OCP, scan rate 0.5 µm/s (r_{tip} = 12.5 µm, RG = 10), mediator: 1.5 mM $K_4[W(CN)_8]$/0.2 M KNO_3. (b) Embedded graph: Cu thin film after measurement. Strong corrosion of the mediator exposed Cu surface at the center of the sample.

Titanium tungsten

The approach curves towards the conductive TiW thin films show a similar behavior as the curves recorded towards the TaN thin film. Again, negative feedback is obtained with FcMeOH and $K_4[W(CN)_8]$ and a positive feedback with $Ru(NH_3)_6Cl_3$. The only difference between the results lies in the fact that the negative current responses are slightly differing from the theoretical calculated curves for TiW thin films. Accordingly, it can be assumed that the regeneration of the active species of FcMeOH and $K_3[W(CN)_8]$ mediator at the TiW surface are under kinetical control. This observed effect can be explained with the help of Pourbaix-diagrams for Ti [9,13,14]. Due to the formation of a semiconductive TiO_2 layer in aqueous solution, the electron transfer is partially hindered causing the effect observed in the negative feedback curves [15]. The positive feedback for $Ru(NH_3)_6Cl_3$ follows the same explanation as in the case of the TaN thin film.

Titanium nitride

The obtained approach curves with FcMeOH and $Ru(NH_3)_6Cl_3$ towards the TiN surface are consistent with the theoretical calculation for the positive feedback. Therefore, it can be said that the regeneration of these mediators is diffusion controlled without any interfering influences of an oxide formation in aqueous solution. In contrast, the current response obtained with $K_4[W(CN)_8]$ mediator deviates significantly from the theoretical predictions. This effect can be explained by using the previously obtained results for thin film Cu. In this context, the presented investigations have shown that $K_3[W(CN)_8]$ has strong oxidative properties that cause the surface of Cu to corrode. Consequently, it is possible that the surface of TiN may become oxidized in $K_3[W(CN)_8]$ mediator [14]. As in the case of TiW thin film, the formation of TiO_2 is limiting the electron transfer. As a result, the regeneration of the active mediator species is under kinetic control at the substrate interface [15].

4.2.4 Conclusion

Electrochemical surface characterization of relevant thin film materials in semiconductor industry in classical feedback mode is presented. Based on the obtained results, it can be concluded that surface oxide formation in aqueous solution has a significant impact on the current response obtained in feedback mode. Additionally, it must be considered that a mediator-based modification of the surface can occur during measurements which is expressed by the formation of a metal oxide or surface corrosion. Consequently, it is recommended to bias the semi-precious metal thin films during measurement in feedback mode to avoid the effects described above. After elimination of these disrupting influences, the regeneration of the active mediator species will be under diffusion-control.

References

[1] M. Baklanov, P.S. Ho, E. Zschech, Advanced interconnects for ULSI technology, John Wiley & Sons, 2012.

[2] S. Armini, H. Philipsen, Z. El-Mekki, A. Redolfi, A. Van Ammel, A. Radisic, W. Ruythooren, others, Seedless Copper Electrochemical Deposition on Barrier Materials as a Replacement/Enhancement for PVD Cu Seed Layers in HAR TSVs, in: Meet. Abstr., 2010: p. 1280.

[3] M. Sun, T.J.O. Keefe, The Effect of Additives on the Nucleation and Growth of Copper onto Stainless Steel Cathodes, Metall. Trans. B. 23 (1992) 591–599. doi:10.1007/BF02649719.

[4] P. Hanekamp, W. Robl, F.M. Matysik, Development and application of a multipurpose electrodeposition cell configuration for studying plating processes on wafer specimen and for characterizing surface films by scanning electrochemical microscopy, J. Appl. Electrochem. 47 (2017) 1305–1312. doi:10.1007/s10800-017-1124-8.

[5] C. Lee, C.J. Miller, A.J. Bard, Scanning electrochemical microscopy: preparation of submicrometer electrodes, Anal. Chem. 63 (1991) 78–83. doi:10.1021/ac00001a016.

[6] R. Cornut, C. Lefrou, A unified new analytical approximation for negative feedback currents with a microdisk SECM tip, J. Electroanal. Chem. 608 (2007) 59–66. doi:10.1016/j.jelechem.2007.05.007.

[7] R. Cornut, C. Lefrou, New analytical approximation of feedback approach curves with a microdisk SECM tip and irreversible kinetic reaction at the substrate, J. Electroanal. Chem. 621 (2008) 178–184. doi:10.1016/j.jelechem.2007.09.021.

[8] U. Emekli, A.C. West, Effect of additives and pulse plating on copper nucleation onto Ru, Electrochim. Acta. 54 (2009) 1177–1183. doi:10.1016/j.electacta.2008.08.065.

[9] M. Pourbaix, Atlas of electrochemical equilibria in aqueous solution, NACE. 307 (1974).

[10] E. McCafferty, Introduction to corrosion science. 2010, Alexandria: Springer. (n.d.).

[11] S. Ezhilvalavan, T.-Y. Tseng, Electrical properties of Ta 2 O 5 thin films deposited on Ta, Appl. Phys. Lett. 74 (1999) 2477–2479.

[12] A. Gulino, S. Parker, F.H. Jones, R.G. Egdell, Influence of metal--metal bonds on electron spectra of MoO2 and WO2, J. Chem. Soc. Faraday Trans. 92 (1996) 2137–2141.

[13] V.M.C.A. de Oliveira, C. Aguiar, A.M. Vazquez, A.L.M. Robin, M.J.R. Barboza, Corrosion Behavior Analysis of Plasma-assited PVD Coated Ti-6Al-4V alloy in 2 M NaOH Solution, Mater. Res. 20 (2017) 436–444.

[14] Y. Ju, M. Wang, Y. Wang, S. Wang, C. Fu, Electrical properties of amorphous titanium oxide thin films for bolometric application, Adv. Condens. Matter Phys. 2013 (2013).

[15] A. Asserghine, D. Filotás, L. Nagy, G. Nagy, Scanning electrochemical microscopy investigation of the rate of formation of a passivating TiO 2 layer on a Ti G4 dental implant, Electrochem. Commun. (2017). doi:10.1016/j.elecom.2017.08.018.

4.3 Material contrast studies of conductive thin films on semiconductor substrates using scanning electrochemical microscopy

Patrick Hanekamp, Timo Raith, Christian Iffelsberger, Tobias Zankl, Werner Robl and Frank-Michael Matysik

Journal of Applied Electrochemistry (2019): 1-9

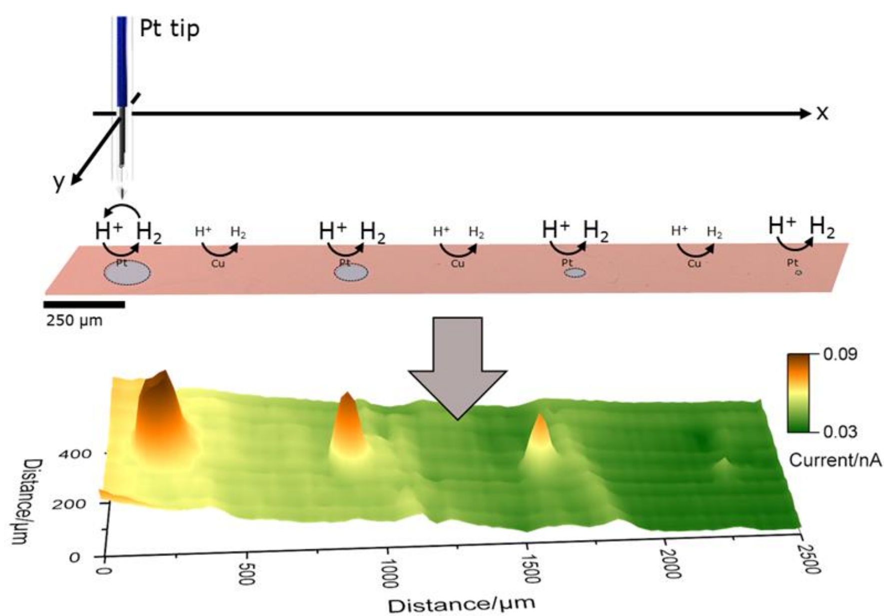

Abstract

In this paper a mediator-free scanning electrochemical microscopy (SECM) imaging concept is presented, which is capable of generating high electrochemical contrast and high spatial resolution between two conductive materials. The methodical approach is based on the hydrogen evolution reaction which shows potential dependent material selectivity. Various conductive thin films deposited on silicon substrates were studied. The investigated materials included copper, ruthenium, platinum, tantalum nitride, and titanium nitride. The hydrogen evolution was studied with chronoamperometry ($E_{substrate}$ = -1 V vs. Ag/AgCl/3 M KCl) to characterize the material selectivity of this reaction for the above listed thin films. SECM imaging in the substrate generation-tip collection (SG/TC) mode was carried out and applied to study the boundary regions of thin copper films in combination with the aforementioned thin film materials. In

addition, the spatial resolution of hydrogen based SG/TC SECM imaging was characterized using lithographically fabricated platinum/copper structures as test substrates. For comparison, the common feedback mode was also applied for SECM imaging of the conducting thin film combinations. It was found, that only the hydrogen based SG/TC mode enabled SECM imaging with clear material contrast between different conductive materials which was not possible in the feedback mode.

4.3.1 Introduction

In semiconductor manufacturing copper (Cu) based metallization is typically realized by electrochemical deposition from an acidic electrolyte with various additives on a Cu seed layer. This conductive seed layer acts as a starting layer for the electrolytic deposition and is formed by chemical vapor deposition (CVD) or physical vapor deposition (PVD) on a silicon substrate. A deposition of a thin barrier layer of tungsten nitride (WxN), titanium nitride (TiN), tantalum (Ta), or tantalum nitride (TaN) is carried out prior to the Cu seed coating [1] to inhibit the Cu diffusion into the surrounding dielectric. With the ongoing trend of downscaling feature sizes, a conformal and defect-free seed layer coating of structured surfaces is challenging when applying conventional methods [2,3]. Consequently, new deposition techniques are under evaluation for direct electroplating of the Cu metallization on barrier films like ruthenium (Ru) [4-6], TaN [7,8], TiN [9–11], W2N [12], osmium (Os) [13] or iridium (Ir) [14]. Even though various approaches are investigated for direct electrochemical deposition of Cu on these barriers [15], the absence of studies on local electrochemical surface characterization by scanning electrochemical microscopy (SECM) of such conductive reactive materials is identifiable. One possible reason is the fact that the measuring mode most commonly used in SECM, the feedback mode, has its strength in the high local contrast between conductive and insulating surfaces [16–18]. This can be attributed to the measurable conductivity dependent surface interaction of the electrochemical active species. In this process, a signal increase is obtained over conductive surfaces as the species can be regenerated. Contrary, a signal decrease is received over insulating areas which act as blocking sites. As a consequence, this mode of operation reaches its limit in resolution as materials with similar conductivity are studied. Hence, a measurable material selective reaction is required to distinguish between the electrochemical activities of different conductive materials in surface characterization with SECM. One approach is the usage of the material selective hydrogen evolution reaction (HER) [19,20] to generate the reactive species. Furthermore, using such a mediator-free system is advantageous in terms of prevention of a mediator-based surface

interaction. HER as measurable reaction in SECM is realizable with the generation collection operation mode. Thereby, hydrogen can be either generated at the tip and collected at the substrate (TG/SC) [21–25] or in converse direction (SG/TC) [26,27]. Comparing both modes, SG/TC is more promising because biasing the substrate on a reductive potential for hydrogen evolution is simultaneously inhibiting thin film corrosion and oxide formation during measurement. Concerning this topic, it was already shown that HER SG/TC is an applicable method for electrochemical surface characterization at very high hydrogen evolution rates with forced convection applied to the system [28]. In this paper, we introduce an imaging concept based on HER SG/TC mode, which is capable of generating high contrast between different conductive thin film materials on a silicon substrate. First results on material selectivity, electrochemical contrast and spatial resolution for semiconductor manufacturing relevant materials are presented.

4.3.2 Experimental

4.3.2.1 Reagents and materials

For all experiments 4 x 3 cm² silicon wafer specimen with a thermally grown oxide (SiO2) were used. Thin layers of TiN (50 nm, PVD), TaN (50 nm, PVD), Ru (50 nm, PVD), Pt (50 nm with 30 nm Ti adhesion layer, PVD) and Cu (300 nm with 50 nm TiW adhesion layer, PVD) were deposited on these substrates. Electrochemical Cu deposition on the above mentioned materials and the composition of the utilized mediators for electrochemical characterization were based on the reagents described in Table 4.2. The aqueous solutions were prepared using ultrapure water with a resistivity > 18 MΩ cm.

Table 4.2: Reagents for electroplating and electrochemical surface characterization with SECM.

Reagent	Manufacturer
copper sulfate pentahydrate ($CuSO_4 \cdot 5H_2O$)	analytical grade, Merck
ammonium citrate ($(NH_4)_3C_6H_5O_7$)	analytical grade, VWR Chemicals
ammonium sulfate ($(NH_4)_2SO_4$)	analytical grade, Merck
ammonia (NH_3)	28%, analytical grade, BASF
sulfuric acid (H_2SO_4)	analytical grade, Merck
hydrochloric acid (HCl)	analytical grade, Merck
potassium hydroxide (KOH)	analytical grade, Honeywell Chemicals
ferrocenemethanol (FcMeOH)	99%, ABCR
hexaammineruthenium(III) chloride ($Ru(NH_3)_6Cl_3$)	98%, Sigma-Aldrich
potassium nitrate (KNO_3)	analytical grade, Merck

All potentials of the electrochemical deposition as well as the SECM studies refer to an Ag/AgCl/3 M KCl reference electrode. The ultramicroelectrodes (UME) were fabricated from soda-lime glass capillaries and 25 µm Pt wire (99.99%, Goodfellow, Huntingdon, England) resulting in an electrode radius of the tip of r_{tip} of 12.5 µm following the procedure described in [29]. Since the ratio between the electrode radius and the surrounding glass mantle (RG value) has a large impact on the measurement results, the utilized UME's were characterized before the investigations. The electrode dimensions were determined from negative feedback approach curves towards a glass slide. The UMEs used for the recording of the approach curves had a RG value of 10. In the case of imaging experiments, UMEs with a RG value of 2 were used.

4.3.2.2 Electroplating experiments for sample preparation

Electrochemical deposition of Cu on thin films of Ru, Pt, TiN, and TaN was carried out with a multipurpose cell as published in [30]. Using this special sample holder, the thin films on the silicon wafer specimen are simultaneously sealed and electrically contacted. Accordingly, only a small circular opening with a diameter d = 4.52 mm was exposed to the electrolyte. The electroplating experiments were performed in three electrode configuration consisting of the multipurpose cell, an Ag/AgCl/3 M KCl reference electrode

and an iridium coated Ti plate as counter electrode. Potentiostatic deposition was carried out without agitation in a Smart Cell 1000w (Yamamoto MS, Tokyo, Japan) using an Autolab PGST302N potentiostat (Metrohm, Herisau, Switzerland) and the copper electrolytes described in Table 4.3. The target Cu film thickness was d_{Cu} = 200 nm ± 50 nm. The thickness of the deposited film was determined using a laser microscope LEXT OSL400 (Olympus, Tokyo, Japan).

Table 4.3 Composition of the electrolytes for thin film Cu electroplating based on [4,31,32,33].

Copper electrolyte	Components	pH value
Standard acidic copper bath	0.63 M $CuSO_4$, 0.3 M H_2SO4, 1.4 mM HCl	pH < 1
Neutral complexed copper bath	0.08 M $CuSO_4$, 0.1 M $(NH_3)_3C_6H_5O_7$	pH = 5.5 (with NH_4OH)
Alkaline copper bath	0.08 M $CuSO_4$, 0.4 M $(NH_4)_2SO_4$	pH = 10 (with NH_4OH)

Large area copper depositions on Ru, Pt, TiN, and TaN were performed with the multipurpose cell according to the following protocols. Electroplating on thin film Ru was carried out following the two-step procedure described in [4]. According to this process, the native oxide layer was removed at -0.3 V for 60 s in 1.8 M H_2SO_4 with a subsequent deposition in the standard acidic copper bath at -0.05 V for 10 s. Electrochemical deposition of Cu on the Pt thin film was carried out without any further sample preparation at -0.3 V for a time of 5 s using the same copper bath. Cu deposition on TiN was adapted from [31] using the neutral complexed copper bath. Cu deposition was carried out without any pretreatment in this electrolyte at -1.3 V for 15 s. Deposition on TaN was based on the method of Starosvetsky et al. [32,33] utilizing an alkaline Cu bath. In this multiple bath process, the native oxide on TaN was removed at -1.9 V for 60 s in 0.9 M KOH. To prevent the formation of a new oxide layer, 1.5 ml of the alkaline Cu bath was added with 57 s pre clean time and the potential was shifted to -1.2 V for 5 s in order to obtain a continuous Cu thin film. Subsequently, the wafer specimen was transferred into the alkaline Cu bath for Cu deposition at -1.2 V for 5 s. Samples with a structured surface were prepared with a lithographic step prior to the electrochemical deposition. The wafer specimen with a Pt thin film were coated with a Microposit S1805 photoresist (DOW Electronic Materials Semiconductor Technologies, Midland, Michigan) in a WS-650MZ-8NPPB spin coater (Laurell Technologies Corporation, North Wales,

Pennsylvania). Textures of a photomask were transferred to the photoresist using a MA56 mask aligner (Süss Microtec AG, Garching, Germany). The exposed resist was subsequently developed in a AZ726MIF developer (MicroChemicals, Ulm, Germany). Cu electroplating on this lithographic patterned Pt surface was carried out with the procedure of the above mentioned large area deposition from the standard acidic copper bath. After deposition, the photoresist was carefully removed with acetone. The patterned Cu thin film consisted of circular structures with varying spot sizes (d_1 = 150 µm, d_2 = 110 µm, d_3 = 75 µm, d_4 = 30 µm, spacing l = 700 µm) on Pt and also the inverse structures of Pt inlets in a Cu film exhibited the same pattern layout.

4.3.2.3 Scanning electrochemical microscopy studies

SECM studies were performed with a measuring cell consisting of a customized Teflon tub placed above the opening of the multipurpose cell in conjunction with a commercially available SECM CH Instruments CHI920C (Austin, Texas) as already described in [30]. The setup was used in a four electrode configuration with the multipurpose cell containing the substrate electrode, the UME as probe, a Pt wire as counter electrode and an Ag/AgCl/3 M KCl as reference electrode. The measuring configuration was placed on a damped working bench inside a laboratory constructed Faraday cage. Prior to each measurement the substrate was leveled with an integrated circular level. The composition of the utilized mediators are summarized in Table 4.4.

Table 4.4: Composition of the mediators for electrochemical surface characterization.

Mediator	Active species	Supporting electrolyte
FcMeOH	1.5 mM FcMeOH	0.2 M KNO_3
$Ru(NH_3)_6Cl_3$	1 mM $Ru(NH_3)_6Cl_3$	0.2 M KNO_3
Mediator-free solution	-	0.2 M KNO_3, 1.4 mM HCl

Probe scan curves in z-direction were carried out with the substrate at open circuit potential in deaerated FcMeOH at an electrode potential of the UME of E_{tip} = 0.45 V or in deaerated $Ru(NH_3)_6Cl_3$ solution at E_{tip} = -0.2 V with a scan rate of 2.5 µm s^{-1} using an UME of r_{tip} = 12.5 µm and RG = 10. The tip-to-substrate

distance was calculated based on the signal change during contact of the tip with the substrate. For chronoamperometric measurements the multipurpose cell was used as working electrode 1 and set to a substrate potential of $E_{substrate}$ = -1.0 V for 600 s in the mediator-free solution. Imaging experiments were carried out after probe approach to a predefined distance towards the substrate. This distance is related to the ratio between the measured tip current and the measured value in bulk solution far away from the substrate as $I_T/I_{T,\infty}$. The UME was approached to $I_T/I_{T,\infty}$ = 140% at E_{tip} = 0.45 V in FcMeOH mediator which corresponds to a tip to substrate distance of d = 15.6 µm. Subsequently, imaging in SG/TC mode was carried out in the mediator-free solution at E_{tip} = -0.1 V and $E_{substrate}$ = -1.0 V with an idle time of t_{idle} = 600 s if not specified otherwise. Afterwards, imaging in feedback mode was performed in FcMeOH mediator at E_{tip} = 0.45 V and $E_{substrate}$ = -0.5 V. The substrate was biased on this negative potential to prevent interaction of the species generated at the tip with the surface of the substrate [34].

4.3.3 Result and discussion

4.3.3.1 Approach curves on conductive thin film layers in feedback mode

Prior to the imaging experiments, the thin films on the Si substrate were electrochemically characterized with SECM in feedback mode. For this reason approach curves were recorded in order to obtain and compare the local electrochemical surface reactivity of the studied materials. These probe scan curves were recorded in FcMeOH and $Ru(NH_3)_6Cl_3$ mediator for unbiased thin films of Ru, Pt, Cu, TiN, TaN, and SiO_2 as described in the experimental section and were compared to theoretical feedback. These two mediator systems were selected due to their difference in surface interaction in feedback mode on conductive surfaces: The tip generated oxidized form of FcMeOH is reduced whereas the tip generated reduced form of $Ru(NH_3)_6Cl_3$ is oxidized. As depicted in Fig. 4.9, the measured approach curves were in good agreement with the calculated negative [35] and positive [36] feedback curve (r_{tip} = 12.5, RG = 10) proving that the reaction of the active species was diffusion controlled. Accordingly, pure positive feedback was observed for both mediator systems on Ru, Pt, Cu, and TiN due to their high conductivity. In contrast to the other thin films, a significant difference in feedback response between FcMeOH and $Ru(NH_3)_6Cl_3$ was observed at the TaN film. For FcMeOH the feedback was negative and for $Ru(NH_3)_6Cl_3$ a positive feedback response was found. This behavior can be attributed to the surface interaction of the active species of the mediators with the Ta_2O_5 surface oxide natively formed at open circuit potential in

aqueous solution. This insulating layer inhibited the regeneration of the tip generated oxidized species generated at the tip, which resulted in a negative feedback during probe approach. In contrast to FcMeOH, the regeneration of the $Ru(NH_3)_6Cl_3$ species generated at the tip led to a local Ta_2O_5 oxide reduction, resulting in a positive feedback. Nevertheless, the obtained results revealed that no electrochemical "material contrast" between the aforementioned conductive materials was to be expected while imaging in feedback mode at a fixed distance L.

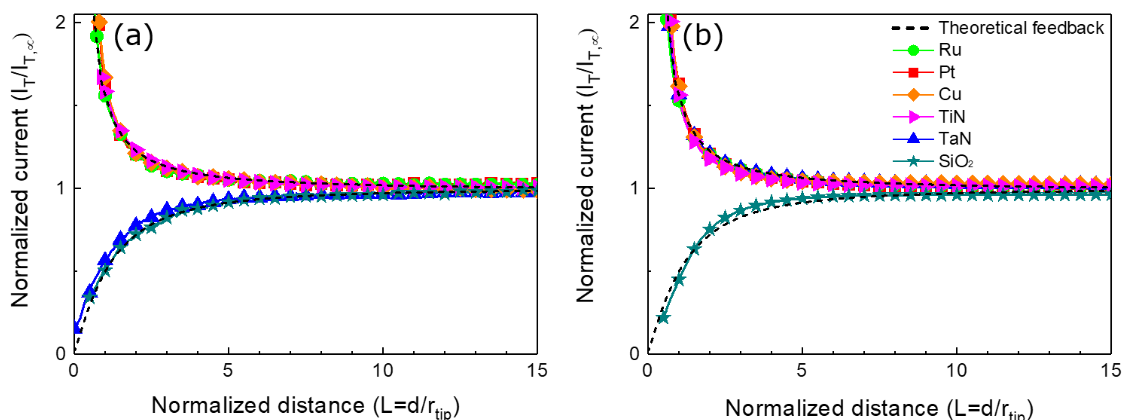

Figure 4.9: Approach curves towards the surface of various thin films on a Si substrate recorded with an ultramicroelectrode (r_{tip} = 12.5 µm, RG = 10). Thin films: Ru (green), Pt (red), Cu (orange), TiN (magenta), TaN (blue). Experimental conditions: (a) 1.5 mM FcMeOH/0.2 M KNO_3 (E_{tip} = 0.45 V) and (b) 1 mM $Ru(NH_3)_6Cl_3$/0.2 M KNO_3 (E_{tip} = -0.1 V). The theoretical (positive and negative) feedback responses are plotted in black.

4.3.3.2 Chronoamperometric transients

According to the approach curves, a measurable material selective reaction is required to distinguish between the electrochemical activities of different conductive materials in surface imaging with SECM. Based on [19], the usage of HER is promising as a material selective reaction. Since hydrogen evolution depends strongly on thin film metals it is suitable to generate local contrast in SECM imaging. For this reason, chronoamperometric measurements were carried out with Ru, Pt, Cu (ECD), Cu (PVD), TiN, and TaN thin films on Si substrates to characterize the material selectivity of this reaction. A suitable substrate potential of $E_{substrate}$ = -1 V was identified by preliminary experiments. Applying this potential reduced the risk of hydrogen embrittlement of metals due to small evolution rates while still providing sufficient

hydrogen formation rates on all investigated semiprecious thin films. The obtained current curves were normalized to the exposed area of the multipurpose cell and were plotted as current density vs time transients in Fig. 4.10. Comparing the transients of the investigated substrates, it can be seen that at a fixed potential the hydrogen evolution rate is strongly dependent on the thin film material specified before. Ru shows the strongest hydrogen evolution followed by Pt, Cu, TiN, and TaN with the lowest signal. Moreover, it was possible to distinguish between Cu (PVD) and Cu (ECD) since the hydrogen evolution was slightly increased on Cu (ECD) in comparison to Cu (PVD). It should be annotated, that the measured current signal was changing until t = 400 s due to growth of the diffusion layer. Consequently, an idle time of t > 400 s was necessary before imaging with SECM to obtain reproducible results.

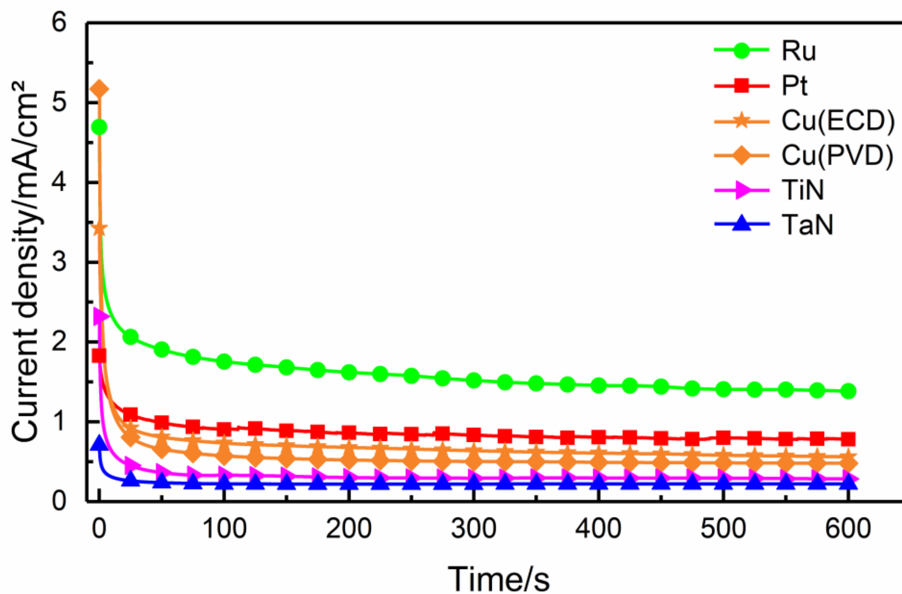

Figure 4.10: Chronoamperometric current transients for various thin films on a Si substrate. Thin films: Ru (green), Pt (red), Cu (ECD) (orange, star symbol), Cu (PVD) (orange, diamond symbol), TiN (magenta), TaN (blue) with a circular exposed area of r = 2.26 mm. Experimental conditions: $E_{substrate}$ = -1.0 V in 0.2 M KNO_3/1.4 mM HCl.

4.3.3.3 Imaging with SECM

Based on the chronoamperometric current transients, material contrast studies were carried out by imaging the boundary region between a thin Cu layer and various semiprecious thin films in HER SG/TC mode. For this reason, a very thin Cu film was electrochemically deposited on Ru, Pt, TiN, and TaN as described in the experimental section. The Cu coated 4 x 3 cm^2 silicon wafer specimen were mounted in the multipurpose cell exposing the boundary region between the thin films to the mediator solution. Since imaging was carried out at a tip to substrate distance of d = 15.6 µm ($I_T/I_{T,\infty}$ = 140%, r_{tip} = 12.5 µm , RG = 2), it was assumed that the influence of the thin Cu film of d_{Cu} = 200 nm ± 50 nm on the topography during imaging is negligible and a superimposition of the local height and the electrochemical activity during imaging was nonexistent. Consequently, the measured local currents represented the activity of the materials during imaging in HER SG/TC and classical feedback mode.

4.3.3.3.1 Comparison of feedback mode and HER SG/TC mode

The boundary region between Ru and Cu was imaged both in HER SG/TG mode at E_{tip} = -0.1 V and $E_{substrate}$ = -1.1 V in mediator-free solution and in feedback mode using FcMeOH as the mediator at E_{tip} = 0.45 V and $E_{substrate}$ = -0.5 V applying a scan rate of 105 µm s^{-1}. Comparing the optical micrograph (a) with the imaged area in HER SG/TC mode (b) and in feedback mode (c) in Fig. 4.11, it can be seen that the boundary region between Cu and Ru was well resolved in SG/TC mode. It was observable, that the measured local current above Cu differed by a factor of 2 from the signal above the Ru surface at $E_{substrate}$ = -1.1 V. This is in good agreement with the transients at t > 400 s depicted in Fig. 2 with a larger current density observed on Ru in comparison to Cu. No contrast was visible in feedback mode as expected from the results of the probe approach curves presented in Fig. 4.9.

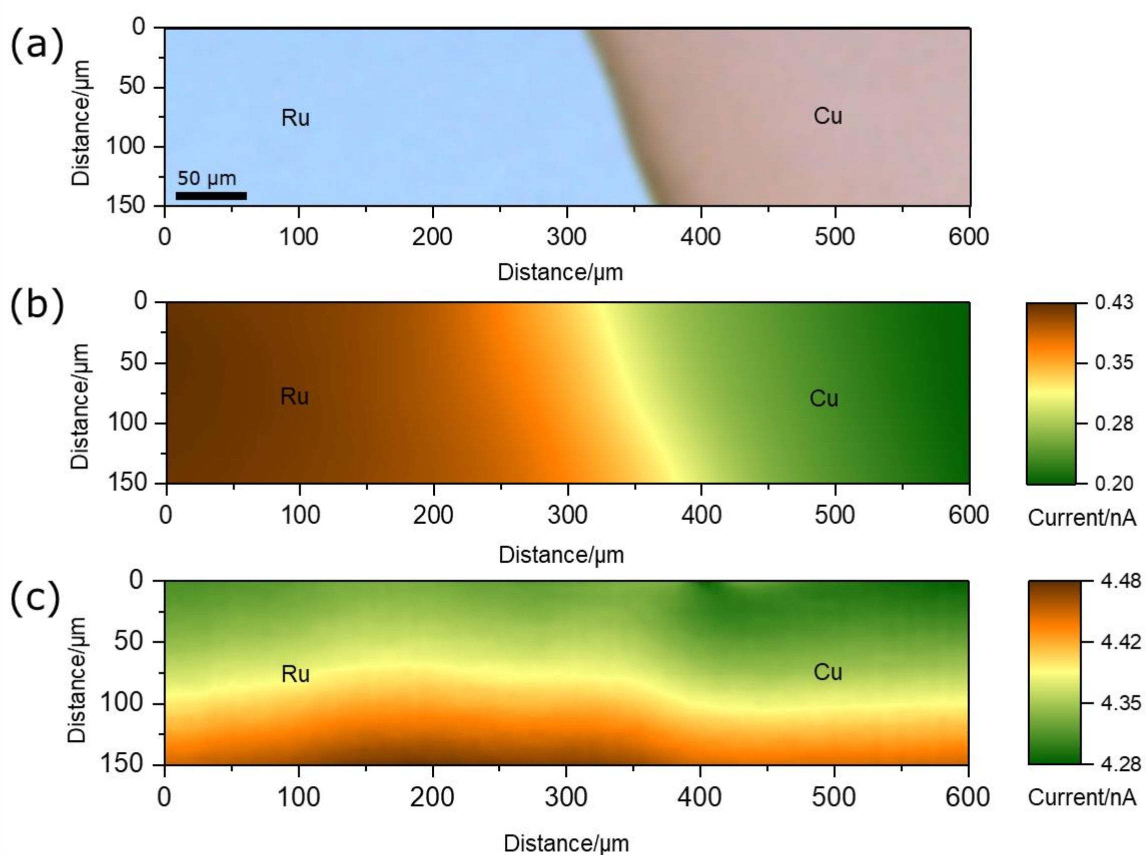

Figure 4.11: SECM image of the boundary region of a Cu thin film on Ru thin film on a Si substrate (a) Optical micrograph of the imaged area, (b) SECM imaging in SG/TC in 0.2 M KNO_3/1.4 mM HCl (E_{tip} = -0.1 V, $E_{substrate}$ = -1.1 V, scan rate: 105 µm s^{-1}), and (c) SECM imaging in feedback mode in 1.5 mM FcMeOH/0.2 M KNO_3 (E_{tip} = 0.45 V, $E_{substrate}$ = -0.5 V, scan rate: 105 µm s^{-1}).

The same SG/TC mode experiments were carried out for different conductive metal combinations of Ru/Cu, Pt/Cu, TiN/Cu, and TaN/Cu at $E_{substrate}$ = -1.0 V. The deposition procedure for this Cu (ECD) thin films is described in the experimental section. In Fig. 4.12 it can be seen that for all imaged layer combinations a clear “material contrast” was achievable with HER SG/TC, which is in good agreement with the current transients in Fig. 4.10.

4.3.3.3.2 Material contrast of different conductive thin films in HER SG/TC mode

The same SG/TC mode experiments were carried out for different conductive metal combinations of Ru/Cu, Pt/Cu, TiN/Cu, and TaN/Cu at $E_{substrate}$ = -1.0 V. The deposition procedure for this Cu (ECD) thin films is described in the experimental section. In Fig. 4.12 it can be seen that for all imaged layer combinations a clear "material contrast" was achievable with HER SG/TC, which is in good agreement with the current transients in Fig. 4.10.

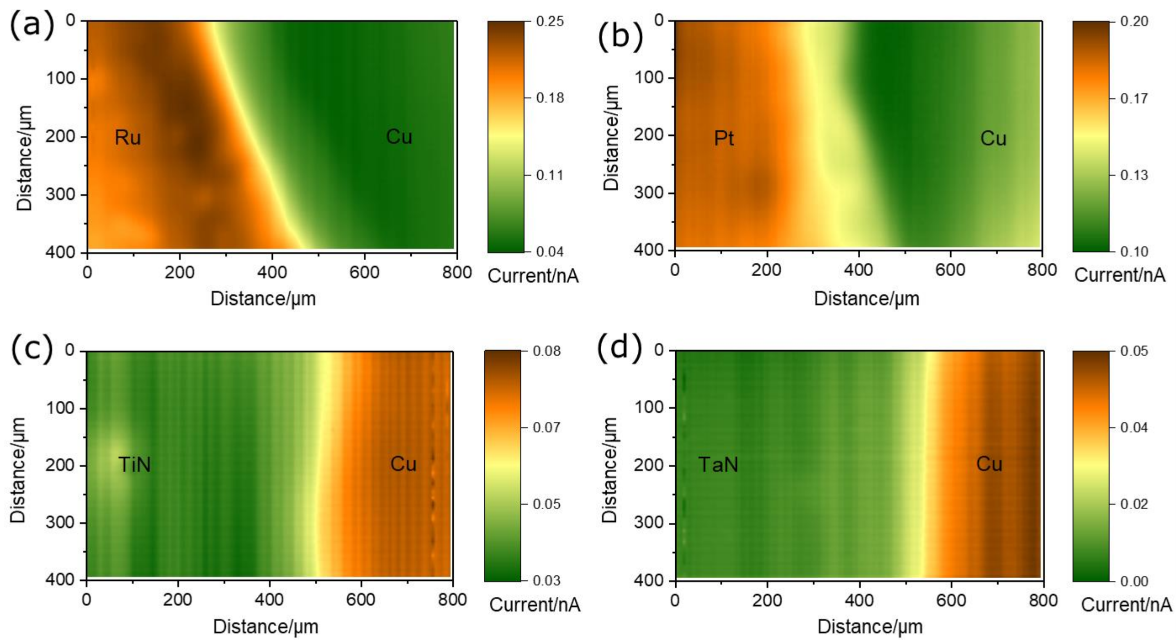

Figure 4.12: SECM image of the boundary region of Cu film on various thin film materials on a Si substrate. Thin films: (a) Ru, (b) Pt, (c) TiN and (d) TaN. Experimental conditions: E_{tip} = -0.1 V, $E_{substrate}$ = -1.0 V in 0.2 M KNO_3/1.4 mM HCl, scan rate 105 µm s^{-1}.

A quantification of the electrochemical material contrast can be expressed by adapting the interferometric visibility (Michelson visibility) [37] to the SECM measurements in SG/TC mode. Using equation 46, the material contrast Cm between two materials can be calculated using the measured current above the first material im1 and the second material im2. The obtained contrast value is independent of total current.

$$C_m = \frac{|I_{m1} - I_{m2}|}{(I_{m1} + I_{m2})/2} \tag{46}$$

Thus, the material contrast was calculated from the HER TG/SC measurements of Fig. 4.12. A high contrast is expressed by a large value and a contrast free situation by zero. The obtained results are depicted in Table 4.2.

Table 4.2: Material contrast C_m of thin film combinations calculated with equation 46 based on the imaging studies in HER SG/TC of Fig. 4.12.

Material combination	C_m(HER SG/TC)
TaN/Cu	1.76
Ru/Cu	1.44
TiN/Cu	0.88
Pt/Cu	0.72

Comparing the calculated C_m values, there is an obvious a trend is observable with TaN/Cu exhibiting the highest contrast and Pt/Cu the lowest one. This result is in good agreement with the results of the chronoamperometric studies in Fig. 4.10. Accordingly, HER SG/TC is a viable option to image local electrochemical activity of different conductive semiprecious thin film materials.

4.3.3.3.3 Characterization of resolution in HER SG/TC mode

In order to evaluate the resolution capabilities of imaging in HER SG/TC mode, defined structures of Cu and Pt thin films were investigated. Surface structuring was carried out by electrochemical Cu deposition using a lithographic process step as described before. For this study the Pt/Cu system was used as it showed the lowest "electrochemical" contrast of the material combinations presented in Table 4.2. Sample preparation and imaging of these structures both in HER SG/TC and in feedback mode was carried out as described in the experimental section. As can be seen in Fig. 5, the circular Pt inlets in the Cu thin film were well resolved in HER SG/TC recordings (b) at a scan rate of 416 µm s^{-1}. The circular structures with a diameter of d_1 = 150 µm, d_2 = 110 µm and d_3 = 75 µm were in good agreement with the microscopic image (a). The resolution was not influenced by diffusive broadening effects because the hydrogen

evolution on Pt and Cu was in the same current range. The smallest Pt spot with d_4 = 30 µm could barely be resolved as the structure size was in the range of the tip dimension r_{tip} = 12.5 µm (RG = 2). Furthermore, streaks of contaminations were observable, which were not visible in the microscopic image. Hence, HER SG/TC is very sensitive to surface impurities as these spots are acting as blocking sites for hydrogen generation. The impurities could be attributed to the removal step of the photoresist in the sample preparation process. In contrast to SG/TC mode, the structures could not be resolved in feedback mode (c) due to the similar conductivity of Pt and Cu as already indicated in Fig. 4.9.

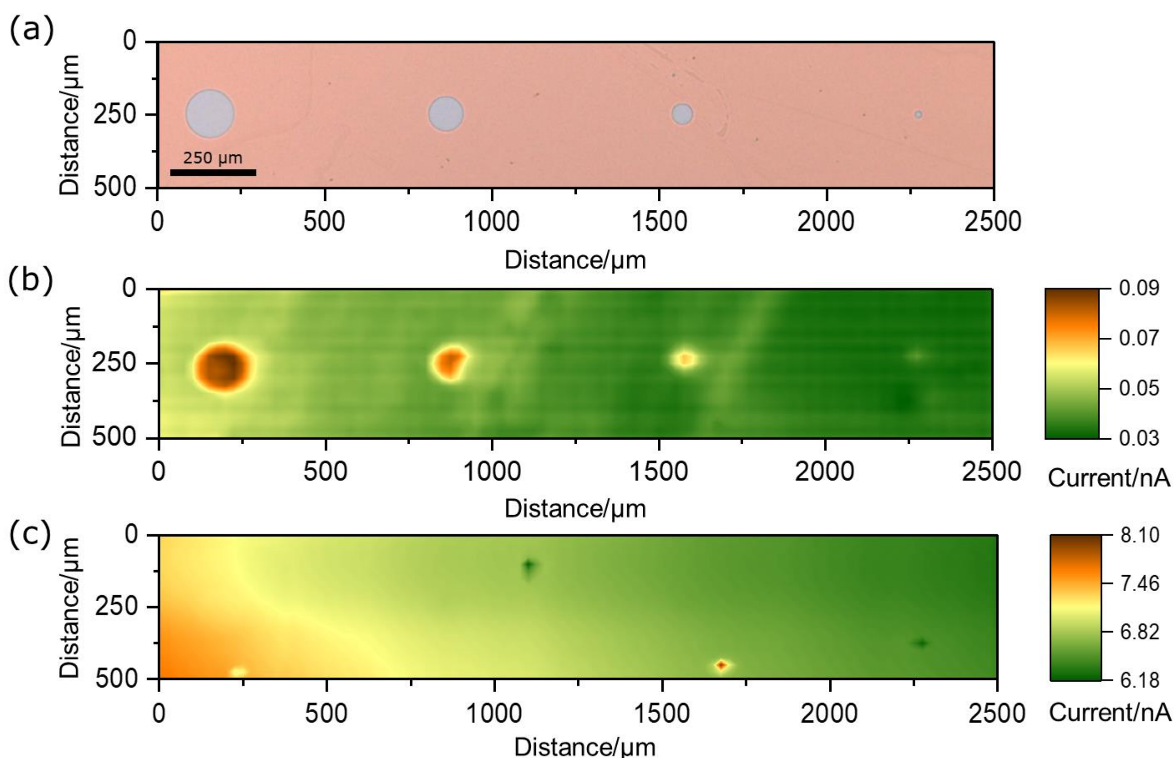

Fig. 4.13: SECM image of a Cu thin film with lithographically formed Pt inlets of varying diameters on a Si substrate. (a) Optical micrograph of the imaged area, (b) SECM imaging in SG/TC in 0.2 M KNO_3/1.4 mM HCl (E_{tip} = -0.1 V, $E_{substrate}$ = -1.0 V, scan rate: 416.6 µm s^{-1}) and (c) SECM imaging in feedback mode in 1.5 mM FcMeOH/0.2 M KNO_3 (E_{tip} = 0.45 V, $E_{substrate}$ = -0.5 V, scan rate: 100 µm s^{-1})

Subsequently, HER SG/TC and feedback mode were used to image the inverted thin film pattern with the same structure sizes as depicted in Fig. 4.14. These pattern of lithographically formed Cu spots on a Pt surface were selected to study the impact of structure shape on spatial resolution. In comparison to Fig. 4.13, imaging in HER SG/TC was carried out at $E_{substrate}$ = -0.7 V due to strong hydrogen generation above

the Cu thin film spots. No sharp resolution of the structures could be obtained at more negative potentials as the tip movement caused some distortion during surface imaging. Consequently, the previously described effect can still be observed at the much lower potential of $E_{substrate}$ = -0.7 V.

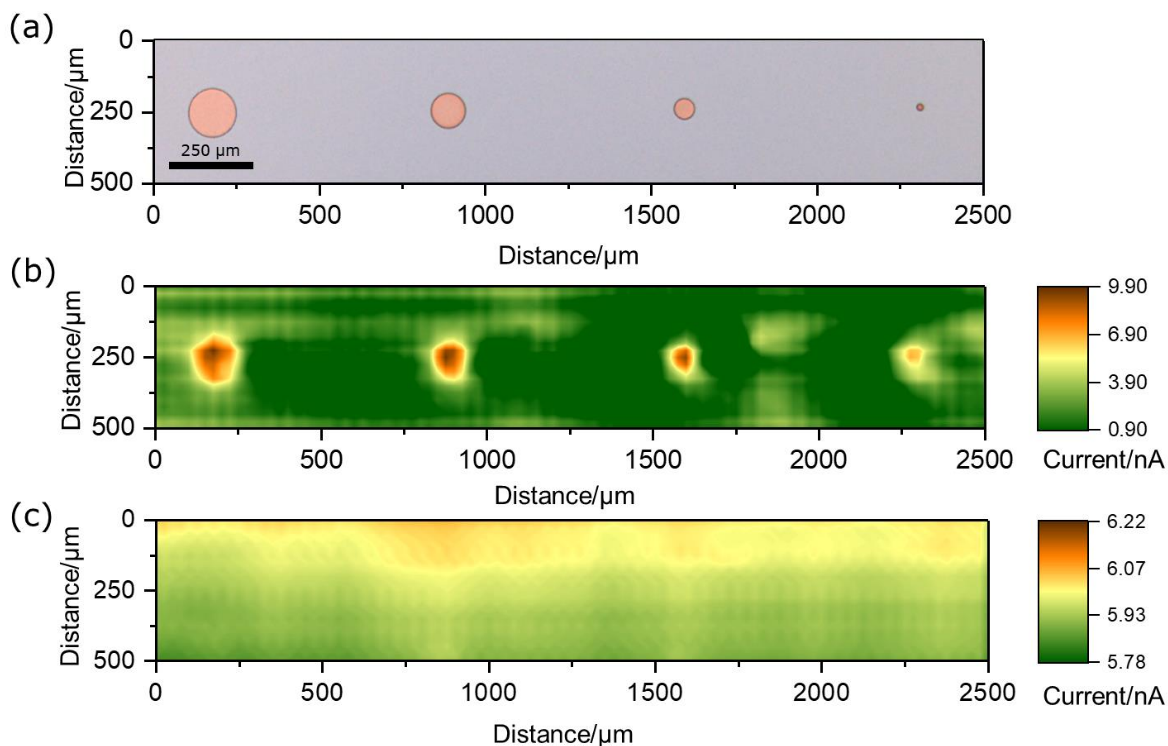

Fig. 4.14: SECM image of lithographically formed thin film Cu spots with varying diameters on a thin film Pt surface on Si substrate. (a) Optical micrograph of the imaged area, (b) SECM imaging in SG/TC in 0.2 M KNO_3/1.4 mM HCl (E_{tip} = -0.1 V, $E_{substrate}$ = -0.7 V, scan rate: 416.6 µm s^{-1}) and (c) SECM imaging in feedback mode in 1.5 mM FcMeOH/0.2 M KNO_3 (E_{tip} = 0.45 V, $E_{substrate}$ = -0.5 V, scan rate: 100 µm s^{-1}).

Comparing the measured current above both materials in Fig. 4.14 (a) it can be concluded that hydrogen evolution is 10 times more intense on Cu in comparison to Pt. Furthermore, the strong hydrogen evolution on the Cu surface was responsible for the distortion of the imaged patterns in SG/TC mode. The circular Cu structures were enlarged due to diffusive broadening of hydrogen towards the Pt surface with a much lower hydrogen evaluation rate. The effect was most pronounced at the smallest Cu spot with d_4 = 30 µm in comparison to the microscopic image in Fig. 4.14 (a). Nonetheless, contrast between Cu and Pt was

possible in HER SG/TC in contrast to feedback mode, shown in Fig. 4.14 (c). Comparing Fig. 4.13 (b) and Fig. 4.14 (b), it can be concluded that hydrogen evolution is not merely dependent on the surface potential but also on material combination (Ru on Cu, Cu on Ru).

4.3.3.4 Conclusion

A mediator-free SECM concept with clear contrast between materials with similar conductivity is presented. This methodical approach is necessary since the conventional feedback mode shows limited resolution. Based on chronoamperometric investigations on Ru Cu, Pt, TiN, and TaN, it was shown that hydrogen evolution is a suitable material selective reaction. Thus, imaging of the boundary region between Cu and the aforementioned thin films in HER SG/TC resulted in a sharp contrast between various conducting materials. In addition, lithographically structured conductive surfaces with defined pattern have been studied to characterize the attainable resolution. It was found that high spatial resolution and high electrochemical contrast is simultaneously achievable with HER SG/TC in contrast to conventional feedback mode.

Acknowledgements

Timo Raith gratefully acknowledges the financial support from the Studienstiftung des deutschen Volkes.

References

[1] M. Baklanov, P.S. Ho, E. Zschech, Advanced interconnects for ULSI technology, John Wiley & Sons, 2012.

[2] M.W. Lane, C.E. Murray, F.R. McFeely, P.M. Vereecken, R. Rosenberg, Liner materials for direct electrodeposition of Cu, Appl. Phys. Lett. 83 (2003) 2330–2332. doi:10.1063/1.1610256.

[3] S. Armini, Z. El-Mekki, M. Nagar, A. Radisic, P.M. Vereecken, Wafer Scale Copper Direct Plating on Thin PVD RuTa Layers: A Route to Enable Filling 30 nm Features and Below?, J. Electrochem. Soc. 161 (2014) D564–D570. doi:10.1149/2.1031410jes.

[4] T.P. Moffat, M. Walker, P.J. Chen, J.E. Bonevich, W.F. Egelhoff, L. Richter, C. Witt, T. Aaltonen, M. Ritala, M. Leskelä, D. Josell, Electrodeposition of Cu on Ru Barrier Layers for Damascene Processing, J. Electrochem. Soc. 153 (2006) C37. doi:10.1149/1.2131826.

[5] U. Emekli, A.C. West, Effect of additives and pulse plating on copper nucleation onto Ru, Electrochim. Acta. 54 (2009) 1177–1183. doi:10.1016/j.electacta.2008.08.065.

[6] P.M. Vereecken, A. Radisic, F.M. Ross, Differential Inhibition during Cu Electrodeposition on Ru: Combined Electrochemical and Real-Time TEM Studies, J. Electrochem. Soc. 166 (2019) D3129--D3135. doi:10.1149/2.0121901jes.

[7] S. Kim, D.J. Duquette, Growth of conformal copper films on TaN by electrochemical deposition for ULSI interconnects, Surf. Coatings Technol. 201 (2006) 2712–2716. doi:10.1016/j.surfcoat.2006.05.022.

[8] A. Radisic, Y. Cao, P. Taephaisitphongse, A.C. West, P.C. Searson, Direct Copper Electrodeposition on TaN Barrier Layers, J. Electrochem. Soc. 150 (2003) C362–C367. doi:10.1149/1.1565137.

[9] S. Kim, D.J. Duquette, Nucleation Characteristics of Directly Electrodeposited Copper on TiN, J. Electrochem. Soc. 153 (2006) C673. doi:10.1149/1.2219712.

[10] G. Oskam, P.M. Vereecken, P.C. Searson, Electrochemical Deposition of Copper on n-Si/TiN, J. Electrochem. Soc. 146 (1999) 1436–1441. doi:10.1149/1.1391782.

[11] L. Graham, C. Steinbrüchel, D.J. Duquette, Nucleation and Growth of Electrochemically Deposited Copper on TiN and Copper from a Cu NH 3 Bath, J. Electrochem. Soc. 149 (2002) C390–C395. doi:10.1149/1.1487836.

[12] M.J. Shaw, S. Grunow, D.J. Duquette, “Seedless” electrochemical deposition of copper on physical vapor deposition-W2N liner materials for ultra large scale integration (ULSI) devices, J. Electron. Mater. 30 (2001) 1602–1608. doi:10.1007/s11664-001-0179-8.

[13] D. Josell, C. Witt, T.P. Moffat, Osmium barriers for direct copper electrodeposition in damascene processing, Electrochem. Solid-State Lett. 9 (2006) C41–C43. doi:10.1149/1.2149214.

[14] D. Josell, J.E. Bonevich, T.P. Moffat, T. Aaltonen, M. Ritala, M. Leskelä, Iridium Barriers for Direct Copper Electrodeposition in Damascene Processing, Electrochem. Solid-State Lett. 9 (2006) C48–C50. doi:10.1149/1.2179770.

[15] B. Pesic, Copper Electrodeposition on Diffusion Barrier Films- A Literature Review, ECS Trans. 2 (2007) 243–256. doi:10.1149/1.2408879.

[16] J. Izquierdo, J.J. Santana, S. González, R.M. Souto, Scanning microelectrochemical characterization of the anti-corrosion performance of inhibitor films formed by 2-mercaptobenzimidazole on copper, Prog. Org. Coatings. 74 (2012) 526–533. doi:10.1016/j.porgcoat.2012.01.019.

[17] C. Li, L. Li, C. Wang, Study of the inhibitive effect of mixed self-assembled monolayers on copper with SECM, Electrochim. Acta. 115 (2014) 531–536. doi:10.1016/j.electacta.2013.11.029.

[18] G. Wittstock, T. Asmus, T. Wilhelm, Investigation of ion-bombarded conducting polymer films by scanning electrochemical microscopy (SECM)., Fresenius. J. Anal. Chem. 367 (2000) 346–51. doi:10.1007/s002160000389.

[19] W. Vielstich, H.A. Gasteiger, H. Yokokawa, Handbook of Fuel Cells: Fundamentals Technology and Applications: Advances in Electrocatalysis, Materials, Diagnostics and Durability, John Wiley & Sons, 2009.

[20] D.T. Jantz, K.C. Leonard, Characterizing Electrocatalysts with Scanning Electrochemical Microscopy, Ind. Eng. Chem. Res. (2018). doi:10.1021/acs.iecr.8b00922.

[21] J. Kim, C. Renault, N. Nioradze, N. Arroyo, K.C. Leonard, A.J. Bard, Nanometer Scale Scanning Electrochemical Microscopy Instrumentation, Anal. Chem. 88 (2016) acs.analchem.6b03024. doi:10.1021/acs.analchem.6b03024.

[22] J. Kim, C. Renault, N. Nioradze, N. Arroyo-Currás, K.C. Leonard, A.J. Bard, Electrocatalytic Activity of Individual Pt Nanoparticles Studied by Nanoscale Scanning Electrochemical Microscopy, J. Am. Chem. Soc. 138 (2016) 8560–8568. doi:10.1021/jacs.6b03980.

[23] T. Kai, C.G. Zoski, A.J. Bard, Scanning electrochemical microscopy at the nanometer level, Chem. Commun. 54 (2018) 1934–1947. doi:10.1039/C7CC09777H.

[24] A.R. Kucernak, P.B. Chowdhury, C.P. Wilde, G.H. Kelsall, Y.Y. Zhu, D.E. Williams, Scanning electrochemical microscopy of a fuel-cell electrocatalyst deposited onto highly oriented pyrolytic graphite, Electrochim. Acta. 45 (2000) 4483–4491. doi:10.1016/S0013-4686(00)00504-1.

[25] J. Zhou, Y. Zu, A.J. Bard, Scanning electrochemical microscopy - Part 39. The proton/hydrogen mediator system and its application to the study of the electrocatalysis of hydrogen oxidation, J. Electroanal. Chem. 491 (2000) 22–29. doi:10.1016/S0022-0728(00)00100-5.

[26] J.L. Fernández, C.G. Zoski, Voltammetric and Scanning Electrochemical Microscopy Investigations of the Hydrogen Evolution Reaction in Acid at Nanostructured Ensembles of Ultramicroelectrode Dimensions: Theory and Experiment, J. Phys. Chem. C. 122 (2018) 71–82. doi:10.1021/acs.jpcc.7b08976.

[27] J. Meier, K.A. Friedrich, U. Stimming, Novel method for the investigation of single nanoparticle reactivity, Faraday Discuss. 121 (2002) 365–372. doi:10.1039/b200014h.

[28] C. Iffelsberger, P. Vatsyayan, F.-M. Matysik, Scanning Electrochemical Microscopy with Forced Convection Introduced by High-Precision Stirring, Anal. Chem. 89 (2017) 1658–1664. doi:10.1021/acs.analchem.6b03764.

[29] C. Lee, C.J. Miller, A.J. Bard, Scanning electrochemical microscopy: preparation of submicrometer electrodes, Anal. Chem. 63 (1991) 78–83. doi:10.1021/ac00001a016.

[30] P. Hanekamp, W. Robl, F.M. Matysik, Development and application of a multipurpose electrodeposition cell configuration for studying plating processes on wafer specimen and for characterizing surface films by scanning electrochemical microscopy, J. Appl. Electrochem. 47 (2017) 1305–1312. doi:10.1007/s10800-017-1124-8.

[31] S. Kim, D.J. Duquette, Effect of Chemical Composition on Adhesion of Directly Electrodeposited Copper Film on TiN, J. Electrochem. Soc. 153 (2006) C417–C421. doi:10.1149/1.2189971.

[32] D. Starosvetsky, N. Sezin, Y. Ein-Eli, Seedless copper electroplating on Ta from an alkaline activated bath, Electrochim. Acta. 82 (2012) 367–371. doi:10.1016/j.electacta.2012.03.033.

[33] D. Starosvetsky, N. Sezin, Y. Ein-eli, Electrochimica Acta Seedless copper electroplating on Ta from a “ single ” electrolytic bath, Electrochim. Acta. 55 (2010) 1656–1663. doi:10.1016/j.electacta.2009.10.044.

[34] M. Sheffer, D. Mandler, Why is copper locally etched by scanning electrochemical microscopy?, J. Electroanal. Chem. 622 (2008) 115–120. doi:10.1016/j.jelechem.2008.05.005.

[35] J. Galceran, J. Cecı, J. Puy, Analytical Expressions for Feedback Currents at the Scanning Electrochemical Microscope, J. Phys. Chem. B. 104 (2000) 7993–8000. doi:10.1021/jp001564s.

[36] Y. Shao, M. V. Mirkin, Probing Ion Transfer at the Liquid / Liquid Interface by Scanning Electrochemical Microscopy (SECM), J. Phys. Chem. B. 102 (1998) 9915–9921. doi:10.1021/jp9828282.

[37] F.G. Smith, T.A. King, Optics and photonics: an introduction, John Wiley & Sons, 2007.

4.4 Nucleation studies on ruthenium from various electrolytes

4.4.1 Introduction

Copper (Cu) is slowly replacing aluminum as metallization in semiconductor industry due to its higher electrochemical and thermal conductivity and resistance against electromigration [1]. These Cu layers are usually deposited by electrochemical deposition from an acidic electrolyte with additives on a Cu seed layer. The seed layer acts as conductive starting layer for the electroplating process and is formed by physical vapor deposition (PVD), chemical vapor deposition (CVD) or atomic layer deposition (ALD). In order to inhibit the diffusion of copper into the surrounding dielectrics, a thin barrier film is deposited prior to the seed layer. This barrier layer typically consists of tungsten nitride (W_xN), titanium nitride (TiN), tantalum (Ta), or tantalum nitride (TaN) [2]. Due to the ongoing trend of scaling down feature sizes, it is demanding to conformally coat trenches and vias with a seed layer using the previously described methods [3]. As a result, alternative approaches are under evaluation to address this issue. One promising strategy is the direct electrochemical deposition of Cu on the barrier thin film in order to fill the aforementioned structures without a seed layer [4]. In this case, ruthenium (Ru) based barriers are most promising due to their immiscibility with Cu, good adhesion to Cu and their capability to act as a barrier layer even at very thin layer thicknesses of 5 nm [5]. For successful void-free filling of sub-µm range structures by direct electroplating, the formation of a continuous Cu film inside the trenches and vias is crucial. This critical layer thickness formed by coalescence d_{coal} is dependent on the nucleation density N_d in the early stages of electrocrystallization. Consequently, it is favorable to have a high initial nucleation density for fast film formation according to the correlation $\mathrm{d_{coal}} = 1/2\sqrt{\mathrm{N_d}}$ [6]. Recently, it was shown that it is possible to increase nucleation density by adding small amounts of citric acid to the Cu electrolyte [7,8].

Contemporaneously, such grain-refined layers exhibit an increased mechanical stability based on the Hall-Petch relation [9]. Up to now, the electrochemical deposition of such a grain refined copper was only shown on a Cu seed layer [10]. In order to verify that this effect is also obtainable in galvanic direct deposition, electrochemical copper nucleation from a citric acid containing electrolyte is studied and is compared to a commercially available acidic copper electrolyte. First results on the nucleation behavior of galvanically deposited Cu on Ru thin films are presented.

4.4.2 Experimental

4.4.2.1 Materials and chemicals

For all studies 4 x 4 cm^2 wafer specimen with thermally grown oxide were used. A thin layer of Ru (50 nm, PVD) or Cu (300 nm with 50 nm Ti adhesion layer, PVD) was deposited on these substrates. For electroplating experiments two Cu electrolytes were used. The first bath was a standard acidic bath [11] of 0.63 M copper sulfate pentahydrate ($CuSO_4*5H_2O$, analytical grade, Merck, Darmstadt), 0.3 M sulfuric acid (H_2SO_4, analytical grade, Merck, Darmstadt, Germany), 1.4 mM hydrochloric acid (HCl, analytical grade, Merck, Darmstadt, Germany), further denoted as virgin make up solution (VMS) with and without commercial additives. The second bath was adapted from [7] and contained 0.4 M $CuSO_4*5H_2O$, 0.38 M ammonium sulfate ($(NH_4)_2SO_4$ analytical grade, Merck, Darmstadt, Germany), and 0.03 M citric acid ($C_6H_8O_7$, Analytical grade, Sigma-Aldrich, St. Louis, Missouri). This electrolyte is denoted as low acidic electrolyte and was used with and without adding 1.4 mM HCl. The pH of this bath was varied by adding H_2SO_4 or ammonia (NH_3, 28%, analytical grade, BASF, Ludwigshafen, Germany).

4.4.2.2 Electrochemical deposition experiments

Electrochemical deposition was carried out with a special multipurpose cell for wafer-based samples in conjunction with a Smart Cell 1000w (Yamamoto MS, Tokyo, Japan) and an Autolab PGST302N potentiostat (Metrohm, Herisau, Switzerland) as described in [12]. Using this cell, the thin films on the silicon substrate are areal contacted and sealed at the same time. Therefore, a homogenous current and potential distribution for homogenous electrochemical deposition was obtained in the small exposed

circular opening of d = 4.52 mm. Linear sweep voltammetry studies were carried out in three electrode configuration with the multipurpose cell containing the sample as working electrode, an Ag/AgCl/3 M KCl as reference electrode and an iridium coated titanium plate as counter electrode at a scan rate of 0.05 V/s from open circuit potential E_{OCP} to E = -1 V. The obtained current responses were subsequently normalized to the active deposition area and were plotted as current density vs potential. Galvanic Cu deposition was performed in a two-electrode configuration with the multipurpose cell including the wafer specimen as cathode and an iridium coated titanium plate as counter electrode at a current density of cathodic j = 30 mA/cm^2 at fixed deposition times t_{dep} of 1 s, 1.5 s, 2 s, 5 s and 15 s. In order to remove the natively formed RuO, a pre-cleaning step at cathodic j = 0.25 mA/cm^2 for t = 180 s in 1.8 M H_2SO_4 was carried out prior to Cu deposition using the same setup with subsequent wet-transfer into the Cu electrolyte for electroplating. After deposition, the samples were carefully cleaned with isopropanol and dried with nitrogen gas.

4.4.2.3 Evaluation of nucleation

Evaluation of Cu nucleation was carried out with SEM images of a Zeiss Gemini Ultra 55 (Zeiss, Oberkochen, Germany). All pictures were taken at the same magnification and working distance (10000 x, WD = 6.9 mm) during recording. The nuclei size and their distribution were characterized with the software ImageJ (open source). In this process, the two-dimensional area of all nuclei was determined and their counts n_x were plotted in a histogram in dependence of their area size A. Subsequently, the mean area of these nuclei $A_m \pm \sigma_A$ was gained by fitting the obtained results with a Gauss-function in Origin 2017G (OriginLab Corporation Inc., Northampton, Massachusetts). The mean radius $r_m \pm \sigma_r$ can be derived by assuming all nuclei are circularly shaped. A visual presentation of this procedure is depicted in Fig 4.15. Moreover, nuclei density N_d and Cu coverage $A_{Cu\%}$ were also obtained utilizing ImageJ. Here, N_d is the amount auf nuclei N normalized to one picture section with the unit µm^{-2} and $A_{Cu\%}$ is the percentual Cu area coverage of the same section. For the cases where no software-based evaluation with ImageJ was possible, a manual determination of $r_m \pm \sigma_r$ was performed with DIPS 2.9 (Point electronic, Halle, Germany) as can be seen in Fig 4.17. Furthermore, adhesion of the deposited Cu was tested with a galvanic tape with the samples of t = 15 s deposition time. A good adhesion was achieved if no peeling of Cu from the Ru surface was observed.

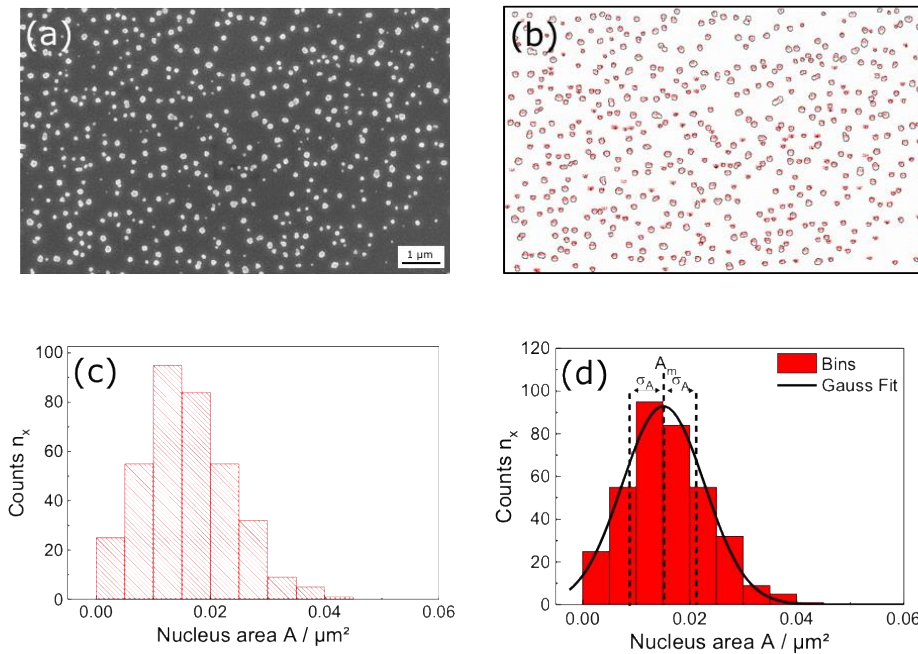

Figure 4.13: Visual presentation of the evaluation process of nuclei size distribution determination. (a) original SEM image, (b) software-based detection and labeling of nuclei with ImageJ, (c) histogram of the counts n_x in dependence of nucleus area A and (d) determination of mean area A_m and standard deviation σ_A of the histogram by fitting of a Gauss function with Origin 2017G.

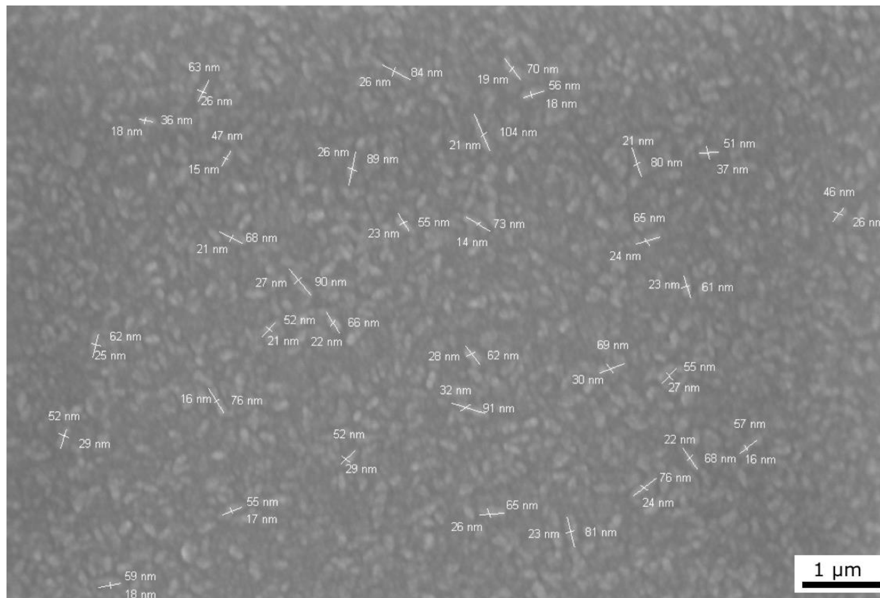

Figure 4.14: Manual determination of nuclei radii with software DIPS 2.9. Mean radius and standard deviation are calculated based on average diameter of the nuclei.

4.4.3 Result and discussion

4.4.3.1 Linear sweep voltammetry

In advance to the nucleation studies, the potential dependent deposition of Cu was electrochemically characterized with linear sweep voltammetry using the electrolytes described in the experimental section. Experiments were carried out using the wafer specimen with a Cu-seed layer to analyze the deposition potential without the superposition of direct deposition-based phenomena. As the effect of grain growth suppression and nucleation enhancement is dependent on the pH dependent complexation between Cu ions and citric acid [13], the initial pH value of the low acidic electrolyte of pH = 2.2 was adjusted to pH = 1 and pH = 2.5 for the characterization with linear sweep voltammetry. The scan curves are depicted in Fig 4.17.

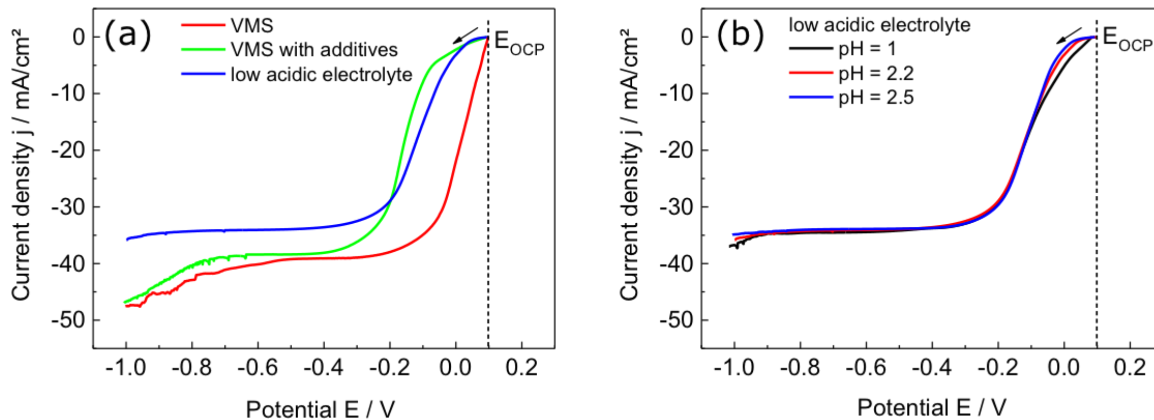

Figure 4.15: Linear sweep voltammetry of different copper electrolytes on a Cu thin film on Si. (a) Comparison of VMS (0.63 M $CuSO_4$, 0.3 M H_2SO_4, 1.4 mM HCl), VMS with commercially available bath additives and low acidic electrolyte (0.4 M $CuSO_4$, 0.38 M $(NH_4)_2SO_4$, 0.03 M $C_6H_8O_7$) and (b) low acidic electrolyte with varying pH value of pH = 1, pH = 2.2 and pH = 2.5.

As can be seen in Fig. 4.17 a), the current responses of the studied electrolytes differed significantly between each other. On this occasion, the suppressor component of the commercial additive system is strongly hindering copper deposition in the lower potential regime between E_{OCP} and E = -0.3 V in

comparison to the additive-free VMS solution. This ability to restrain copper deposition decreases with increasing overpotential as the effect of surface interaction of the additives is potential dependent. Consequently, the influence of the additives on deposition decreased and the current responses were almost identical in the potential range of E = -0.3 V to E = -0.6 V for the additive-free and additive-containing VMS electrolyte. A similar hindering effect was also observable for the low acidic electrolyte in the lower potential regime between E_{OCP} and E = -0.2 V. This behavior can be assigned to Cu grain growth suppression due to the pH dependent complex formation of citric acid at the Cu surface [8]. This model is further supported by the scan curves of the low acidic electrolyte recorded at different pH values of pH = 1, pH = 2.2 and pH = 2.5, represented in Fig. 4.17 b). As it can be seen, the inhibition effect increased with higher pH values and is nearly non-existent at strong acidic pH values. In contrast to VMS, deposition was also strongly inhibited at potentials lower than E = -0.3 V, indicating that $(NH_4)_2SO_4$ had a strong potential-independent influence on Cu deposition due to the formation of a shielding, positively charged NH_4^+ ion film at the substrate electrolyte interface [14]. Consequently, it can be assumed that the studied electrolytes will show different nucleation behavior as the obtained current responses were strongly influenced by bath composition.

4.4.3.2 Characterization of nucleation behavior

Since high nucleation rate is required for defect free filling of structures and the nuclei formation is dependent on overpotential [15], a high deposition potential is favorable for application-oriented direct plating of Cu. Based on the results of linear sweep voltammetry, galvanic deposition studies are carried out at a fixed current density of j = 30 mA/cm^2 with the parameters described in the experimental section. At this current density, electrochemical Cu deposition is not diffusion limited and subsequently the risk of hydrogen formation during the galvanic process is reduced. Cu nucleation is studied on Ru thin film on silicon substrates which is a promising candidate as a plateable thin film barrier in the semiconductor industry. In comparison to other barriers, corrosion or oxide formation is not present across the whole pH range which is crucial for electroplating of adherent Cu films [16]. Nucleation behavior on Ru thin film was studied from the VMS electrolyte without additives and the low acidic electrolyte. Furthermore, 1.4 mM HCl was added to the low acidic electrolyte to study the influence of chloride on nucleation. It is crucial to understand these effects, since the surface interaction of additives requires the presence of chloride in the electrolyte [17]. As it is known that Ru forms a native conductive oxide RuO [18], the impact

of oxide removal on nuclei formation and layer growth were also studied. Therefore, deposition experiments were carried out with untreated and pre-cleaned Ru thin films at the same deposition parameters.

Copper nucleation on untreated thin film ruthenium

In the first step untreated Ru thin films on silicon substrate were used for galvanic deposition studies at j = 3 mA/cm^2 at fixed deposition times of t = 1 s, 1.5 s, 2 s, 5 s and 15 s. The SEM images of the corresponding deposition times are depicted in Fig. 4.18. As the illustration shows, the growth of the Cu layer is dominated by island formation and 3D grain growth in the early electrocrystallization stages with different nucleation types dependent on electrolyte composition. For all electrolytes no dense layer was formed at t = 15 s.

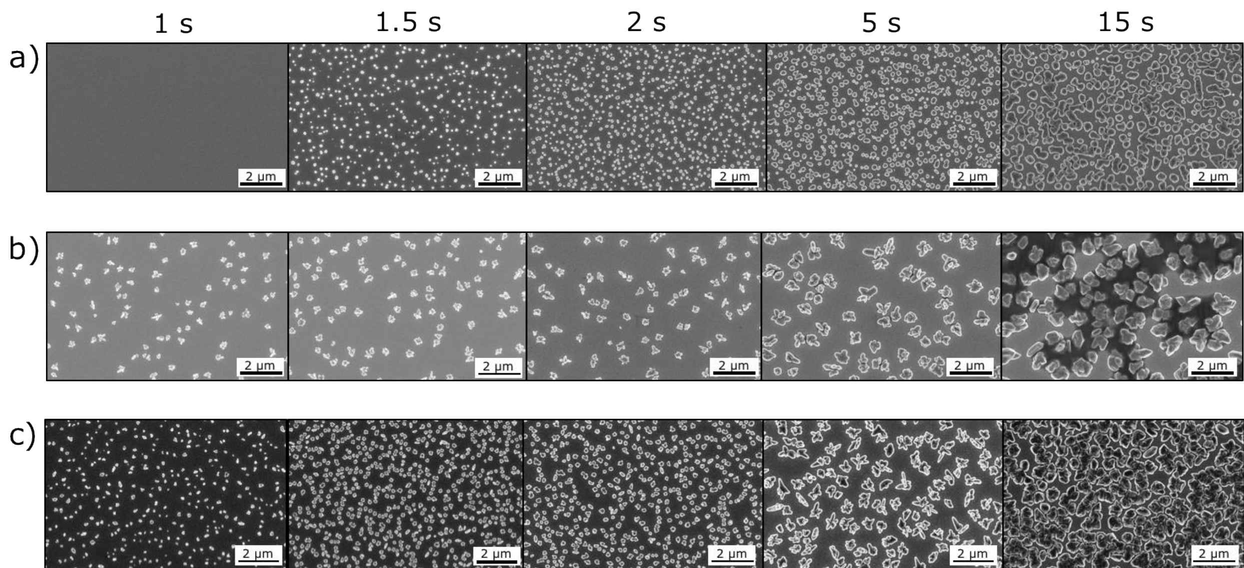

Figure 4.16: Galvanic Cu nucleation on untreated Ru thin film on Si substrate from different electrolytes at fixed deposition times. (a) VMS (0.63 M $CuSO_4$, 0.3 M H_2SO_4, 1.4 mM HCl), (b) low acidic electrolyte (0.4 M $CuSO_4$, 0.38 M $(NH_4)_2SO_4$, 0.03 M $C_6H_8O_7$) and (c) low acidic electrolyte with HCl (0.4 M $CuSO_4$, 0.38 M $(NH_4)_2SO_4$, 0.03 M $C_6H_8O_7$, 1.4 mM HCl). Deposition parameters: j = 30 mA/cm^2 at t = 1 s, 1.5 s, 2 s, 5 s and 15 s. All SEM images are recorded with the same magnification.

In order to characterize the underlying nucleation mechanism, the mean nuclei radius r_m, the nucleation density N_d and the Cu coverage of the surface $A_{Cu\%}$ were evaluated using the SEM images as described in the experimental section. Using the obtained information, the growth mechanism can be categorized in progressive nucleation, instantaneous nucleation or a mixed form of both types. Here, instantaneous nucleation is characterized by the formation of all nuclei at the initial deposition stage and a subsequent uniform growth of these nuclei until coalescence. Consequently, this mechanism is expressed by a constant N_d value and a linear increase of r_m during deposition time. Contrary, progressive nucleation describes continuous formation and individual growth of nuclei across deposition time. Therefore, this mechanism is described by an increase of N_d and an increase of scattering of the r_m value with deposition time. Comparing the software-based evaluation results in Fig 4.19, the growth mechanism at j = 3 mA/cm^2 can be derived for each electrolyte.

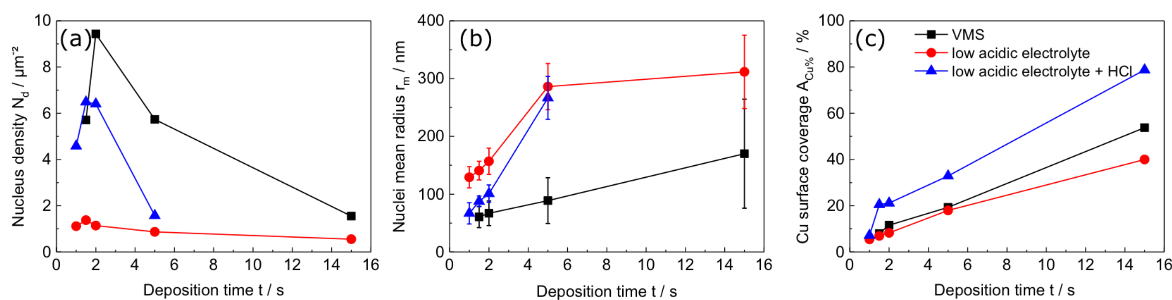

Figure 4.17: Characterization of Cu nucleation on an untreated Ru surface from different electrolytes in dependence of deposition time. (a) Nucleus density N_d, (b) nuclei mean radius r_m and (c) surface coverage $A_{Cu\%}$. Electrolytes: VMS (black, 0.63 M $CuSO_4$, 0.3 M H_2SO_4, 1.4 mM HCl), low acidic electrolyte (red, 0.4 M $CuSO_4$, 0.38 M $(NH_4)_2SO_4$, 0.03 M $C_6H_8O_7$) and low acidic electrolyte with HCl (blue, 0.4 M $CuSO_4$, 0.38 M $(NH_4)_2SO_4$, 0.03 M $C_6H_8O_7$, 1.4 mM HCl). Deposition parameters: j = 3 mA/cm^2 at t = 1 s, 1.5 s, 2 s, 5 s and 15 s.

Based on Fig. 4.19 a) and Fig. 4.19 b), it can be said that Cu nucleation from the VMS electrolyte is progressive as N_d and the scattering of r_m are increasing with deposition time before coalescence. In contrast, electrochemical deposition of Cu from the low acidic electrolyte is dominated by instantaneous nucleation since nearly no change of N_d as well as a linear increase of r_m were observed. Therefore, it can be concluded, that citric acid is actively inhibiting nuclei formation on the untreated Ru surface and favors grain growth at the early deposition stage. Despite the different growth mechanism, $A_{Cu\%}$ is nearly equal

for both electrolytes as it can be seen in Fig. 4.19 c). Hence, the larger N_d value achieved with the VMS electrolyte is counterbalanced by the overall larger nuclei of the low acidic electrolyte in the deposition time of $t \leq 5$ s. The addition of 1.4 mM HCl to the low acidic electrolyte had a large impact on the nucleation behavior as well as on $A_{Cu\%}$ in the early deposition stages. Here, N_d was heavily shifted towards larger values and was no longer constant with deposition time. Furthermore the r_m value was halved. It can be deducted that chloride counteracts the effect of citric acid on Cu nucleation because nucleation behavior showed a more progressively pronounced growth mechanism. Thus, faster coalescence was achieved as it can be seen in Fig 4.19 c). The adhesion of the formed Cu layer was tested with the samples of t = 15 s deposition time using an adhesive tape. Complete peeling of the Cu film from the untreated Ru surface was observed, indicating that adhesion is rather poor independent of the used electrolyte.

Copper nucleation on pre-cleaned ruthenium thin film

In the second step, a pre-cleaning step at cathodic j = 0.25 mA/cm^2 in 0.8 M H_2SO_4 for t = 180 s was carried out prior to galvanic deposition to remove the native oxide from the Ru surface. The same galvanic deposition experiments were performed with the pre-cleaned samples at j = 3 mA/cm^2 at deposition times of t = 1 s, 1.5 s, 2 s, 5 s and 15 s. The corresponding SEM images are depicted in Fig 4.20.

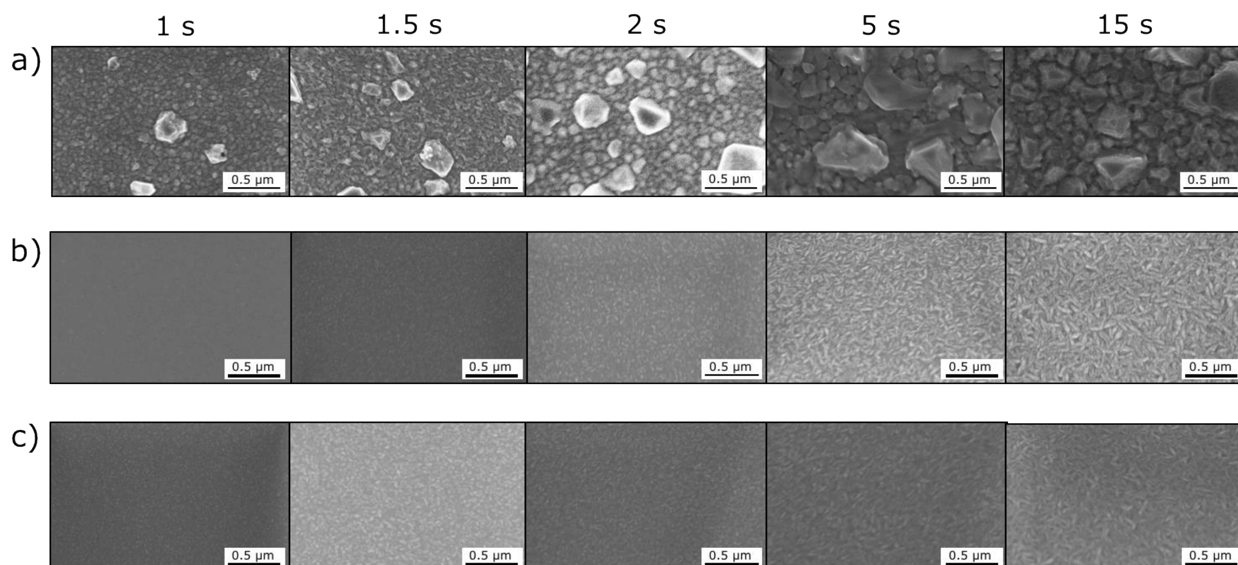

Figure 4.18: Galvanic Cu nucleation on pretreated Ru thin film on Si substrate from different electrolytes at fixed deposition times. (a) VMS (0.63 M $CuSO_4$, 0.3 M H_2SO_4, 1.4 mM HCl), (b) low acidic electrolyte (0.4 M $CuSO_4$, 0.38 M $(NH_4)_2SO_4$, 0.03 M $C_6H_8O_7$) and (c) low acidic electrolyte with HCl (0.4 M $CuSO_4$, 0.38 M $(NH_4)_2SO_4$, 0.03 M $C_6H_8O_7$, 1.4 mM HCl). Pre-cleaning step: cathodic $j = 0.25$ mA/cm^2 for $t = 180$ s in 1.8 mM H_2SO_4. Deposition parameters: $j = 30$ mA/cm^2 for $t = 1$ s, 1.5 s, 2 s, 5 s and 15 s. All SEM images are recorded with the same magnification.

Comparing Fig. 4.18 with Fig. 4.20, it is evident that oxide removal has a large impact on nucleation. Here, nucleation on oxide-free Ru is dominated by two-dimensional layer growth. In the case of the VMS electrolyte, 2D layer formation is further superimposed by 3D island growth. These results are in good agreement with the observed layer by layer growth of Cu on Ru in potentiostatic deposition studies described in literature [19]. Since the Cu nuclei are hardly distinguishable from the Ru surface in the SEM images, a software-based determination of N_d and A_{dep} is not possible. Consequently, characterization of the deposition mechanism cannot be achieved. Correspondingly, a manual evaluation of r_m on the samples with the deposition time of t = 1 s, 1.5 s and 2 s were carried out as described in the experimental section. The characterization procedure was not conducted for t = 5 s and 15 s samples, since the formation of dense Cu layer was already observable. The results are depicted in Fig. 4.21.

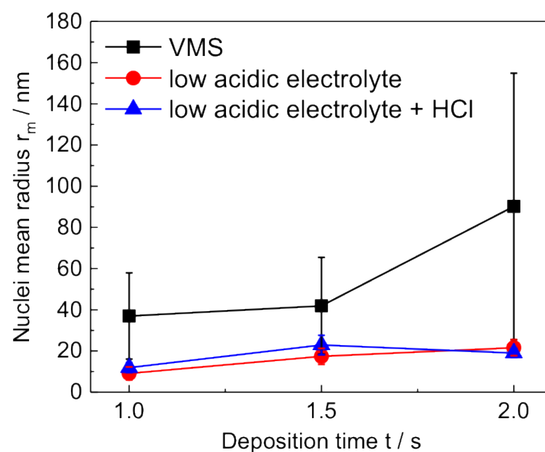

Figure 4.19: Characterization of Cu nuclei radius on pretreated Ru surface from different electrolytes in dependence of deposition time at $j = 3\ mA/cm^2$. Electrolytes: VMS (black, 0.63 M $CuSO_4$, 0.3 M H_2SO_4, 1.4 mM HCl), low acidic electrolyte (red, 0.4 M $CuSO_4$, 0.38 M $(NH_4)_2SO_4$, 0.03 M $C_6H_8O_7$) and low acidic electrolyte with HCl (blue, 0.4 M $CuSO_4$, 0.38 M $(NH_4)_2SO_4$, 0.03 M $C_6H_8O_7$, 1.4 mM HCl). Pre-cleaning step: $j = 0.25\ mA/cm^2$ for t = 180 s in 1.8 mM H_2SO_4. Deposition parameters: cathodic $j = 3\ mA/cm^2$.

Comparing r_m at the early deposition stage, it is evident that r_m of the VMS-deposited Cu as well as its scattering were significantly larger than the obtained values for the low acidic electrolyte. Simultaneously, it is observable that r_m of the citric acid containing electrolytes was only increasing slightly with deposition time. This can be attributed to the inhibition of grain growth and consequently the enhancement of nuclei formation by surface interaction of citric acid [8]. The mean radius r_m is obviously not influenced by the addition of 1.4 mM HCl to the low acidic electrolyte as the obtained values are almost identical within the accuracy of analysis. Therefore, influencing effects of chloride on the surface interaction of citric acid during electrocrystallization can be ruled out. Cu adhesion on pretreated Ru was also characterized with the samples of t = 15 s deposition time following the same protocol as for the untreated Ru samples. No peeling of the Cu layer was observed, indicating that adhesion between the thin film Cu and the pre-cleaned Ru is independent of electrolyte composition.

Nucleation characteristics in dependence of Ru surface condition

Comparing the results from Fig. 4.19 with Fig. 4.21, it is evident that the wetting behavior of Cu in the early nucleation phase is heavily dependent on the condition of the Ru surface. On this occasion, electrochemical Cu nucleation on untreated Ru occurred as a three-dimensional island growth. Therefore, it can be concluded that Cu deposition is electrochemically preferred on Cu and not on the RuO surface. Furthermore, grain growth inhibition of citric acid could not be detected in this case, which was shown by the comparison of the nuclei sizes of citric acid containing electrolytes and the acidic VMS copper bath in Fig 4.19 b). One plausible reason for this observed effect is a stronger interaction of citric acid with the natively formed conductive oxide compared to the copper surface. In contrast to this result, a two-dimensional layer by layer Cu growth was observable on the pre-cleaned oxide-free Ru surface. This indicates that Cu preferentially attaches to pure Ru rather than to the Cu nuclei. This is also the reason that causes the Cu nuclei on pure Ru to be 10 times smaller than on the RuO surface. Contrary to the case of untreated Ru, Cu grain growth inhibition was observed from the citric acid containing electrolytes independent of chloride concentration. Here, small nuclei sizes of r_m = 10 nm were obtained in comparison to r_m = 40 nm for the acidic VMS bath as it can be seen in Fig. 4.21. Surface pretreatment does not only affect the nucleation behavior but also the adhesion of the Cu nuclei on the Ru surface. Hence, removal of the oxide is crucial for electrochemical deposited Cu thin films with good adhesion to the substrate independent of electrolyte composition.

4.4.4 Conclusion

Investigations on electrochemical nucleation and growth of Cu on Ru thin film on a silicon substrate were performed to study the grain growth inhibition effect of citric acid in the early deposition stage in a direct plating process. Based on galvanic Cu deposition experiments with a commercial acidic plating bath and a low acidic electrolyte containing citric acid, it could be shown that Cu grain refinement and a high nuclei density is achievable with a citric acid electrolyte. The deposition of nanocrystalline Cu with good adhesion was only possible on pure Ru, indicating that the removal of natively formed RuO is crucial for galvanic thin film coating. Since the addition of chloride to the citric acid containing electrolyte had not affected grain growth suppression, organic additives for direct Cu deposition on Ru can be utilized. Consequently,

defect-free conformal filling of structures in the sub-µm ranges should be feasible with a citric acid as grain refiner.

References

[1] P.C. Andricacos, C. Uzoh, J.O. Dukovic, J. Horkans, H. Deligianni, Damascene copper electroplating for chip interconnections, IBM J. Res. Dev. 42 (1998) 567–574.

[2] M. Baklanov, P.S. Ho, E. Zschech, Advanced interconnects for ULSI technology, John Wiley & Sons, 2012.

[3] S. Armini, H. Philipsen, Z. El-Mekki, A. Redolfi, A. Van Ammel, A. Radisic, W. Ruythooren, others, Seedless Copper Electrochemical Deposition on Barrier Materials as a Replacement/Enhancement for PVD Cu Seed Layers in HAR TSVs, in: Meet. Abstr., 2010: p. 1280.

[4] B. Pesic, Copper Electrodeposition on Diffusion Barrier Films- A Literature Review, ECS Trans. 2 (2007) 243–256. doi:10.1149/1.2408879.

[5] T.N. Arunagiri, Y. Zhang, O. Chyan, M. El-Bouanani, M.J. Kim, K.H. Chen, C.T. Wu, L.C. Chen, 5 nm ruthenium thin film as a directly plateable copper diffusion barrier, Appl. Phys. Lett. 86 (2005) 83104.

[6] A. Radisic, Y. Cao, P. Taephaisitphongse, A.C. West, P.C. Searson, Direct Copper Electrodeposition on TaN Barrier Layers, J. Electrochem. Soc. 150 (2003) C362–C367. doi:10.1149/1.1565137.

[7] S.D. Kang, J. Joon Yoo, H.-K. Lyeo, J. Yong Song, S. Lee, J. Yu, Assessing the thermal conductivity of non-uniform thin-films: Nanocrystalline Cu composites incorporating carbon nanotubes, J. Appl. Phys. 110 (2011) 23506.

[8] H. Natter, R. Hempelmann, Nanocrystalline copper by pulsed electrodeposition: The effects of organic additives, bath temperature, and pH, J. Phys. Chem. 100 (1996) 19525–19532. doi:10.1021/jp9617837.

[9] C.S. Pande, K.P. Cooper, Nanomechanics of Hall-Petch relationship in nanocrystalline materials, Prog. Mater. Sci. 54 (2009) 689–706.

[10] M.J. Kim, S. Choe, H.C. Kim, S.K. Cho, S.-K. Kim, J.J. Kim, Electrochemical Behavior of Citric Acid

and Its Influence on Cu Electrodeposition for Damascene Metallization, J. Electrochem. Soc. 162 (2015) D354–D359. doi:10.1149/2.0561508jes.

[11] A. Radisic, O. Lühn, H.G.G. Philipsen, Z. El-Mekki, M. Honore, S. Rodet, S. Armini, C. Drijbooms, H. Bender, W. Ruythooren, Copper plating for 3D interconnects, Microelectron. Eng. 88 (2011) 701–704. doi:10.1016/j.mee.2010.06.030.

[12] P. Hanekamp, W. Robl, F.M. Matysik, Development and application of a multipurpose electrodeposition cell configuration for studying plating processes on wafer specimen and for characterizing surface films by scanning electrochemical microscopy, J. Appl. Electrochem. 47 (2017) 1305–1312. doi:10.1007/s10800-017-1124-8.

[13] F.I. Lizama-Tzec, L. Canché-Canul, G. Oskam, Electrodeposition of copper into trenches from a citrate plating bath, Electrochim. Acta. 56 (2011) 9391–9396. doi:10.1016/j.electacta.2011.08.023.

[14] H. Fischer, Elektrolytische Abscheidung und Elektrokristallisation von Metallen, Springer-Verlag, 2013.

[15] L. Guo, P.C. Searson, On the influence of the nucleation overpotential on island growth in electrodeposition, Electrochim. Acta. 55 (2010) 4086–4091.

[16] M.W. Lane, C.E. Murray, F.R. McFeely, P.M. Vereecken, R. Rosenberg, Liner materials for direct electrodeposition of Cu, Appl. Phys. Lett. 83 (2003) 2330–2332. doi:10.1063/1.1610256.

[17] P.M. Vereecken, R. a. Binstead, H. Deligianni, P.C. Andricacos, The chemistry of additives in damascene copper plating, IBM J. Res. Dev. 49 (2005) 3–18. doi:10.1147/rd.491.0003.

[18] U. Emekli, A.C. West, Effect of additives and pulse plating on copper nucleation onto Ru, Electrochim. Acta. 54 (2009) 1177–1183. doi:10.1016/j.electacta.2008.08.065.

[19] T.P. Moffat, M. Walker, P.J. Chen, J.E. Bonevich, W.F. Egelhoff, L. Richter, C. Witt, T. Aaltonen, M. Ritala, M. Leskelä, D. Josell, Electrodeposition of Cu on Ru Barrier Layers for Damascene Processing, J. Electrochem. Soc. 153 (2006) C37. doi:10.1149/1.2131826.

5 Summary

In this work, evaluation of the applicability of electrochemical scanning microscopy (SECM) for semiconductor industry-relevant thin film materials was carried out. These investigations were focused on the local electrochemical characterization of electrodeposited copper layers and their growth behavior on a variety of barrier materials such as Pt, Ru, TiN, TaN, Ta, Ti, W, and TiW. A special holding device for wafer-based samples was developed to be able to handle this combined task on a laboratory scale. This multipurpose cell provided electrical contact for the thin films deposited on the silicon substrate while simultaneously sealing the sample with only a small exposed area without any complex sample preparation. Based on preliminary studies, it could be shown that local surface characterization by means of SECM as well as electrochemical copper deposition in a commercial laboratory tool on the aforementioned materials with this cell was feasible. Consequently, deposition protocols for electroplating of dense Cu films with good adhesion on various barrier materials were developed for surface characterization studies with SECM. It became apparent that conventional commercial acidic copper electrolytes were only suitable for deposition of dense and adherent films on Cu or platinoids such as Ru or Pt. In contrast, direct electroplating on Ta-, Ti- and W-based barrier thin films had shown that the deposition of dense and adherent layers was heavily dependent on potential, on electrolyte composition and process handling and was therefore inappropriate for galvanic coating on a wafer scale. On the other side, implementation of the multipurpose cell into the SECM setup revealed that the local surface characterization of semi-precious metals in conventional feedback mode was strongly restricted. It could be shown, that oxide formation and corrosion of the thin film surface on the basis of surface interaction effects in aqueous solution had a strong influence on the measurement results. Moreover, the local resolution of this technique is limited, since materials with similar conductivity cannot be distinguished as shown by approach curves studies on different metallic thin films such as Ru, Pt, Cu, TiN, TiW, W and TaN. Based on these results a non-destructive measuring concept was developed which would ensure a high electrochemical contrast between different metallic materials without mediator-based surface interferences on the measured signal. It was demonstrated that the hydrogen evolution reaction had the necessary material selectivity according to the results of chronoamperometric studies on different barrier thin films. Therefore, a mediatorless SECM concept in SG/TC mode was characterized from these findings, which showed that the aforementioned requirements were achieved. In the next step, the measurement concept was used for the electrochemical characterization of the growth of direct electroplated Cu on Ru thin films. This model system was selected since Ru did not restrict the composition of the Cu electrolyte.

Therefore, it was possible to study the influence of a grain refiner such as citric acid on the early electrocrystallization stage of Cu on Ru. In a preliminary SEM-supported study, it was shown that citric acid had a strong impact on the nucleation since it effectively inhibited grain growth in the deposition process. Thus, nanocrystalline and adherent Cu layers with a grain radius of 10 nm could be formed on pure Ru surface. Since the local resolution of the SECM is dependent on the probe size, ultramicroelectrodes with a size of $r_{tip} < 10$ nm are required. The fabrication of electrodes of this dimensions cannot be accomplished with existing methods. In order to electrochemically characterize the nucleation behavior of Cu on foreign substrates electrochemically, new manufacturing processes for ultramicroelectrodes in the lower nanometer range have to be developed.

6 Zusammenfassung in deutscher Sprache

Im Rahmen dieser Arbeit wurden die Analysemöglichkeiten von relevanten Materialien aus der Halbleiterindustrie mittels elektrochemischer Rastermikroskopie (SECM) evaluiert. Im Fokus dieser Untersuchungen stand die lokale Oberflächencharakterisierung von elektrochemisch abgeschiedenen Kupferschichten und deren Wachstumsverhalten auf unterschiedlichen Barrierematerialien (Direct Copper Plating, DCP). Um diese gekoppelte Aufgabenstellung im Labormaßstab ohne komplexe Probenpräparation bewältigen zu können, wurde eine spezielle Haltevorrichtung für Wafer-basierte Proben entwickelt. Die Bauweise dieser sogenannten Multifunktionszelle ermöglicht die elektrische Kontaktierung der Dünnschichten auf dem Siliziumträgersubstrat bei gleichzeitiger Versiegelung der Probe. Hierdurch wurde die lokale Oberflächencharakterisierung mittels SECM als auch die elektrochemische Kupferabscheidung in einem kommerziellen Labortool ermöglicht. Um das elektrochemische Wachstumsverhalten von Kupfer auf vorab eigeschränkten Barrierematerialien untersuchen zu können, wurden geeignete Cu Abscheideprotokolle mithilfe der Multifunktionszelle erstellt und getestet. Es konnte hierfür gezeigt werden, dass konventionelle schwefelsäurehaltige Kupferelektrolyte nur für die Abscheidung auf Kupfer oder Platinoide geeignet sind. Die direkte elektrochemische Abscheidung von dichten und haftenden Kupferfilmen auf Ta-, Ti- und W-basierende Barrieren war hingegen stark Potential abhängig, benötigte spezielle Elektrolytzusammensetzung sowie Abscheideprotokolle und war folglich für eine galvanische Beschichtung im Wafer-Maßstab ungeeignet. Implementiert man die Multifunktionszelle in das SECM zur Untersuchung der vorab genannten Materialien, so zeigt sich, dass die lokale Oberflächencharakterisierung von Halbedelmetallen mittels SECM im konventionellen Feedback Modus nur unter Einschränkungen verwendbar ist. Die Messresultate werden hierbei stark von Oberflächenwechselwirkungseffekten wie etwa Oxidbildung oder Korrosion in der wässrigen Lösung beeinflusst. Das Auflösungsvermögen war weiterhin stark limitiert, da Materialien mit ähnlichen elektrischen Eigenschaften mit dieser Messmethode nicht differenziert werden konnten. Dies konnte mit Hilfe von Annährungskurven auf unterschiedlichen metallischen Dünnschichten wie Ru, Pt, Cu, TiN, TiW, W und TaN gezeigt werden. Aufgrund dieser Erkenntnisse wurde ein zerstörungsfreies Messkonzept entwickelt, welches einen hohen Kontrast zwischen unterschiedlichen metallischen Materialien ohne Störeffekte durch mediatorbasierte Oberflächenwechselwirkungseffekte gewährleisten sollte. Mithilfe von chronomamperometrischen Studien an unterschiedlichen metallischen Dünnfilmen konnte demonstriert werden, dass die Wasserstoffentwicklungsreaktion die nötige Materialselektivität besitzt. Basierend auf diesen Resultaten wurde ein Mediator-freier experimenteller SECM-Ansatz im

SG/TC Modus entwickelt, welcher die zuvor genannten Anforderungen erfüllte. Das entwickelte Messkonzept sollte im nächsten Schritt zur elektrochemischen Charakterisierung des Nukleations- und Wachstumsverhaltens von galvanisch aufwachsendem Cu auf Ru eingesetzt werden. Dieses Modellsystem wurde gewählt, da Ru die Zusammensetzung des Cu-Elektrolyten nicht einschränkt und folglich der Einfluss von Zusatzstoffen wie etwa des Kornverfeinerers Zitronensäure, auf die Direktabscheidung untersucht werden kann. In einer REM-gestützten Vorabstudie konnte gezeigt werden, dass Zitronensäure das Kornwachstum aktiv hemmt und sehr feinkristalline und gut haftende Cu-Schichten mit einem Kornradius von 10 nm auf reinem Ru abgeschieden werden konnten. Da das lokale Auflösungsvermögen des SECM von der Sondengröße abhängig ist, werden Ultramikroelektroden mit einer Größe von $r_{tip} < 10$ nm zur Oberflächencharakterisierung benötigt. Die Herstellung von Elektroden dieser Dimensionen ist mit bekannten Verfahren nicht möglich. Um das Nukleationsverhalten von Cu auf artfremden Substraten elektrochemisch charakterisieren zu können, müssen folglich neue Herstellungsprozesse für Ultramikroelektroden im unteren Nanometerbereich entwickelt werden.

Erklärung

Ich erkläre hiermit an Eides statt, dass ich die vorliegende Arbeit ohne unzulässige Hilfe Dritter und ohne Benutzung anderer als der angegebenen Hilfsmittel angefertigt habe; die aus anderen Quellen direkt oder indirekt übernommenen Daten und Konzepte sind unter Angabe des Literaturzitats gekennzeichnet.

Weitere Personen waren an der inhaltlich-materiellen Herstellung der vorliegenden Arbeit nicht beteiligt. Insbesondere habe ich hierfür nicht die entgeltliche Hilfe eines Promotionsberaters oder anderer Personen in Anspruch genommen. Niemand hat von mir weder unmittelbar noch mittelbar geldwerte Leistungen für Arbeiten erhalten, die im Zusammenhang mit dem Inhalt der vorgelegten Dissertation stehen.

Die Arbeit wurde bisher weder im In- noch im Ausland in gleicher oder ähnlicher Form einer anderen Prüfungsbehörde vorgelegt.

Regensburg, den 17. Dezember 2019

____

(Patrick Hanekamp)